UNIVERSITY OF OKLAHOMA

GRADUATE COLLEGE

ASSESSING THE IMPACT OF MICROORGANISMS CAPABLE OF DEGRADING BIODIESEL AND DIESEL FUEL IN STORAGE TANKS

A DISSERTATION

SUBMITTED TO THE GRADUATE FACULTY

in partial fulfillment of the requirements for the

Degree of

DOCTOR OF PHILOSPOHY

By

JAMES GREGORY FLOYD

Norman, Oklahoma

2021

ASSESSING THE IMPACT OF MICROORGANISMS CAPABLE OF DEGRADING BIODIESEL AND DIESEL FUEL IN STORAGE TANKS

A DISSERTATION APPROVED FOR THE
DEPARTMENT OF MICROBIOLOGY AND PLANT BIOLOGY

BY

Dr. Anne Dunn, Chair

Dr. Bradley Stevenson, Co-Chair

Dr. Kara De León

Dr. Andrew Madden

Every student's journey in graduate school is unique, mine can only be described as a rollercoaster of highs and lows. I met my wife during my PhD journey and was married by my advisor Bradley Stevenson. On the other end of the spectrum, I was unsure I would even be alive to finish this dissertation as I was diagnosed with metastatic cancer. I cannot thank my wife enough for her unyielding love and compassion during those trying times. To my mother, I cannot thank you enough for supporting me throughout my life and helping to guide me into the man that I am today. Additionally, I would like to thank my uncle Greg for his continual support through my life.

"You cannot hope to build a better world without improving the individuals."

-Marie Curie

Acknowledgements

I must thank all my committee members, past and present, for all your insights and guidance along this journey. To my advisor Dr. Bradley Stevenson, you took me under your wing and enlightened me to new ways to view and understand the world around us. Outside of the professional scope you also provided pillars of support and understanding from the many trials I confronted during my time as your student. You provided a strong foundation and gave me the tools and attention that allowed me to excel.

This dissertation is a product of the numerous people that I have interacted with during my time at OU. I would first like to thank each member of the Stevenson lab. Emily, thank you for your inquisitive nature and providing useful insights on this work. Blake, thank you for always being around to answer my numerous bioinformatic questions and providing useful insights into this work. Brian, thank you for not only your insights, but you were the best friend that I made during my time at OU. Heather, thank you for your contributions to this work, as well as being like the sister I never had. Finally, Oderay although our time together was short, I can't thank you enough for your input and the friendship that we had.

Finally, I must thank the entire Microbiology and Plant Biology Department. During my cancer diagnosis it was inspiring to see everyone come together and rally around me during my time of need. I would not have made it through those trying times without everyone that supported my family and me.

Table of Contents

List of Tables viii

List of Figures ix

Abstract xvi

Chapter 1. Introduction 1

Assessing the Impact of Microorganisms Capable of Degrading Biodiesel and Diesel Fuel in Storage Tanks 1

Microbiologically Influenced Corrosion (MIC) in Biodiesel and Diesel Fuel Systems 4

Investigating Microbial Communities in Fuel Systems 6

Microbial Ecology in Fuel Storage Systems 7

Scientific Contributions 10

Works Cited 12

Chapter 2. Locating and Quantifying Carbon Steel Corrosion Rates Linked to Fungal B20 Biodiesel Degradation 20

Foreword 21

Abstract 22

Importance 22

Introduction 23

Results 26

Characterization and Phylogenetic Identification of Fungi Isolated from B20 Biodiesel 26

Fungal Growth in Bioreactors 27

Acidification of Aqueous Medium 28

Direct Measurement of Corrosion 29

Colocation of Biology and Corrosion 30

Fuel Degradation 33

Discussion 35

Materials and Methods 38

Isolation, Identification, and Growth of Fungal Isolates. 38

Quantification and Characterization of Microbiologically Influenced Corrosion in Bioreactors 40
Localizing Corrosion in Fuel, Interphase, and Aqueous Phases 42
Calculation of Corrosion Rates from Mass Loss Measurements 44
Quantification and Characterization of B20 Biodiesel Fuel Biodegradation. 45
Statistical Analysis and Data Visualization 46
Acknowledgements 46
Works Cited 47
Chapter 3. Connection Between Fuel Composition and the Microbiological Communities Contaminating Fuel Storage Tanks 54
Foreword 55
Abstract 56
Importance 57
Introduction 57
Results 60
Characterization of n-Alkanes and FAME Components in Fuels 60
Taxonomic Analysis of Contaminated Fuels 63
Redundancy Analysis Correlating Fuel Components to Taxonomy 65
Physiological Characterization of Isolates to Test Correlations Predicted from Fungal RDA 80
Discussion 81
Materials and Methods 85
Fuel Tank Sampling Protocol 85
DNA Extraction, SSU rRNA Gene Library Preparation, and Sequencing 86
Quantification and Characterization of FAME and Alkanes in Fuels 88
Analysis of SSU rRNA Gene Sequencing Libraries 89
Redundancy Analyses (RDA) 90
Validation of the Fungal Redundancy Analysis Model 90
Statistical Analyses and Data Visualization 92
Acknowledgements 92
Works Cited 93

Chapter 4. Transcriptomic Analysis of *Paecilomyces* AF001 Grown on B20 Biodiesel and Ultra-Low Sulfur Diesel 101

Foreword 102
Abstract 103
Importance 103
Introduction 104
Results 106
Fuel Sterilization and Selection 106
Determining *Paecilomyces* AF001 Growth Stages on Fuels 107
Biomass-based Growth Measurements and Lipase Assay 108
Transcriptome Analysis 109
Discussion 114
Materials and Methods 117
Fuel Sterilization and Selection 117
Determining *Paecilomyces* AF001 Growth Stages on Fuels 119
Biomass Growth Measurements and Lipase Assay 120
RNA Extraction and Sequencing 122
Transcriptome Analysis 123
Statistical Analyses and Data Visualization 123
Acknowledgements 123
Works Cited 125
Chapter 5. Conclusions 131

Locating and Quantifying Carbon Steel Corrosion Rates Linked to Fungal B20 Biodiesel Degradation 131
Microbial Communities in Biodiesel Storage Tanks Correlate with Fuel Composition 135
Transcriptomic Analysis of *Paecilomyces* AF001 Grown on B20 Biodiesel and Ultra-Low Sulfur Diesel 137
Final Conclusions 138
Works Cited 140
APPENDIX 146

List of Tables

Table 3.1. Forward selection of significant ($p \leq 0.05$) fuel variables based on an adonis permutational multivariate analysis of variance on the bacterial Hellinger transformed taxonomic data. 68

Table 3.2. Correlation coefficients for fuel compounds for RDA1 and RDA2 axes for the bacterial RDA plot. 71

Table 3.3. Forward selection of significant ($p \leq 0.05$) fuel variables based on an adonis permutational multivariate analysis of variance on the fungal Hellinger transformed taxonomic data. 75

Table 3.4. Correlation coefficients for fuel compounds for RDA1 and RDA2 axes for the fungal RDA plot. 78

Table 4.1. Primers and probes used to quantify potential bacterial contamination in B20 biodiesel and B5 ULSD. 118

Table 4.2. Primers and probes used to quantify potential fungal contamination in B20 biodiesel and B5 ULSD 118

Table A.1. Fuel sample descriptions used in Chapter 3 for the meta-analysis. 146

Table A.2. n-Alkane composition of fuels in parts per million (PPM) used in the analyses from Chapter 3. Values provides are the average PPM from 3 technical replicates analyzed from the same fuel. Sample descriptions can be seen in table A.1 151

Table A.3. Fatty acid methyl ester concentrations in parts per million (PPM) used in the analyses from Chapter 3. Values provides are the average PPM from 3 technical replicates analyzed from the same fuel. Sample descriptions can be seen in table A.1 157

List of Figures

FIG 1.1 Illustration of an underground fuel storage tank showing the separation of vapor, fuel, and water phases. Gradients on the right demonstrate where the highest concentrations (Blue) of each category are found in these tanks (lowest concentrations White). 9

FIG 2.1. Maximum likelihood tree based on ITS sequence similarity among close phylogenetic relatives (NCBI accession numbers in parentheses) of the Paecilomyces sp. AF001 (A) and Wickerhamomyces SE3 (B) isolates. Bootstrap values above 50 percent for 500 samples are shown at relevant nodes 27

FIG 2.2. Density of planktonic populations (circles) and biofilms (squares) in bioreactors inoculated with Paecilomyces AF001 (MPNs; Black) or Wickerhamomyces SE3 (CFUs; Gray). Error bars represent 95% confidence intervals for mean Paecilomyces AF001 MPNs or Wickerhamomyces SE3 CFUs (n=3). 28

FIG 2.3. Violin plot showing pH values of the aqueous phase in bioreactors inoculated with Paecilomyces AF001(Blue), Wickerhamomyces SE3 (Green), or controls (Tan) over time. Bold dashed lines represent the median (biological replicates n=3) while the nonbold dashed lines represent the data quartiles. Wider sections of this violin plot represent a higher probability that the data will have the corresponding value, while skinnier sections represent a lower probability. Asterisks indicate a significant difference between the pH of inoculated and uninoculated controls. 29

FIG 2.4. A. Violin plot showing corrosion rates in milliinches per year (MPY) of carbon steel coupons in bioreactors inoculated with Paecilomyces (Blue), Wickerhamomyces (Green), and uninoculated controls (Tan) over time. The bold dashed line represents the median (biological replicates n=3 and n=3 technical replicates) and nonbold dashed lines represent the data

quartiles. B. Violin plot showing total pitted area on carbon steel coupons from bioreactors inoculated with Paecilomyces (Blue), Wickerhamomyces (Green), and uninoculated controls (Tan). The bold dashed line represents the median (biological replicates n=3 and n=3 technical replicates) and nonbold dashed lines represent the data quartiles. C. Violin plot showing maximum pit depths on carbon steel coupons in uninoculated bioreactors (Tan) and bioreactors inoculated with Paecilomyces (Blue) and Wickerhamomyces (Green) over time. The bold dashed line represents the median (biological replicates n=3 and n=3 technical replicates) and nonbold dashed lines represent the data quartiles. 30

FIG 2.5. A. Violin plot showing pH values of the aqueous phases after incubation of carbon steel brads with Paecilomyces (Blue), Wickerhamomyces (Green) and uninoculated controls (Tan). The bold lines represent the median and the nonbold lines on the plots represent the data quartiles (biological replicates n=5). **B.** Violin plot showing corrosion rates of carbon steel brads in the organic phases, organic-aqueous interface, and aqueous phase after exposure to the fungal isolates. The bold lines represent the median and the nonbold lines on the plots represent the data quartiles (biological replicates n=5). 31

FIG 2.6. A. Violin plot showing total pitted area on carbon steel coupons (pits > 20µm below mean surface average) inoculated with Paecilomyces (Blue) compared to uninoculated controls (Tan). The bold line represents the medium of the data and the nonbold lines represent the data quartiles (biological replicates n=3). **B.** Violin plot showing maximum pit depths on carbon steel coupons in abiotic controls (Tan) and flasks inoculated with Paecilomyces (Blue) over 90 days. The bold line represents the median of the data and the nonbold lines represent the data quartiles (biological replicates n=3). 32

FIG 2.7. Surface depth profiles of carbon steel coupons exposed to the filamentous fungus Paecilomyces and uninoculated controls after 90 days. Biological replicates are show next to each other and depth was calculated from the highest point on the surface of the coupon representing 0 μm. The color scale bar represents depths in microns. The dashed bar represents where the interface was located on the coupons with the fuel phase above and the aqueous phase below. 33

FIG 2.8. Degradation of alkanes and FAME in B20 biodiesel by Wickerhamomyces and Paecilomyces after 7, 14 and 21 days of incubation. Conditions were replicated (biological replicates n=3) and the average remaining percent of the compound compared to abiotic controls is shown. The scale bar represents the percent of remaining compound compared to the unexposed control with white indicating no degradation and black indicating complete degradation. 34

FIG 3.1. PCA ordination of fuel samples based on n-alkane composition. Biodiesel (circles) and diesel (triangles) fuel samples from different geographical areas in the continental U.S. are represented with different colors with Central (Orange), Northwest (Green), Southeast (Blue), and Southwest (Purple). Blue vectors represent the different n-alkanes and their contribution to the separation of the fuel samples in this ordination space. 61

FIG 3.2. PCA ordination of fuel samples based on FAME composition. Biodiesel (circles) and diesel (triangles) fuel samples were from different bases are represented with different colors and the corresponding geographical location is indicated by Northwest, Southeast, Central, or Southwest. Blue vectors represent the different FAME components and their contribution to the separation of the fuel samples in this ordination space. Many FAME components had low

eigenvectors in this PCA, and their chemical names are excluded for simplicity; however, their vectors remain in this PCA to give a better overview of how fuel samples are separated. 62

FIG 3.3. Heatmap representing the relative abundance of bacterial populations in microbial communities from contaminated fuels. Relative abundance of 100% is represented by dark blue, while gray represents 0% of the reads. Samples are sorted by the dendrogram on the left y-axis, which was based on bacterial population similarity. Bacterial families are denoted along the x-axis and sample names are denoted on the right y-axis. Bacterial families with less than 5 sequences remaining after rarefication were removed from this heatmap for simplicity. 64

FIG 3.4. Heatmap representing the relative abundance of fungal populations in microbial communities from contaminated fuels. Relative abundance of 100% is represented by dark blue, while gray represents 0% of the reads. Samples are sorted by the dendrogram on the left y-axis, which was based on fungal population similarity. Fungal families are denoted along the x-axis and sample names are denoted on the right y-axis. Fungal families with less than 5 sequences remaining after rarefication were removed from this heatmap for simplicity. 65

FIG 3.5. Redundancy analysis (RDA) of the Hellinger-transformed bacterial populations constrained by the fuel composition. Bacterial families are denoted as red text. In this RDA the red crosses are bacterial families that still contribute to this ordination space, but not specifically named due to their central clustering indicating a low correlation coefficient. Fuel component variables are represented by blue vectors. Blue vectors lengths indicate the relative weight of a fuel component in the ordination. 67

FIG 3.6. Redundancy analysis (RDA) of the Hellinger-transformed fungal communities constrained by the fuel composition. Fungal families are denoted as red text. In this RDA the red crosses are fungal families that still contribute to this ordination space, but not specifically

named due to their central clustering indicating a low correlation coefficient. Fuel component variables are represented by blue vectors. Blue vectors lengths indicate the relative weight of a fuel component in the ordination. 74

FIG 3. 7. Growth curve of the fungal isolates Paecilomyces AF001 (Filled circles; Trichocomaceae) and Wickerhamomyces SE3 (Open circles; Debaryomycetaceae) when grown on palmitoleic acid methyl ester as a sole carbon and energy source. Error bars represent standard deviation for mean Paecilomyces AF001 or Wickerhamomyces SE3 (n=3). **B:** Growth curve of the fungal isolates Paecilomyces AF001 (Filled circles; Trichocomaceae) and Wickerhamomyces SE3 (Open circles; Debaryomycetaceae) when grown on pentadecanoic acid methyl ester as a sole carbon and energy source. Error bars represent standard deviation for mean Paecilomyces AF001 or Wickerhamomyces SE3 (biological replicates n=3). 80

FIG 3.8. A map on the U.S where fuel samples were obtained for this analysis. Due to DoD confidentiality a rough overview of where the fuel samples are shown representing different regions in the U.S. from the Southeast (Red), Northwest (Blue), Southwest (Brown), and Central (Green). Map generated from https://mapchart.net/usa.html. 86

FIG 4.1. Growth of Paecilomyces AF001 with on B5 ULSD (open circle) and B20 biodiesel (closed circle) as the sole carbon and energy source. Error bars represent standard deviation of mean MPNs (n=3). 107

FIG 4.2. Total biomass as dry weight of Paecilomyces AF001 during growth with B5 (open circle) or B20 (closed circle) as the sole carbon and energy source. The total volume filtered was 10 mL ASW and 40 mL fuel for a total volume of 50 mL with most of the biomass being localized at the interface. Error bars represent standard deviation of the mean of the biomass (mg) (n=3). 108

FIG 4.3. Lipase activity of Paecilomyces AF001 when grown on B5 (open circle) or B20 (closed circle) normalized to biomass collected at each timepoint. Data is presented as units of lipase per mg of dry biomass. Error bars represent standard deviations for each mean (biological replicates n=3). 109

FIG 4.4. Principal component analysis (PCA) of transcripts produced by Paecilomyces AF001 grown on B20 biodiesel or B5 ULSD. B20 samples are represented by circles. The day 14 B20 samples are represented by orange while the day 8 B20 samples are represented by green. B5 samples are represented by squares. The day 14 B5 samples are teal while the day 8 B5 samples are purple. 110

FIG 4.5. Quantification of transcripts per million (TPM) mapped to a monooxygenase (GO:0016705) with oxidoreductase activity that incorporates molecular oxygen into reduced donors. Boxplots represent bootstrap values (n=3) from each replicate's transcripts per million that map to the genome of Paecilomyces AF001..... 111

FIG 4.6. Quantification of transcripts per million (TPM) mapped to a dioxygenase (GO:0051213) with oxidoreductase activity that incorporates both atoms of molecular oxygen into reduced donors. Boxplots represent bootstrap values (n=3) from each replicate's transcripts per million that map to the genome of Paecilomyces AF001. 112

FIG 4.7. Quantification of transcripts per million (TPM) mapped to a lipase (GO:0052689) that is known to be involved with the catalysis of the hydrolysis of carboxylic ester bonds. Cultures grown in B20 (top) and B5 ULSD (B5, bottom) for 8 and 14 days. Boxplots represent bootstrap values (n=3) from each replicate's transcripts per million that map to the genome of Paecilomyces AF001. 113

FIG 4.8. Quantification of transcripts per million (TPM) that mapped to an acetyl transferase (GO:0006635) used in the beta-oxidation pathway of fatty acid. Samples are normalized to transcripts per million (TPM) reads for each sample. Boxplots represent bootstrap values (n=3) from each replicate transcripts per million that map to the genome of Paecilomyces AF001. .. 114

Abstract

Microbiological contamination in petroleum-based fuels has been exacerbated with the addition of fatty acid methyl esters to diesel fuels. Consequences of microbiological contamination of these fuels can lead to degraded fuels, fouling and clogging of infrastructure, and potentially lead to microbiologically influenced corrosion (MIC) from the formation of organic acids as these microbes metabolize the fuel components. Additionally, operators are typically unaware of any potential contamination in their fuel tanks as the formation of biofilms can interfere with current technology designed to alert them of ongoing problems. As part of this dissertation, the fungal isolates *Paecilomyces* AF001 and *Wickerhamomyces* SE3 were characterized as being capable of degrading B20 biodiesel and using it as the sole carbon and energy source. The metabolism of B20 biodiesel led to an acidification of the medium and caused an increase in pitting corrosion and generalized corrosion on carbon steel. Additionally, this research has provided evidence that corrosion risks in contaminated fuel storage tanks are greatest at the interface of the fuel and any water that becomes entrapped in the fuels.

Prior to this research, limited information was known about the microbiological communities in ultra-low sulfur diesel (ULSD) and B20 biodiesel. This research expands the knowledge of microbial communities in fouled fuels by analyzing contaminated fuels from 106 fuel tanks at 17 military bases across the continental U.S. This research has demonstrated the bacterial communities in contaminated fuels are far more diverse than fungal communities in fuels when they are present. When fungal contamination occurred in fuels it was primarily composed of the filamentous fungal family Trichocomaceae. Fuel composition of B5 ULSD and B20 biodiesel was determined and used to correlate microbial community families to the fuel components. The same problematic fungal isolates *Paecilomyces* AF001 and *Wickerhamomyces*

SE3 used to evaluate corrosion of carbon steel when grown on B20 were used to determine if the correlations predicted by RDA analysis were accurate. Trichocomaceae (representative isolate *Paecilomyces* AF001) had positive correlations with fuels containing more palmitoleic acid methyl ester and the fungal family Debaryomycetaceae (representative isolate *Wickerhamomyces* SE3) had a positive correlation with increases in pentadecanoic acid methyl esters in fuels. Both isolates were grown on these substrates to determine their ability to utilize them as a sole carbon and energy source. *Paecilomyces* AF001 was able to grow on palmitoleic acid methyl ester and was unable to grow on pentadecanoic acid methyl esters while *Wickerhamomyces* SE3 was able to grow on both substrates.

Fungal families are less diverse than bacterial families in contaminated fuels and were primarily present when contamination occurred. Due to this, the fungal family Trichocomaceae which was present at many contaminated fuel storage tanks, was selected for enzymatic and transcriptomic analyses on B5 ULSD and B20 biodiesel as the sole carbon and energy sources. *Paecilomyces* AF001, a member of the Trichocomaceae family, has already been shown to be able to utilize hydrocarbons and FAME (Fatty Acid Methyl Ester) components in fuels and leads to increased corrosion risks. Transcriptomics was done to see any differences in metabolic utilization of genes associated with the metabolism of hydrocarbons and FAME. *Paecilomyces* was able to grow on both B5 ULSD and B20 biodiesel. Transcripts associated with hydrocarbon degradation, such as mono and dioxygenases, were higher than those seen when this fungus grew in B20 biodiesel. Additionally, lipase activity and transcripts associated with lipase genes were observed in both fuel types; however, more lipase activity and transcripts were found when *Paecilomyces* AF001 was grown on B20 fuel instead of B5 ULSD. Understanding how *Paecilomyces* AF001 grows on different fuel types can lead to the development of biosensors

that can help operators detect contamination in their tanks sooner and hopefully lead to less costs associated with remediating contaminated tanks. Overall, this work has demonstrated that microbial contamination of B5 ULSD and B20 is a rampant problem across the U.S. This work has linked the filamentous fungus *Paecilomyces* AF001 to increased corrosion risks to carbon steel when grown on B20 biodiesel, demonstrated that the fungal family Trichocomaceae (representative isolate *Paecilomyces* AF001) is a predominant fouler when storage tanks are contaminated, and demonstrates that this organism transcribes different genes associated with fuel metabolism based on if this organism is grown on B5 ULSD or B20 biodiesel.

Chapter 1. Introduction

Assessing the Impact of Microorganisms Capable of Degrading Biodiesel and Diesel Fuel in Storage Tanks

Transportation energy demand in both the United States (U.S.) and the European Union (EU) is largely met by liquid hydrocarbon fuel consumption such as diesel. Demand for diesel has steadily increased from 2016-2021 except for 2020 due to the economic shut down at the onset of the COVID-19 pandemic (1, 2). Diesel fuel consumption in the U.S. transportation sector amounted to 3100 million barrels used daily in 2019 and accounted for 77% of the total U.S. distillate consumption (3). While diesel fuel is an established energy source in the transportation sector, it is a finite resource. To prepare for the inevitable depletion of diesel, entities such as the U.S. Department of Defense (DoD), the U.S. Environmental Protection Agency (EPA), and the EU have mandated increasing the use of renewable fuel substitutes such as biodiesel (4–6).

The U.S. EPA and EU require the use of desulfurized diesel fuel, (*i.e.,* fuels having less than 15 ppm and 10 ppm sulfur, respectively) which caused a loss of lubricity in diesel fuel due to the depletion of organosulfur compounds in the fuels (7, 8). To counteract this loss, suppliers have begun adding biodiesel, which has much greater lubricity. Ultra-low sulfur diesel, which contains up to 5% FAME (Fatty Acid Methyl Esters) in the U.S. and 7% FAME in the EU, is still considered to be "diesel", and is handled as such (9–11). While biodiesel does offer certain advantages over diesel fuel such as offsetting carbon emissions, improving lubricity of fuels, and is a renewable resource, it also comes with drawbacks such as crystallization in colder weather and greater susceptibility to microbial oxidation (12, 13). It is therefore imperative that we better

understand the risks associated with these fuel sources and how contamination could impact infrastructure engineered to contain these fuels.

Biodiesel is chemically different from petroleum diesel. It is commonly composed of FAME produced through a transesterification of fatty acids from plant, animal, or microbial feedstocks and methanol (14). Biodiesel is not typically used as a sole combustible energy source in engines due to engine modifications being needed for combustion. It is rather mixed in various blends with petroleum based ultra-low sulfur diesel (ULSD). The most common blend of biodiesel is B20 biodiesel which contains up to 20% biodiesel and 80% ULSD (9). The B20 biodiesel blend was chosen because it provides acceptable cold weather performance, increases in fuel lubricity relative to unmixed ULSD, and high materials compatibility (*e.g.* materials in fuel storage tanks and engines) that required little to no change in existing vehicles or infrastructure for use (15). Additionally, up to 5% biodiesel is regularly added to ULSD to improve the fuels lubricity (10). While the addition of biodiesel to B5 ULSD can have a net positive impact including the reduction in overall carbon emissions, microorganisms are also much more likely to oxidize biodiesel blends over petroleum based ULSD (16). This leads to the loss of fuel due to contamination, fouling, failure of infrastructure from biofilms, and ultimately leads to microbiologically influenced corrosion (MIC) through the generation of organic acids produced during the metabolism of FAME as well as forming oxygen corrosion cells on metallic surfaces (17–19). Microorganisms can also degrade hydrocarbons in petroleum based ULSD; however, since the addition of biodiesel to B5 ULSD, risks associated with storage and distribution of all fuels blended with even low concentrations of biodiesel have become more common (20).

To understand how both B20 biodiesel and B5 ULSD fuels are at risk of contamination by microorganisms and the consequence of this contamination to storage infrastructure, this dissertation examines two fungi that were isolated from contaminated B20 biodiesel. Numerous studies involving the degradation of diesel and biodiesel focused on anaerobic bacteria with minimal information outlining the risks associated with fungi degrading fuels in active fuel distribution systems (21–23). Our group has shown previously that microbiologically influenced corrosion occurred in operational B20 storage tanks and the primary contaminants appeared to be fungal. However, since these were operational systems, it was difficult to delineate what factors could have contributed to the observed corrosion such as fuel additions to storage tanks or mechanical agitation in the tanks caused by draining potential rainfall runoff (24). To link fungal isolates that degrade B20 biodiesel to microbiologically influenced corrosion in the field, I undertook a series of controlled lab-based experiments that demonstrated how these organisms degrade B20 biodiesel and the effects of their metabolism of fuel on increasing the risk of carbon steel corrosion, which is discussed in Chapter 2 (25).

I continued by exploring the geography of microbial communities in contaminated B20 biodiesel and diesel from across the United States. Previous work in the Stevenson lab focused on examining microbial contamination at two military bases in the US (26). However, I have expanded this work to include 17 military bases from across the continental U.S. from which 106 fuel samples. Fuels that were collected included B20 biodiesel and B5 ULSD. The microbial communities present were examined using small subunit ribosomal RNA gene (SSU rRNA gene) sequencing techniques. Available oxidizable substates impact microbial community structure and can influence bacterial community structure in B5 ULSD and B20 storage tanks (27). Next, I expanded our understanding of fuel composition on microbial community structure by

determining how overall concentrations of individual FAME and n-alkane components in both B20 and B5 ULSD correlate to both bacterial and fungal community structure using redundancy analyses (RDA). Correlations identified by this analysis were then tested *post hoc* with the fungal isolates introduced in Chapter 2 to confirm both the correlations observed in the RDA. By testing correlations between organisms known to enhance corrosion in fuel storage systems and how they selectively degrade fuel components, insights maybe provided to operators on what organisms they can expect to grow or be selected for based on fuel composition. This information could also be used to dictate which feedstocks are used for biodiesel to minimize contamination risks of fuel stored for longer terms.

Finally, I examined the transcriptional and enzymatic response of a common B20 fuel contaminant, *Paecilomyces* sp. AF001 when grown on B5 ULSD and B20 biodiesel. This fungus was chosen due to it being linked to fuel degradation, higher risks of corrosion when grown on B20 biodiesel, and that it is ubiquitous in storage tanks that have fungal contamination (24, 25). Finally, I provide a foundation for how *Paecilomyces* AF001 on fuel and which genes are actively transcribed during both germination and stationary phases. These insights will not only increase our understanding of how this organism grows on these fuels, but it can provide potential transcript targets and enzymes for the development of bioassays that can be deployed in storage tanks.

Microbiologically Influenced Corrosion (MIC) in Biodiesel and Diesel Fuel Systems

Microbiologically influenced corrosion (MIC) was first described in 1910 in a publication that identified corrosive actions of a bacterium on iron and steel (28). By 2010, the cost of corrosion was estimated to be approximately $1.8 trillion dollars annually and MIC was

estimated to account for 20% of these costs or $360 billion dollars (29, 30). MIC is the result of the microorganisms that are present and their activities, the chemical composition of the environment, as well as the type of material that is being exposed to the microbes and the environment. Microorganisms including bacteria, fungi, archaea, and microalgae can influence corrosion in a system either directly or indirectly through complex processes that include both abiotic and biotic factors (19). Abiotic and biotic factors can influence microbial communities, activities, or even the corrosion dynamics of the exposed material. Some common abiotic influencers of MIC include rainfall, temperature, oxygen concentration, pH, and passivating oxidation while biotic factors can include the production of extracellular polymeric substances (EPS), sulfide production, and organic acid production (31). Defining the contribution of MIC to corrosion is, therefore, very challenging.

In diesel and biodiesel systems, sulfide production by sulfate-reducing microorganisms have largely been attributed to increased corrosion risks of infrastructure (32–34). Some fungi such as *Aspergillus niger* have been described as having a role in microbiologically influenced corrosion, but different groups of bacteria and archaea such as sulfate-reducing bacteria (SRB), sulfate-oxidizing bacteria (SOB), iron-reducing bacteria (IRB), iron-oxidizing bacteria (IOB), and sulfate-reducing archaea (SRA) have largely been implicated in most MIC systems (35, 36). Diesel and biodiesel fuel contains a significant amount of dissolved oxygen and the headspace is comprised of air, therefore aerobic and facultative anaerobic microorganisms are able to establish themselves at the fuel and water interface in storage tanks and scavenge the oxygen that paves the way for anaerobic organisms to thrive below the interface (37, 38). Organic acid production from the metabolism of FAME and hydrocarbons is another mechanism that can increase the risk of MIC (39, 40). Organisms growing at the fuel:water interface can produce

thick biofilms that can limit the diffusion of organic acids products of metabolism, causing a localized drop in pH that can be 2 or 3 times lower than in the planktonic environment (38). Additionally, as biofilms form, they can produce oxygen corrosion cells which cause anaerobic environments beneath the biofilms (41). This can cause oxygen in the fuel and water outside of the biofilm to form an anode on the metallic surface underneath the biofilm and a cathode on the metallic surface away from the biofilm and can exacerbate corrosion. Acid localization and oxygen corrosion cells can cause increased risk of localized corrosion (i.e., pitting) that can lead to infrastructure failure more readily than generalized corrosion. The characterization of microbial metabolism that is active in these systems is important to identify which populations are contributing to MIC.

Investigating Microbial Communities in Fuel Systems

More than 99% of the 10^{12} microbial species are currently unknown aside from their molecular detection, and only a small fraction is culturable with current techniques (42, 43). This can make understanding microbial communities challenging in numerous environments including contaminated fuels. Advances in molecular biology have unlocked the ability to investigate microbial communities using culture-independent methods including denaturing and temperature gradient gel electrophoresis, terminal restriction fragment length polymorphisms, 16S and 18S rRNA gene clone libraries, and small subunit sequencing (44, 45). These tools have allowed scientists to learn more about the genetic diversity and community structures of microorganisms in many environments including fuels (24, 46, 47). Combining these approaches with transcriptomics, metabolomics, or single-cell genomics can provide even more information about how these microbes interact with the environment and each other.

New sequencing technologies have provided a treasure trove of otherwise inaccessible information about uncultured microorganisms, but these approaches also have their limitations. Sequencing techniques only reveal a single point in time of a microbial community independent of any of the intricate dynamics that could occur in the environment. The recovery of nucleic acids from a sample could be skewed based on the method of nucleotide extraction since not all cells maybe lysed (48). If not all cells are lysed in the extraction of the nucleotides, then microorganisms that are present in the community would not appear in the sequencing results. Additionally, PCR amplification of the 16S and 18S rRNA genes may not be equally efficient across all targets, which can also introduce bias in the subsequent data (49). Furthermore, SSU rRNA gene sequencing libraries and metagenomic analyses only provide relative abundances of populations within the broader microbial community in an environment, requiring further analyses to determine absolute microbial abundance. Quantitative PCR is one approach that can be used to estimate absolute abundances of microbial communities; however, it has been demonstrated that many bacterial and fungal species can have multiple copies of their rRNA genes, potentially skewing qPCR and even SSU amplicon libraries to suggest higher abundances of microorganisms than are present (50). It is therefore critical to marry molecular techniques with traditional microbiological techniques including isolation, quantification of viability, enzymatic assays, and microscopy to better understand microbial communities in fuels while understanding the limitations associated with each of the techniques.

Microbial Ecology in Fuel Storage Systems

Fuel storage tanks are complex environments and numerous factors influence the microorganisms present in contaminated tanks and their metabolic activities (FIG 1.1). Fuel storage tanks are open to the external environment through vents that allow hazardous vapors to

escape and compensate for fuel additions to storage tanks to avoid positive pressures in the tanks (38). The vents used to allow safe operation of storage tanks also allow influxes of oxygen and water into the tank, providing the opportunity for the proliferation of a complex community of microorganisms. Aerobic and facultative anaerobic organisms establish themselves at the interface between fuel and any water intrusion, scavenging available oxygen and allowing for anaerobic organisms to thrive in the bottom of tanks (38).

Symbiotic relationships may form between the microorganisms present in the fuel. *Nitrospirillium* and *Burkholderia* were found in contaminated B20 storage tanks. Some members of these genera can fix inorganic nitrogen, providing the microbial communities present with a fixed nitrogen source (24, 51, 52). It is also possible that organisms within each fuel storage tank actively compete for nutrients and resources in these tanks as there are limitations to oxygen availability in the tanks, oxidizable substrates, nutrient such as nitrogen and phosphorous especially at the fuel water interface (38). Filamentous fungi, such as *Paecilomyces* sp. AF001. can extend and branch their hyphae into the fuel allowing for a larger surface for nutrient absorption and transport these nutrients along its hyphae potentially allow it to outcompete other taxa and establish itself in these fuel systems more readily (53, 54). Microorganisms can also actively exclude one another through the production of antimicrobials or by actively modifying the chemical environment, for example, by producing acetic acid and causing a decrease in the environmental pH (55–57).

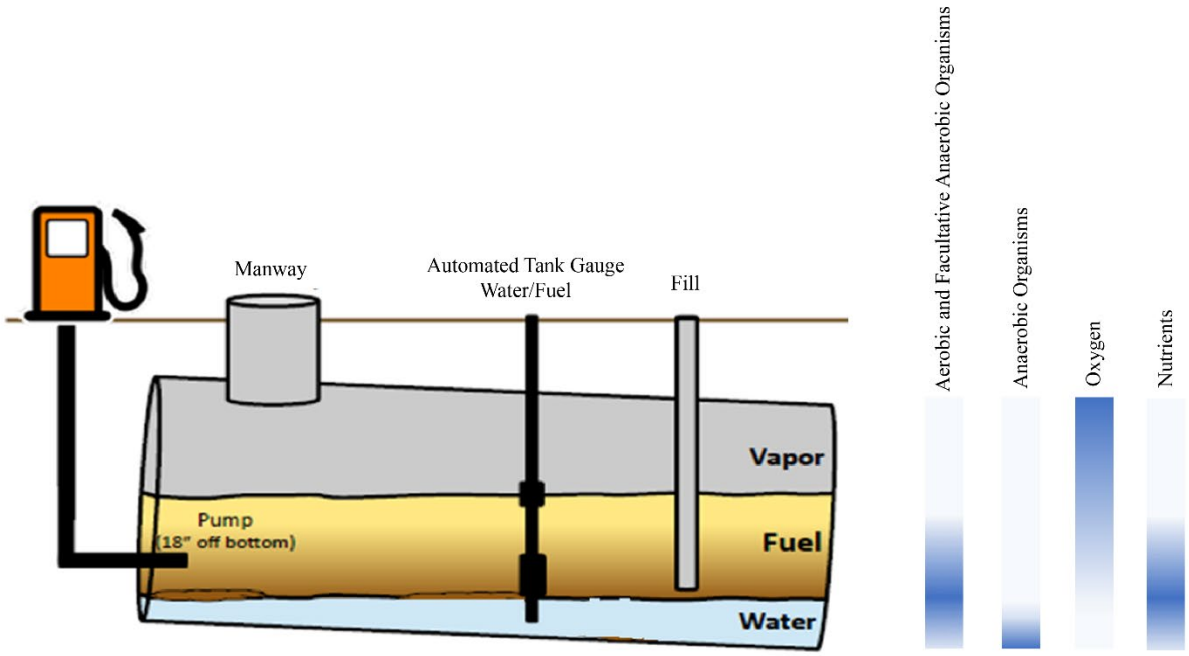

FIG 1.1 Illustration of an underground fuel storage tank showing the separation of vapor, fuel, and water phases. Gradients on the right demonstrate where the highest concentrations (Blue) of each category are found in these tanks (lowest concentrations White).

Aerobic microorganisms readily oxidize FAME and hydrocarbons in fuel using oxygen as a terminal electron acceptor (58). While FAMEs are a key component of biodiesel, they are also natural products and ubiquitous components inside cellular membranes. Due to the ubiquity of FAME, a vast number of microorganisms have the needed genetic machinery to oxidize them. Aerobic and anaerobic FAME metabolism both require de-esterification of a FAME molecule using a lipase (*i.e.,* esterase) producing a free fatty acid and methanol (58, 59). This free fatty acid then undergoes β-oxidation in which two carbon components are subsequently removed from the fatty acid chain producing 1 $FADH_2$, 1 NADH, and 1 acetyl-CoA per oxidation cycle (60). Additionally, hydrocarbons such as alkanes in fuels are readily oxidized by

microorganisms. Typically, aerobic degradation of n-alkanes proceeds by oxidizing the terminal methyl group producing a primary alcohol. This primary alcohol is then converted to an aldehyde using an alcohol dehydrogenase. The next step involves using an aldehyde dehydrogenase that converts the aldehyde to a fatty acid which will undergo β-oxidation (61). While oxidation of fatty acids is ubiquitous among microorganisms, activation of alkanes requires specific enzymes that are much less widespread. These enzymes belong to classes of enzymes termed monooxygenases, cytochrome P-450, and dioxygenases, and each enzyme has a preferred substrate length (61). Anaerobic microorganisms can degrade alkanes as well using many pathways including the subterminal addition to fumarate, intra-aerobic denitrification, and anaerobic hydroxylation. Ultimately the end products of these pathways result in the formation of a fatty acid that undergoes β-oxidation similarly to aerobic oxidation.

Scientific Contributions

In this dissertation I investigated how fungal isolates representative of those found commonly *in situ* degrade fuel components leading to an enhanced risk of corrosion. I also investigate microbial communities from contaminated fuel storage tanks across the U.S. and how these communities correlate to fuel components. Finally, I provide a foundation for understanding how the prominent fungal contaminant, *Paecilomyces* AF001, grows on diesel and biodiesel fuels. In Chapter 2, I hypothesized that the fungal contaminants *Paecilomyces* AF001 and *Wickerhamomyces* SE3 were able to metabolize B20 biodiesel leading to acidic byproducts that can exacerbate corrosion on carbon steel. Additionally, I sought to identify where corrosion risks are the highest in these tanks when these fungi are actively growing on B20 biodiesel as a sole carbon and energy source. In Chapter 3, I investigate different bacterial and fungal communities from over 100 fuel samples. I hypothesized that carbon substrates available in B20

biodiesel and B5 ULSD impacts both bacterial and fungal communities. To explore this hypothesis, modeling using redundancy analyses was conducted to determine correlations between bacterial and fungal communities and fuel components thereby paving the way to formulate fuels from feedstocks less prone to contamination by organisms known to cause MIC. Some of the correlations predicted by these RDA analyses were then tested to determine if the correlations had any validity with fungal isolates representing the prominent fouling families. Finally, in Chapter 4 I sought to better understand how the seemingly ubiquitous filamentous fungus *Paecilomyces* AF001 grows on both diesel and biodiesel fuels. I hypothesized that due to the increased concentration of FAME in B20 biodiesel compared to B5 ULSD the prominent fungal isolate *Paecilomyces* AF001 expresses more transcripts related to FAME degradation than hydrocarbon degradation. This research will provide us with a better understanding of how fungi grow in fuels and elucidate potential targets that can be used in future research to develop methods for earlier detection of contamination from this fungus.

Works Cited

1. U.S. Energy Information Administration. 2021. Short-Term Energy Outlook.

2. Fuels Europe. 2018. Statistical Report 2018.

3. U.S. Energy Information Administration. 2021 Diesel Fuel Explained Use of Diesel.

4. Department of Defense. 2016. 2016 Operational Energy Strategy.

5. U.S. Environmental Protection Agency. 2021. Final Renewable Fuel Standards for 2020, and the Biomass-Based Diesel Volume for 2021.

6. U.S. Department of Energy. 2021. Biodiesel Blend Mandate.

7. EUR-Lex. 2009. Directive 2009/30/EC of the European Parliament and of the Council Amending Directive 98/70/EC as Regards the Specification of Petrol, Diesel and Gas-Oil and Introducing a Mechanism to Monitor and Reduce Greenhouse Gas Emissions and Amending Council Directive 1999/32/EC as Regards the Specification of Fuel Used by Inland Waterway Vessels and Repealing Directive 93/12/EEC.

8. U.S. Environmental Protection Agency. 2021. Diesel Fuel Standards and Rulemakings.

9. Hazrat M, Rasul M, Procedia M. 2015. Lubricity Improvement of the Ultra-Low Sulfur Diesel Fuel with the Biodiesel. Energy Procedia 75:111-117.

10. U.S. Department of Energy. 2021 Alternative Fuels Data Center.

11. National Renewable Energy Laboratory (NREL). 2000. Biofuels for Sustainable Transportation.

12. Bücker F, Peralba M do, Bücker F, Camargo F de, Santestevan N, Bento F, Roesch L, Jacques RJ, Peralba M do, Camargo F de, Bento F. 2011. Impact of Biodiesel on Biodeterioration of Stored Brazilian Diesel Oil. Int Biodeterior Biodegradation 65:172-178.

13. Schleicher T, Werkmeister R, Russ W, Meyer-Pittroff R. 2009. Microbiological Stability of Biodiesel–Diesel-Mixtures. Bioresour Technol. 100:724-730.

14. U.S. Department of Energy. 2021. Alternative Fuels Data Center: Biodiesel Production and Distribution.

15. U.S. Department of Energy. 2021. Alternative Fuels Data Center: Diesel Vehicles Using Biodiesel.

16. Demirbaş A. 2009. Biodegradability of Biodiesel and Petrodiesel Fuels. Energy Sources Part A:169-174.

17. Videla H, Herrera LK. 2005. Microbiologically Influenced Corrosion: Looking to the Future. Int Microbiol. 8:169-180.

18. Szatmari I, Tudosie LM, Cojocaru A, Lingvay M, Prioteasa P, Visan T. 2015. Studies on Biocorrosion of Stainless Steel and Copper in Czapek Dox Medium with *Aspergilus niger* Filamentous Fungus. Chemistry and Materials Science 77:91-102.

19. Little BJ, Lee JS. 2014. Microbiologically Influenced Corrosion: an Update. Int Mater Rev 59:384–393.

20. Das N, Chandran P. 2011. Microbial Degradation of Petroleum Hydrocarbon Contaminants: An Overview. Biotechnology Res Int 2011:941810.

21. Telegdi J, Shaban A, Trif L. 2017. Trends in Oil and Gas Corrosion Research and Technologies. Part III Corros Mech Curr Knowl Gaps Futur Res 191–214.

22. Suflita JM, Aktas DF, Oldham AL, Perez-Ibarra BM, Duncan K. 2012. Molecular Tools to Track Bacteria Responsible for Fuel Deterioration and Microbiologically Influenced Corrosion. Biofouling 28:1003–1010.

23. Skovhus T, Eckert RB, Rodrigues E. 2017. Management and Control of Microbiologically Influenced Corrosion (MIC) in the Oil and Gas Industry—Overview and a North Sea Case Study. Journal Biotechnol 256:31–45.

24. Stamps BW, Bojanowski CL, Drake CA, Nunn HS, Lloyd PF, Floyd JG, Emmerich KA, Neal AR, Crookes-Goodson WJ, Stevenson BS. 2020. In situ Linkage of Fungal and Bacterial Proliferation to Microbiologically Influenced Corrosion in B20 Biodiesel Storage Tanks. Front Microbiol 11:167.

25. Floyd JG, Stamps BW, Goodson WJ, Stevenson BS. 2021. Locating and Quantifying Carbon Steel Corrosion Rates Linked to Fungal B20 Biodiesel Degradation. Appl Environ Microb AEM0117721.

26. Stamps BW. 2016. Measuring the Impact of Microbial Communities and their Proliferation in Engineered Ecosystems. University of Oklahoma Graduate College Dissertation.

27. Mitter EK, Germida JJ, Freitas JR de. 2021. Impact of Diesel and Biodiesel Contamination on Soil Microbial Community Activity and Structure. Sci Rep-uk 11:10856.

28. Gaines RH. 1910. Bacterial Activity as a Corrosive Influence in the Soil. J Industrial Eng Chem 2:128–130.

29. Hays GF. 2010. Now is the time. Advanced Materials Research 95:1-2.

30. Mansfield E, Sowards JW, Crookes-Goodson WJ. 2015. Findings and Recommendations from the NIST Workshop on Alternative Fuels and Materials: Biocorrosion. J Res Natl Inst Stan 120:28–36.

31. Usher K, Kaksonen A, Cole I, Marney D. 2014. Critical review: Microbially Influenced Corrosion of Buried Carbon Steel Pipes. Int Biodeter Biodegr 93:84-106.

32. Liang R, Aydin E, Borgne S, Sunner J, Duncan KE, Suflita JM. 2018. Anaerobic Biodegradation of Biofuels and Their Impact on the Corrosion of a Cu-Ni Alloy in Marine Environments. Chemosphere 195:427-436.

33. Aktas DF, Sorrell KR, Duncan KE, Wawrik B, Callaghan AV, Suflita JM. 2017. Anaerobic Hydrocarbon Biodegradation and Biocorrosion of Carbon Steel in Marine Environments: The Impact of Different Ultra-Low Sulfur Diesels and Bioaugmentation. Int Biodeter Biodegr 118:45–56.

34. Crombie DJ, Moody GJ, Thomas JDR. 1984. Corrosion of Mild Steel Under Diesel Oil by Sulphate-Reducing Bacteria. Mater Chem Phys 10:91–105.

35. Li Y, Xu D, Chen C, Li X, Jia R, Zhang D, Sand W, Wang F, Gu T. 2018. Anaerobic Microbiologically Influenced Corrosion Mechanisms Interpreted Using Bioenergetics and Bioelectrochemistry: A review. J Mater Sci Technol 34:1713–1718.

36. Lugauskas A, Prosycevas I, Ramanauskas R, Griguceviciene A, Selskiene A, Patstas V. 2009. The Influence of Micromycetes on the Corrosion Behaviour of Metals (Steel, Al) Under Conditions of the Environment Polluted with Organic Substances. J Environ Eng Landsc 21:199-208.

37. Passman FJ. 2013. Microbial Contamination and its Control in Fuels and Fuel Systems Since 1980–A Review. Int Biodeter Biodegr 81:88-104.

38. Passman F. 2003. Fuel and Fuel System Microbiology: Fundamentals, Diagnosis, and Contamination Control. American Society for Testing & Materials.

39. Peraza-Reyes L, Berteaux-Lecellier V. 2013. Peroxisomes and Sexual Development in Fungi. Front Physiol 4:244.

40. Bento F, Beech I, Gaylarde C, Englert GE, Muller IL. 2005. Degradation and Corrosive Activities of Fungi in a Diesel–Mild Steel–Aqueous system. World J Microbiol Biotechnology 21:135-142.

41. Dou W, Xu D, Gu T. 2021. Biocorrosion Caused by Microbial Biofilms is Ubiquitous Around us. Microb Biotechnol 14:803–805.

42. Locey KJ, Lennon JT. 2016. Scaling Laws Predict Global Microbial Diversity. Proc National Acad Sci 113:5970–5975.

43. Lloyd KG, Steen AD, Ladau J, Yin J, Crosby L. 2018. Phylogenetically Novel Uncultured Microbial Cells Dominate Earth Microbiomes. mSystems 3:5.

44. Marzorati M, Wittebolle L, Boon N, Daffonchio D, Verstraete W. 2008. How to get More Out of Molecular Fingerprints: Practical Tools for Microbial Ecology. Environ Microbiol 10:1571–1581.

45. Smets W, Leff JW, Bradford MA, McCulley RL, Lebeer S, Fierer N. 2016. A Method for Simultaneous Measurement of Soil Bacterial Abundances and Community Composition via 16S rRNA Gene Sequencing. Soil Biology Biochem 96:145–151.

46. Bodor A, Bounedjoum N, Vincze GE, Kis ÁE, Laczi K, Bende G, Szilágyi Á, Kovács T, Perei K, Rákhely G. 2020. Challenges of Unculturable Bacteria: Environmental Perspectives. Rev Environ Sci Bio Technology 19:1–22.

47. Chaudhary DK, Bajagain R, Jeong S-W, Kim J. 2021. Insights into the Biodegradation of Diesel Oil and Changes in Bacterial Communities in Diesel-Contaminated Soil as a Consequence of Various Soil Amendments. Chemosphere 285:131416.

48. Carrigg C, Rice O, Kavanagh S, Collins G, O'Flaherty V. 2007. DNA extraction method affects microbial community profiles from soils and sediment. Appl Microbiol Biot 77:955–964.

49. Head IM, Saunders JR, Pickup RW. 1998. Microbial Evolution, Diversity, and Ecology: A Decade of Ribosomal RNA Analysis of Uncultivated Microorganisms. Microbial Ecol 35:1–21.

50. Louca S, Doebeli M, Parfrey LW. 2018. Correcting for 16S rRNA Gene Copy Numbers in Microbiome Surveys Remains an Unsolved Problem. Microbiome 6:41.

51. Chung EJ, Park TS, Kim KH, Jeon CO, Lee H-I, Chang W-S, Aslam Z, Chung YR. 2015. *Nitrospirillum irinus* sp. nov., a Diazotrophic Bacterium Isolated from the Rhizosphere Soil of Iris and Emended Description of the Genus *Nitrospirillum*. Antonie Van Leeuwenhoek 108:721–729.

52. Santos PE-DL, Bustillos-Cristales R, Caballero-Mellado J. 2001. *Burkholderia*, a Genus Rich in Plant-Associated Nitrogen Fixers with Wide Environmental and Geographic Distribution. Appl Environ Microb 67:2790–2798.

53. Miller RB, Sadek A, Crouch AL, Floyd JG, Drake CA, Stevenson BS, Crookes-Goodson W, Monty CN, Senko JM. 2020. Novel Mechanism of Microbially Induced Carbon Steel Corrosion at an Aqueous/Non-aqueous Interface. Ind Eng Chem Res 59:15784–15790.

54. Künzler M. 2018. How Fungi Defend Themselves Against Microbial Competitors and Animal Predators. Plos Pathog 14:e1007184.

55. Kotzekidou P. 2014. Encyclopedia of Food Microbiology (Second Edition). Article Titles: B 344–350.

56. Demain AL, Martens E. 2017. Production of Valuable Compounds by Molds and Yeasts. J Antibiotics 70:347–360.

57. Gomes RJ, Borges M, Rosa M, Gomez RJH, Spinosa WA. 2018. Acetic Acid Bacteria in the Food Industry: Systematics, Characteristics and Applications. Food Technol Biotech 56:139–151.

58. Thomas A, Leahy M, Smith JWN, Spence MJ. 2017. Natural Attenuation of Fatty Acid Methyl Esters (FAME) in Soil and Groundwater. Q J Eng Geol Hydroge 50:301-317.

59. Sousa DZ, Pereira MA, Stams AJM, Alves MM, Smidt H. 2006. Microbial Communities Involved in Anaerobic Degradation of Unsaturated or Saturated Long-Chain Fatty Acids. Appl Environ Microb 73:1054–1064.

60. Kumari A. 2018. Chapter 4 – Beta Oxidation of Fatty Acids. *In* Sweet Biochemistry Remembering Structures, Cycles, and Pathways.

61. Rojo F. 2010. Enzymes for Aerobic Degradation of Alkanes, p 781-797. In Timmis KN (eds), Handbook of hydrocarbon and lipid microbiology, Springer, Berlin, Heidelberg.

Chapter 2. Locating and Quantifying Carbon Steel Corrosion Rates Linked to Fungal B20 Biodiesel Degradation

James G. Floyd[1], Blake W. Stamps[2,3], Wendy J. Goodson[4], Bradley S. Stevenson[1]

1 – University of Oklahoma, Department of Microbiology and Plant Biology, Norman OK

2 – 711th Human Performance Wing, Airman Systems Directorate, Air Force Research Laboratory, Wright-Patterson AFB, OH, United States

3 – UES Inc., Integrative Health and Performance Sciences Division, Dayton, OH, United States

4 – Soft Matter Material Branch, Materials and Manufacturing Directorate, Air Force Research Laboratory, Wright-Patterson AFB, OH

Key Words: Biocorrosion, Fungi, B20 Biodiesel, Biodegradation, Carbon Steel, Pitting Corrosion, Surface Analysis.

Foreword

Determining the ability of *Paecilomyces* AF001 and *Wickerhamomyces* SE3 to degrade biodiesel and lead to increased corrosion risks was part a collaborative effort between Bradley Stevenson's lab and the Air Force Research Labs. I performed the ITS phylogenetic analyses, performed corrosion experiments, determined degraded fuel components, gathered data, conducted statistical analyses, generated figures, and wrote the manuscript. Dr. Blake Stamps aided in writing the manuscript as well as provided the foundation for the evaluation of these two fungal isolates. Dr. Wendy Goodson aided in obtaining contaminated fuel samples in which the fungal isolates were obtained as well as provided feedback on experimental design as well as manuscript aid. Bradley Stevenson aided in the writing and editing of the manuscript, the experimental design, sampling the contaminated fuels in which these fungal isolates were obtained, and in data analysis. This manuscript was published in Applied Environmental Microbiology (doi: 10.1128/AEM.01177-21)

Abstract

Fungi that degrade B20 biodiesel in storage tanks have also been linked to microbiologically influenced corrosion (MIC). A member of the filamentous fungal genus *Paecilomyces*, and a yeast from the genus *Wickerhamomyces* were isolated from heavily contaminated B20 storage tanks from multiple Air Force bases. Although these taxa were linked to microbiologically influenced corrosion *in situ*, precise measurement of their corrosion rates and pitting severity on carbon steel was not available. In the experiments described here, we directly link fungal growth on B20 biodiesel to higher corrosion rates and pitting corrosion of carbon steel under controlled conditions. When these fungi were growing solely on B20 biodiesel for carbon and energy, consumption of FAME and n-alkanes was observed. The corrosion rates for both fungi were highest at the interface between the B20 biodiesel and the aqueous medium, where they acidified the medium and produced deeper pits than abiotic controls. *Paecilomyces* produced the most corrosion of carbon steel and produced the greatest pitting damage. This study characterizes and quantifies the corrosion of carbon steel by fungi that are common in fouled B20 biodiesel through their metabolism of the fuel, providing valuable insight for assessing MIC associated with storage and dispensing B20 biodiesel.

Importance

Biodiesel is widely used across the United States and worldwide, blended with ultralow sulfur diesel in various concentrations. In this study we were able to demonstrate that the filamentous fungi *Paecilomyces* AF001 and the yeast *Wickerhamomyces* SE3 were able to degrade fatty acid methyl esters and alkanes in biodiesel causing increases in acidity. Both fungi also accelerated the corrosion of carbon steel, especially at the interface of the fuel and water, where their biofilms were located. This research provides controlled, quantified measurements

and the localization of microbiologically influenced corrosion caused by common fungal contaminants in biodiesel fuels.

Introduction

Biodiesel production within the United States (U.S.) greatly expanded in response to high petroleum prices and an increased need for energy security after the September 11, 2001 terrorist attacks (1, 2). Over two decades afterwards, world biodiesel consumption has continued to increase, reaching 9.3 billion gallons in 56 countries in 2016 (3). Consumption in the U.S. increased from 322 million gallons annually in 2009 to 1.8 billion gallons in 2019 (4). The U.S. increase in biodiesel consumption was largely driven by an increased interest in energy security but there are other advantages to its use. When biodiesel is blended with or used as an additive to ultra-low sulfur diesel (less than 15 ppm sulfur; ULSD), fuel lubricity is restored and emissions of carbon and particulates are partially offset (5, 6). The increased energy independence and fuel performance resulted in widespread adoption of biodiesel blends worldwide. The largest energy consumer in the U.S., the United States Department of Defense (DoD), sought to diversify its energy supplies to reduce fuel security risk through the use of renewable fuels that don't require any changes in existing infrastructure or engines to replace unblended fuels such as ULSD (7). The United States Air Force (USAF), a service within the DoD, rapidly implemented the use of a drop-in fuel in the form of a 20% first-generation biodiesel blend (B20) in non-tactical ground vehicles and equipment. B20 is composed of a 20:80 volume/volume blend of fatty acid methyl esters (*i.e.* FAME biodiesel) and ULSD, which is compatible with existing engines and storage infrastructure (8). The FAME used as biodiesel is a renewable resource produced through an esterification reaction with animal and plant triglycerides and methanol (9). However, the advantages that adoption of B20 represent are tempered by potential limitations.

Biodiesel is more hygroscopic and oxidatively unstable compared to petroleum-based diesel, making fuels containing biodiesel more susceptible to microbiological degradation (10). This is especially true during long term storage as microorganisms can readily degrade the FAME in B20 (11). The half-life of the FAME in B20, as well as C7 to C20 alkanes were 2.1 to 2.8 days in aqueous microcosm experiments, suggesting that both the FAME and alkanes in biodiesel blends are viable oxidizable substrate for microbial growth (12). The biodegradation of FAME is carried out through the β-oxidation pathway, which involves the sequential removal of two-carbon components and production of acetic acid. Acetic acid can then be converted to acetyl-CoA and used in the Krebs cycle or exported from the microbial cell (13–15). Methanol produced from the de-esterification of FAME is readily metabolized by acid-tolerant fungi and bacteria (16). The aliphatic alkanes in B20 are also readily degraded by both fungi and bacteria suggesting that the oxidation of B20 under aerobic conditions is highly favorable (17, 18). Under aerobic conditions alkanes are oxidized by alkane monooxygenases producing a fatty acid that is shuttled into the β-oxidation pathway, producing additional acetic acid (19). Free fatty acids and acidic byproducts produced from the metabolism of many of the components of B20 fuel can acidify both the fuel and any water present within the storage tank, inducing or accelerating corrosion, leading to damaged vehicles and storage infrastructure.

Corrosion directly or indirectly caused by microorganisms is known as microbiologically influenced corrosion, or MIC. Annually, corrosion costs an estimated 2.5 trillion dollars worldwide, up to 20% of which is attributed to MIC (20). MIC occurs on material surfaces, where microorganisms attach and form biofilms. Biofilms affect the physical and chemical environment of metallic surfaces, impacting the kinetics of cathodic or anodic reactions (21, 22). Microorganisms in biofilms can also secrete enzymes that attack metals, increase local acidity,

create differential aeration, and form galvanic cells which accelerate corrosion under otherwise aerobic conditions (23).

Fungi can increase corrosion rates of mild steel when grown on ULSD as a sole carbon and energy source (24). Fungi grow more rapidly and produce more biomass on the FAME in biodiesel blends than ULSD, which could lead to a greater corrosion risk to infrastructure storing or dispensing fuels containing biodiesel (25). Filamentous fungi such as *Penicillium* and *Aspergillus* increase the rate of steel corrosion when degrading diesel fuel (26). It was speculated that the increased steel corrosion rates from these fungi degrading diesel were likely attributed to increased oxygen concentrations in the medium caused by degrading benzene rings and aliphatic hydrocarbons to (-O-CH_2-). The authors also acknowledged that these organisms were likely producing organic acids that could also play a role in the increased corrosion risk. Additionally, studies have shown that fungi contaminating biodiesel storage tanks in Brazil were able to degrade fuels containing 5%, 10%, 20% and 100% biodiesel (25). Although they did not measure corrosion during their investigation, the authors did note that as fungi degraded these fuels, there was an increase in acidity that could impact corrosion risks. There is a critical need to provide quantified rates and measurements of how fungi can degrade fuels, such as B20, and subsequently contribute to MIC in critical fuel storage infrastructure.

When the USAF started using B20 to meet mandated energy requirements, problems quickly arose (27). Numerous USAF bases reported particulates in the fuel from B20 storage tanks and fouled filters on dispensers (28). Subsequent *in-situ* analysis of corrosion confirmed that tanks with obvious fungal contamination had significant pitting corrosion relative to controls. These storage tanks being monitored were still in operation making it difficult to control for other factors that might have contributed to the perceived increase in corrosion risk.

Herein we describe the isolation of organisms responsible for fouling contaminated B20 storage tanks and directly link them to fuel degradation and increased corrosion risks. To address our lack of a direct causative link between the previously identified fungal taxa within USAF B20 tanks and their ability to both increase corrosion rates of carbon steel and degrade B20, members of the abundant taxa *Paecilomyces* and *Wickerhamomyces,* were isolated. These isolates were used to determine their ability to metabolize B20 biodiesel and spatially induce corrosion of carbon steel.

Results

Characterization and Phylogenetic Identification of Fungi Isolated from B20 Biodiesel

The fungal ITS sequences that were sequenced suggested that the filamentous fungal isolate was most closely related to *Byssochlamys nivea* (FIG 2.1A) and the yeast isolate was most closely related to *Wickerhamomyces anomalus* (FIG 2.1B). Although identification of our *Paecilomyces* AF001 isolate is more closely related to *Byssochlamys nivea* (AY53338.1), recent taxonomic changes have caused the genus *Byssochlamys* to be reclassified as *Paecilomyces* (56).

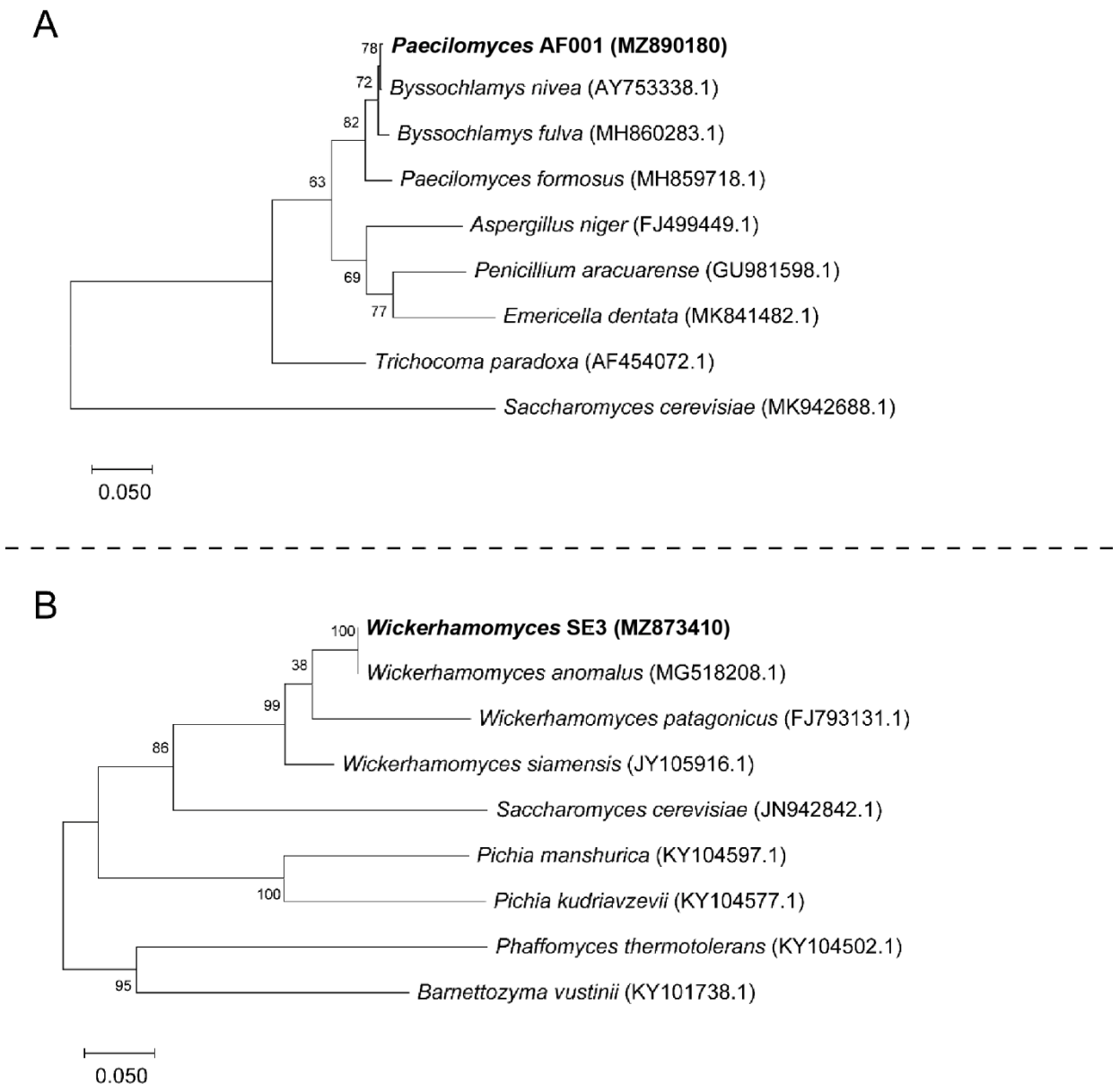

FIG 2.1. Maximum likelihood tree based on ITS sequence similarity among close phylogenetic relatives (NCBI accession numbers in parentheses) of the *Paecilomyces* sp. AF001 (A) and *Wickerhamomyces* SE3 (B) isolates. Bootstrap values above 50 percent for 500 samples are shown at relevant nodes

Fungal Growth in Bioreactors

Paecilomyces AF001 and *Wickerhamomyces* SE3 were presumably in lag phase and had no apparent growth during the first 7 days in the bioreactors. However, after 14 days the MPN of *Paecilomyces* on the surface of the carbon steel witness coupons had increased over an order of

magnitude, the density of *Wickerhamomyces* on the coupon surfaces and the liquid medium had increased in a similar fashion based on CFUs (FIG 2.2).

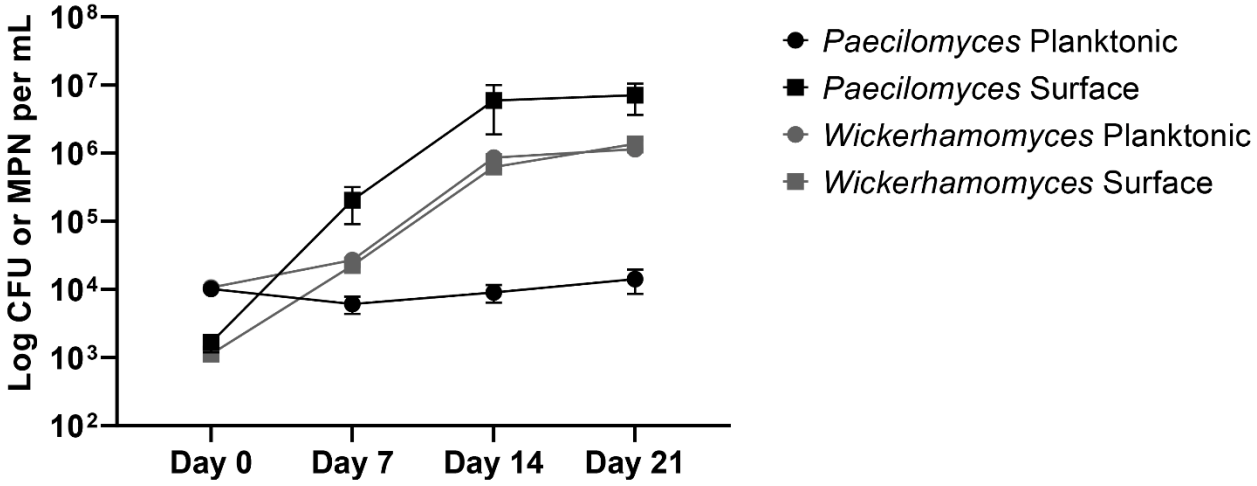

FIG 2.2. Density of planktonic populations (circles) and biofilms (squares) in bioreactors inoculated with *Paecilomyces* AF001 (MPNs; Black) or *Wickerhamomyces* SE3 (CFUs; Gray). Error bars represent 95% confidence intervals for mean *Paecilomyces* AF001 MPNs or Wickerhamomyces SE3 CFUs (n=3).

Acidification of Aqueous Medium

When *Paecilomyces* sp. AF001 and *Wickerhamomyces* sp. SE3 were grown on B20 biodiesel as the sole carbon and energy source, the pH of the aqueous phase did not decrease significantly after 7 days relative to abiotic controls (FIG 2.3). By day 14 and 21 both fungal isolates significantly reduced ($p < 0.05$) the pH of the medium by two or more orders of magnitude compared to the abiotic controls at those times. The *Paecilomyces* isolate was responsible for the greatest reduction in pH to a mean of 4.33 ± 0.31 in the aqueous phase after 21 days. The *Wickerhamomyces* isolate decreased the aqueous pH to a mean of 5.37 ± 0.21 after 21 days.

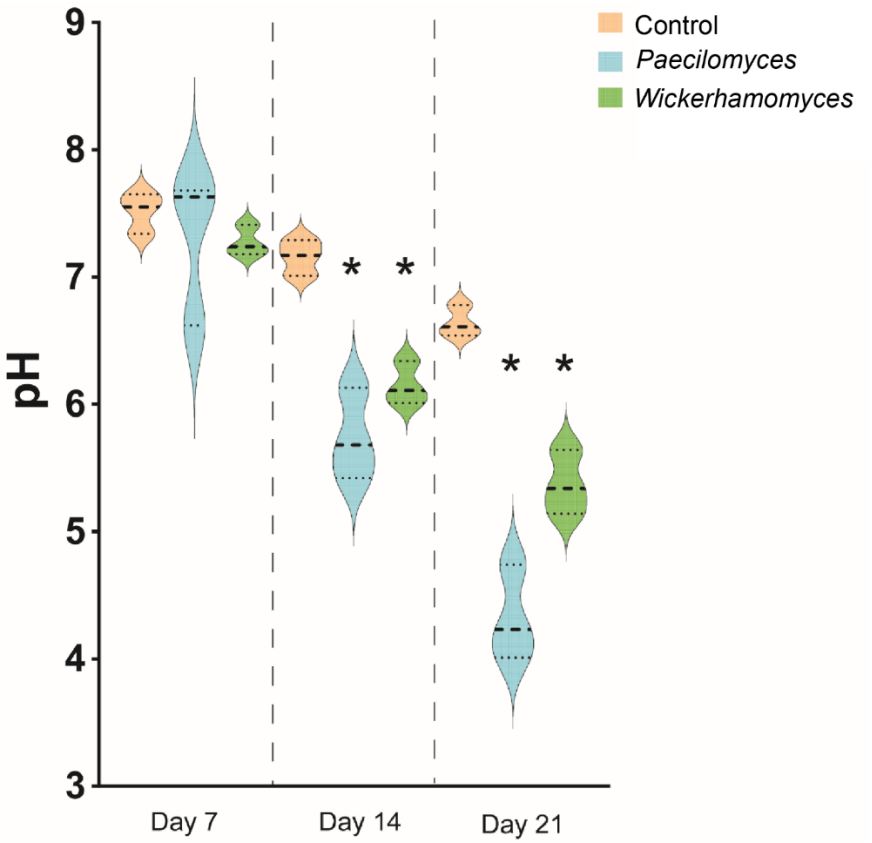

FIG 2.3. Violin plot showing pH values of the aqueous phase in bioreactors inoculated with *Paecilomyces* AF001(Blue), *Wickerhamomyces* SE3 (Green), or controls (Tan) over time. Bold dashed lines represent the median (biological replicates n=3) while the nonbold dashed lines represent the data quartiles. Wider sections of this violin plot represent a higher probability that the data will have the corresponding value, while skinnier sections represent a lower probability. Asterisks indicate a significant difference between the pH of inoculated and uninoculated controls.

Direct Measurement of Corrosion

Corrosion rates (Mils Per Year; MPY) of the carbon steel coupons by each isolate were not significantly different than abiotic controls after 7 and 14 days (FIG 2.4A). After 21 days, incubations with the *Paecilomyces* isolate had significantly greater ($p < 0.05$) corrosion rates compared to abiotic controls. *Wickerhamomyces* SE3 did not produce significantly higher corrosion rates when compared to abiotic controls. The total area pitted of the metal coupons was significantly higher than that of abiotic controls only in bioreactors inoculated with *Paecilomyces*

after 14 and 21 days ($p < 0.05$) (FIG 2.4B). The greatest pit depth recorded for all *Paecilomyces* cultures was 132.7 µm whereas the maximum pit depth recorded for all *Wickerhamomyces* SE3 reactors was 90.7 µm (FIG 2.4C).

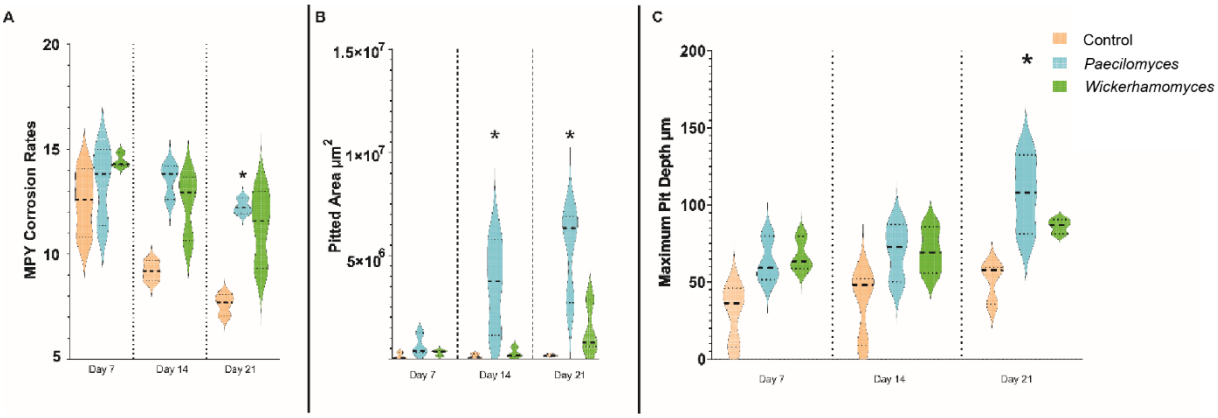

FIG 2.4. A. Violin plot showing corrosion rates in milliinches per year (MPY) of carbon steel coupons in bioreactors inoculated with *Paecilomyces* (Blue), *Wickerhamomyces* (Green), and uninoculated controls (Tan) over time. The bold dashed line represents the median (biological replicates n=3 and n=3 technical replicates) and nonbold dashed lines represent the data quartiles. B. Violin plot showing total pitted area on carbon steel coupons from bioreactors inoculated with *Paecilomyces* (Blue), *Wickerhamomyces* (Green), and uninoculated controls (Tan). The bold dashed line represents the median (biological replicates n=3 and n=3 technical replicates) and nonbold dashed lines represent the data quartiles. C. Violin plot showing maximum pit depths on carbon steel coupons in uninoculated bioreactors (Tan) and bioreactors inoculated with *Paecilomyces* (Blue) and *Wickerhamomyces* (Green) over time. The bold dashed line represents the median (biological replicates n=3 and n=3 technical replicates) and nonbold dashed lines represent the data quartiles.

Colocation of Biology and Corrosion

In static cultures the pH of the aqueous phase was significantly lower ($p < 0.05$) for both *Paecilomyces* and *Wickerhamomyces* compared to abiotic controls after 21 days of incubation (FIG 2.5A). Corrosion rates were lowest in the organic (fuel) phase and elevated in both the aqueous phase (ASW) and at the interface of fuel and medium (FIG 2.5B). Corrosion rates in the fuel phase were significantly higher than abiotic controls ($p<0.05$), six times greater in cultures inoculated with *Paecilomyces* relative to uninoculated controls. In cultures inoculated with

Wickerhamomyces, corrosion rates were not significantly different ($p > 0.05$) from controls in the fuel phase. Corrosion rates at the fuel/medium interface and in the growth medium were significantly higher for both *Paecilomyces* and *Wickerhamomyces* relative to abiotic controls ($p < 0.05$). The greatest corrosion rates (2.1 ± 0.23 MPY *Paecilomyces* and 1.8 ± 0.36 MPY *Wickerhamomyces*) were observed at the fuel/medium interface.

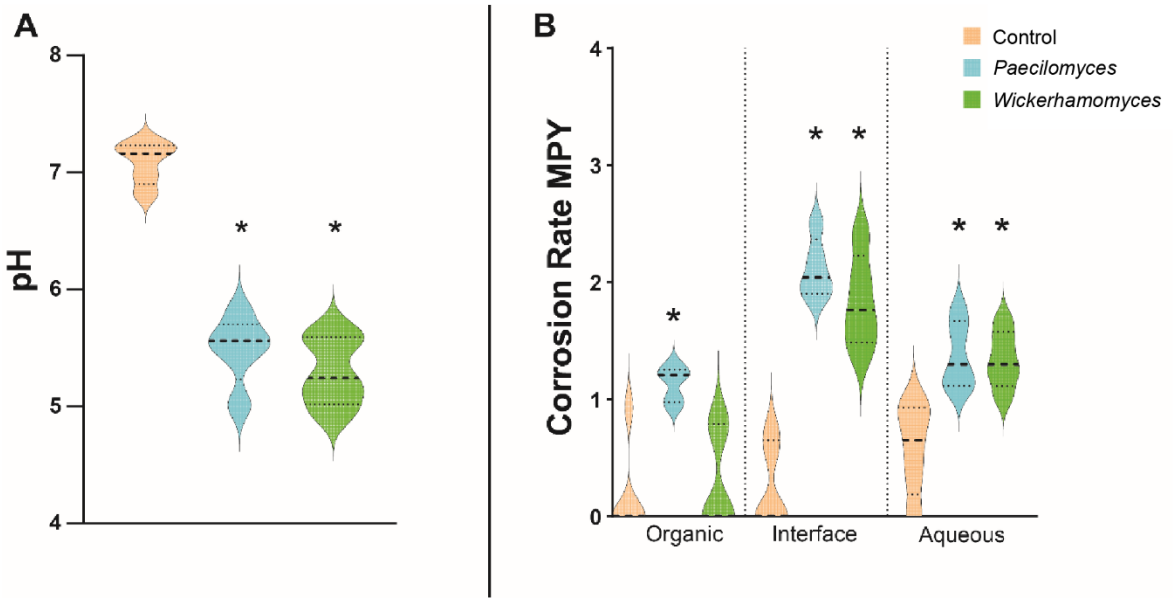

FIG 2.5. A. Violin plot showing pH values of the aqueous phases after incubation of carbon steel brads with *Paecilomyces* (Blue), *Wickerhamomyces* (Green) and uninoculated controls (Tan). The bold lines represent the median and the nonbold lines on the plots represent the data quartiles (biological replicates n=5). **B.** Violin plot showing corrosion rates of carbon steel brads in the organic phases, organic-aqueous interface, and aqueous phase after exposure to the fungal isolates. The bold lines represent the median and the nonbold lines on the plots represent the data quartiles (biological replicates n=5).

Paecilomyces produced more and deeper pitting corrosion at the fuel/medium interface compared to the uninoculated control (FIG 2.6 & 2.7). Both general corrosion rates produced from these fungi growing on B20 biodiesel can be classified as a moderate corrosion risk according to the NACE standards (29).

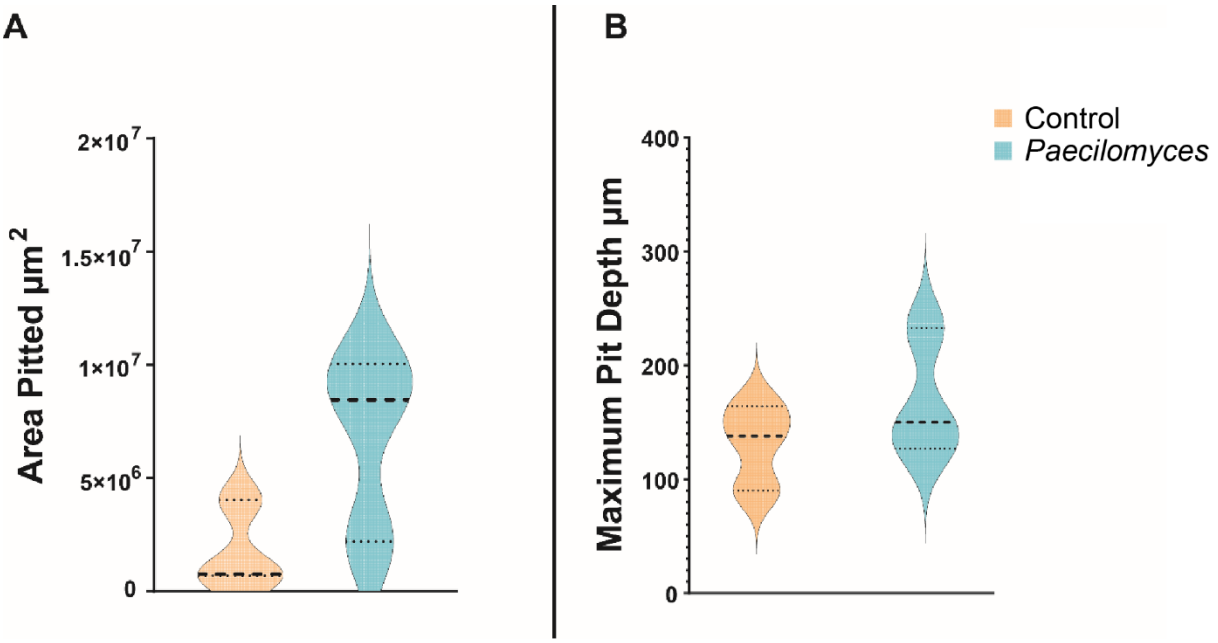

FIG 2.6. A. Violin plot showing total pitted area on carbon steel coupons (pits > 20µm below mean surface average) inoculated with *Paecilomyces* (Blue) compared to uninoculated controls (Tan). The bold line represents the medium of the data and the nonbold lines represent the data quartiles (biological replicates n=3). **B.** Violin plot showing maximum pit depths on carbon steel coupons in abiotic controls (Tan) and flasks inoculated with Paecilomyces (Blue) over 90 days. The bold line represents the median of the data and the nonbold lines represent the data quartiles (biological replicates n=3).

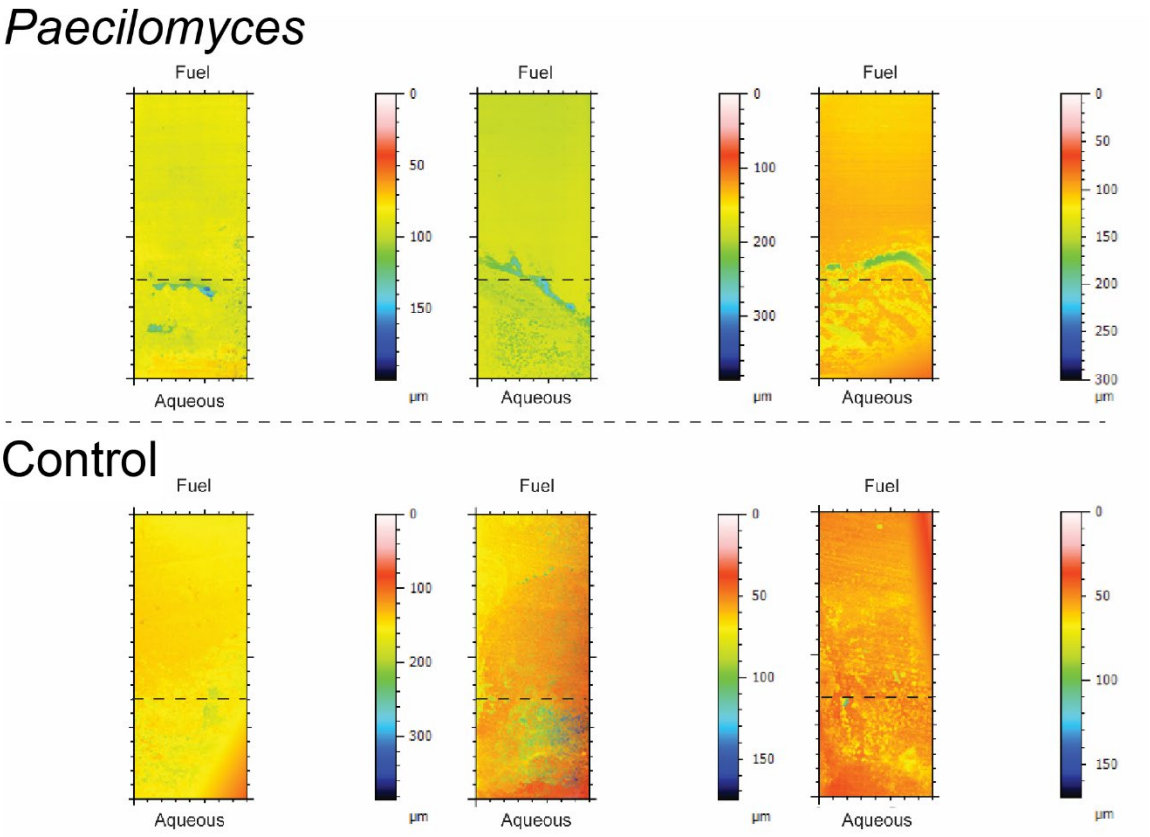

FIG 2.7. Surface depth profiles of carbon steel coupons exposed to the filamentous fungus Paecilomyces and uninoculated controls after 90 days. Biological replicates are show next to each other and depth was calculated from the highest point on the surface of the coupon representing 0 µm. The color scale bar represents depths in microns. The dashed bar represents where the interface was located on the coupons with the fuel phase above and the aqueous phase below.

Fuel Degradation

Both *Paecilomyces* and *Wickerhamomyces* were capable of growth in B20, metabolizing FAME and alkane components of the fuel. As a result, the peak area of all detectable FAME components and alkanes decreased over time in *Paecilomyces* and *Wickerhamomyces* cultures (FIG 2.8). Compared to uninoculated controls, both *Paecilomyces* and *Wickerhamomyces* cultures metabolized greater than 50 % of the Cis-9-Oleic Acid Methyl Ester by day 21. Both fungi decreased the concentration of Cis-9-Oleic Acid Methyl Ester more than any other fuel component after 21 days (measured as peak area). Analysis of the uninoculated controls over the

21 days showed evaporation of fuel components with approximately 15% reduction in the components compared to the unexposed fuel.

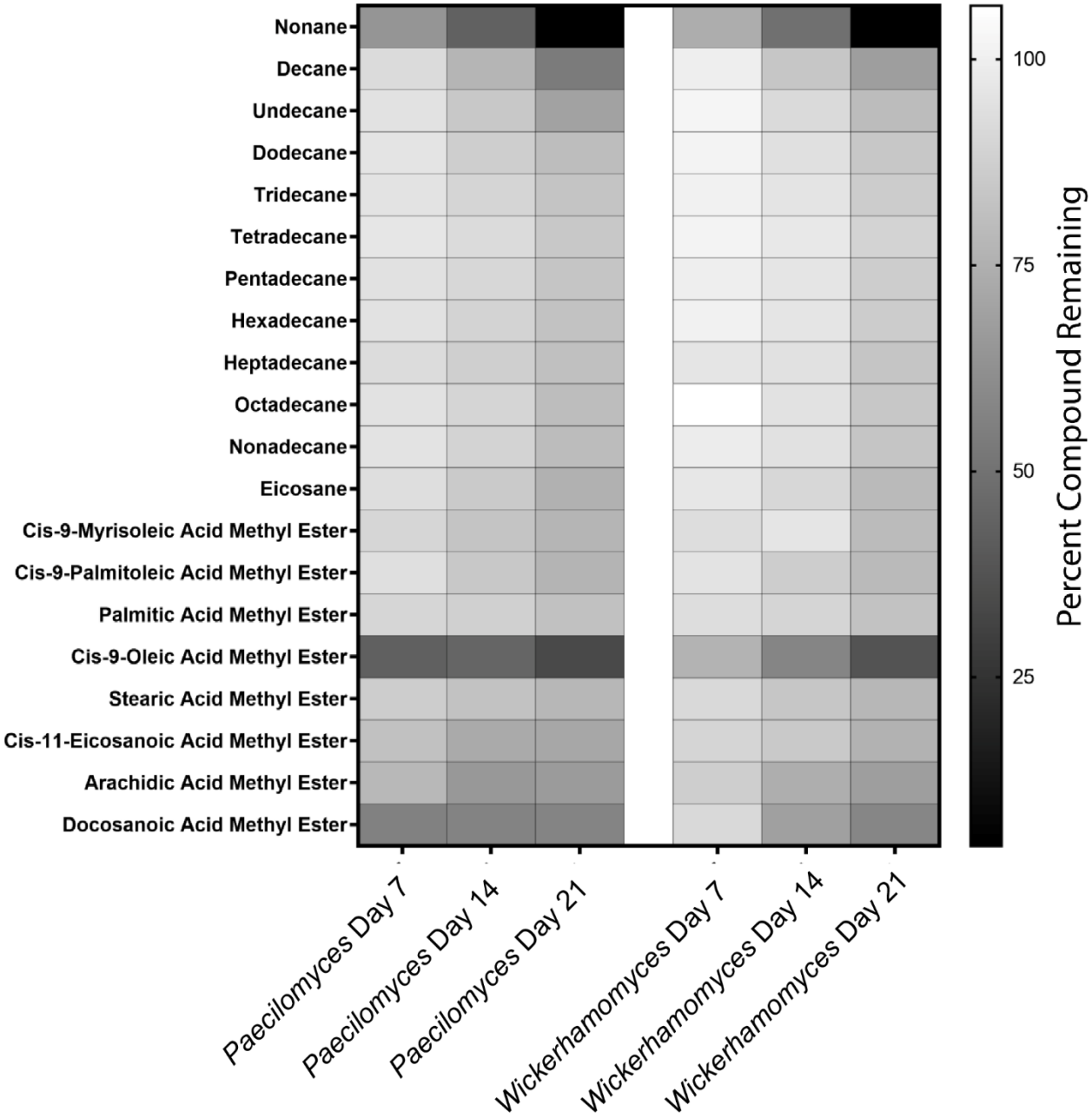

FIG 2.8. Degradation of alkanes and FAME in B20 biodiesel by Wickerhamomyces and Paecilomyces after 7, 14 and 21 days of incubation. Conditions were replicated (biological replicates n=3) and the average remaining percent of the compound compared to abiotic controls is shown. The scale bar represents the percent of remaining compound compared to the

unexposed control with white indicating no degradation and black indicating complete degradation.

Discussion

Complex interactions between microorganisms, fuels, and metallic surfaces *in situ* make it challenging to directly link the microbial degradation of biodiesel to corrosion (30). Isolation of the relevant microorganisms and controlled laboratory experimentation is critical to linking microbial growth and metabolic activity to the corrosion of infrastructure. Both fungi isolated and identified in this study, *Paecilomyces* AF001 and *Wickerhamomyces* SE3*,* represented some of the most abundant fungi identified in a longitudinal study of microbial contamination and microbiologically influenced corrosion in B20 storage tanks (28). We measured the ability of these organisms to both degrade B20 and accelerate corrosion of carbon steel in controlled laboratory experiments. The co-location of microbial biomass and the greatest amount of corrosion at the interface of fuel and water provided a clear link of where the potential for corrosion would be highest in storage tanks, enhancing our ability to more specifically target regions of fuel tanks for mitigation and increasing the chance of early detection of MIC.

Two fungi that were abundant in contaminated B20 fuel samples included a filamentous fungus, *Paecilomyces*, and a yeast, *Wickerhamomyces*. Both were capable of growth on B20 as a sole carbon and energy source by degrading the readily oxidizable FAME components of B20 and several of the alkanes within 21 days. Currently the U.S. DOE and the European Union authorizes the use of B5 and B7 respectively to be added to diesel fuels (31, 32). Our work suggests that even in fuels with low concentrations of FAME such as B5 or B7 (supposedly 'neat' ULSD) biofouling, microbiologically influenced corrosion, and fuel degradation can become more common as biodiesel is added to petroleum diesel.

Biodegradation of both hydrocarbons and FAME in biodiesel blends produces organic acids, which acidifies both the fuel and any aqueous environments, increasing the corrosion of carbon steel (33, 34). Both fungal isolates in this study could degrade alkanes and FAME in B20 biodiesel and appeared to degrade Cis-9-Oleic Acid Methyl Ester and Cis-11-Eicosonic Acid Methyl Ester more readily than the other compounds. Some studies have demonstrated that both fungi and bacteria can metabolize and incorporate unsaturated fatty acids much more rapidly than saturated fatty acids and has been attributed to linear fatty acids being less efficient in entering inside cells for metabolic processes (36, 37).

Biofilms can accelerate corrosion rates by creating localized, concentrated acidic conditions at metallic surfaces or by partitioning oxygen, generating oxygen corrosion cells. Both of these mechanisms increase “pitting” or localized corrosion (35). Surface analysis conducted by white light profilometry showed that pitting corrosion was more severe on coupons exposed to the filamentous fungus *Paecilomyces* AF001 compared to the yeast *Wickerhamomyces*. This difference could be due to the thick biofilms formed by the filamentous fungus. Other filamentous fungi such as *Aspergillus niger* form thick biofilms over steel surfaces, resulting in more pitting corrosion (38). After 21 days, *Paecilomyces* biofilms generated approximately 30-fold more pitted area than the abiotic controls, and 4 times more than on coupons exposed to the yeast *Wickerhamomyces*. The elevated corrosion observed in the *Paecilomyces* cultures confirms previous studies in USAF B20 storage tanks that suggested filamentous fungi contributed to MIC (28).

While we confirmed that both fungi were capable of MIC, materials did exhibit some surface passivation, or reduction in corrosion rates over time. During the corrosion experiments in the bioreactors and test tubes, iron oxide formation was noted during the duration of both

experiments. Corrosion rates decreased slightly over the course of the 21-day bioreactor experiment, possibly due to the formation of passivating iron oxides on the surface of the metal. This passivation could prevent further iron oxidation from occurring as rapidly as when neutral iron is exposed to the medium (39, 40). Corrosion rates plateaued over time similar to the corrosion dynamics that were observed *in situ* where *Paecilomyces* was the most abundant fungal population (28). Although overall corrosion rates decelerated over the course of 12 months, significantly more deep pits were detected, suggesting that long-term corrosion modeling remains challenging.

Both isolated fungi are capable of growth under oxic conditions, and most of the observable fungal and bacterial taxa identified *in situ* were either facultative anaerobes or known aerobic microorganisms (28). As the fungi grew, an obvious biofilm formed at the fuel:water interface. This growth could provide a physical niche in that the fungi could use the available oxygen in the fuel for metabolism while excluding other microorganisms from that space and define which organisms can grow in fuel storage tanks. Biodiesel and biodiesel blends (such as B20) contain more dissolved oxygen than ultra-low sulfur diesel (42). Aerobic metabolism at the fuel:water interface would deplete the oxygen present in the immediate environment, including the aqueous phase. Dissolved oxygen in the much larger volume of the fuel would be limited by diffusion into the aqueous phase, which would more than likely remain anoxic when contaminated with metabolizing microorganisms. The resulting oxygen concentration gradient would be most prominent at the interface of fuel and water where the fungi we isolated are actively growing within a fuel tank, generating an oxygenic corrosion cell and leading to exacerbated, aggressive pitting-type corrosion (41, 43).

Although correlative links between bacterial degradation of both fossil and bio- based fuels and corrosion are well established, the direct connection between fungal taxa and rates or types of corrosion is less developed (44–46). The controlled experiments in this study link active fungal metabolism to the aerobic degradation of B20, the production of biofilms at the fuel/water interface, and pitting corrosion. Future research will address how potential metabolic interactions between *Paecilomyces* and the bacterial populations might affect the rates of fuel degradation and corrosion. The FAME components of biodiesel are more amenable to biodegradation than petroleum-based hydrocarbons (FIG 2.8), suggesting persistent challenges in the long-term storage of biodiesel (47, 48). While we tested a 20% biodiesel blend, biodiesel is also present in ULSD in the U.S. at concentrations up to 5%; added to compensate for the loss of lubricity in diesel fuel from the removal of organosulfur compounds. Blends in the EU contain up to 7% biodiesel. Therefore, even in fuels denoted as "neat" or ULSD the degradation of FAME and hydrocarbons represents an increased corrosion risk within storage infrastructure. These findings have identified the challenges associated with the incorporation of FAME in diesel fuels and will inform best management practices to allow the continued use of renewable fuels, while also reducing the risk of microbiologically influenced corrosion to global energy infrastructure.

Materials and Methods

Isolation, Identification, and Growth of Fungal Isolates.

Paecilomyces sp. strain AF001 and *Wickerhamomyces* sp. strain SE3 were isolated from contaminated B20 biodiesel storage tanks at an Air Force Base in the southeast United States (33). To isolate the fungi, 1 L of B20 fuel was passed through a polyether sulfone Steritop™ bottle top filter unit with a 40 cm^2 filter area and 0.22 μm nominal pore size (Millipore Sigma). This filter was cut out with a sterile scalpel, transferred to a 1.5 mL Eppendorf tube containing

500 µL of phosphate buffered saline (pH 7.4), and the biomass was resuspended by vortexing at maximum speed for 1 min. The biomass suspension was diluted in phosphate buffered saline (pH 7.4), spread onto Hestrin Schramm (HS) agar medium (per L: 20 g glucose, 5 g yeast extract, 5 g peptone, 2.7 g Na_2HPO_4, 1.15 g citric acid, 7.5 g Agar; pH adjusted to 6.0 with diluted HCl or NaOH) (49) and incubated at 25°C for 7 days.

Fungal growth was transferred for isolation repeatedly until pure cultures (repeatedly singular morphologies) were obtained. The fungal isolates were identified by extracting genomic DNA with the *Quick*-DNA Fungal/Bacterial Miniprep Kit (Zymo Research; Irvine (Fig, CA), amplifying and sequencing the internal transcribed spacer (ITS) region. Specifically, the ITS region for each isolate was amplified with the primers ITS1-F (5'CTTGGTCATTTAGAGGAAGTAA-3') and ITS4 (5'-TCCTCCGCTTATTGATATGC-3') in a PCR using 5 PRIME HotMasterMix (Quanta Biosciences, Beverly, MA, United States) (50, 51). The amplified DNA was purified using ExoSap-IT™ (Thermo Fisher Scientific) according to the manufacturer's instructions. Once purified, the amplified DNA was submitted for BigDye® Direct Cycle sequencing with each amplification primer on the 3130xl Genetic Analyzer (Biology Core Molecular Laboratory, University of Oklahoma). The resulting sequences for each amplicon were trimmed for quality to only include nucleotides with a Q-score ≥ 30 and merged using CAP3 (52). The trimmed and merged sequences were then submitted to NCBI to identify their closest neighbor using MegaBLAST. The MEGA X software package (53) was used to build a maximum likelihood tree (Tamura-Nei model, bootstrapped with 500 samplings) containing sequences from the isolates and closest neighbors (FIG 2.1).

A spore suspension of the filamentous fungus *Paecilomyces* sp. was used as the normalized inoculum in the experiments described below. To prepare the spore suspension, 4 mL

of PBS was added to the surface of HS agar containing hyphal growth of *Paecilomyces* sp., and an inoculating loop was used to scrape off the fungal growth. The PBS solution was then collected from the plate and filtered through a 10 μm pore size polyether sulfone filter, to separate spores from hyphal biomass. The spores were then centrifuged at 10,000 x RCF for 1 minute. The supernatant was decanted, and sterilized PBS was added back to the spore pellet and vortexed to resuspend the spores in solution. This was repeated for a total of three washes. Spore concentrations were determined using a Petroff-Hausser counting chamber then diluted to adjust the inoculum concentration to $1x10^4$ spores/mL.

To produce a suspension of yeast cells, *Wickerhamomyces* sp. was grown in HS broth for 48 hours and was centrifuged at 10,000 x RCF to pellet cell mass. The supernatant was decanted, and sterilized PBS was added to the cell pellet. This pellet was centrifuged at 10,000 x RCF for 1 minute. The supernatant was decanted, and more sterilized PBS was added to the cell pellet and vortexed to resuspend the cells in suspension. This was repeated for a total of three washes. Cell concentrations were determined using a Petroff-Hausser counting chamber and diluted to adjust the inoculum concentration to $1x10^4$ cells/mL.

Quantification and Characterization of Microbiologically Influenced Corrosion in Bioreactors

Three CDC biofilm bioreactors® (BioSurface Technologies Corp.) were filled with 3 mL of B20 biodiesel and 297 mL of Artificial Sump Water (ASW, per L: 0.015 g NaCl, 0.035 g NaF, 0.02 g $CaCl_2$, 0.018 g KNO_3, 0.01 g Na_2SO_4, 0.015 g $(NH_4)_2SO_4$, and 0.017 g K_2HPO_4) (1:100 ratio of B20:ASW) and inoculated to a final concentration of $1X10^4$ *Paecilomyces* spores/mL or *Wickerhamomyces* cells/mL. These reactors were run as a closed system at ambient temperature and were stirred at 100 rpm over the duration of the experiment. Grade 1018 carbon

steel circular disk coupons (1.27 cm diameter x 3.82 mm thick; BioSurface Technologies Corp., Bozeman, MT) were washed in acetone to remove any machine oil, weighed to obtain initial mass, and sterilized prior to use by exposing them to UV light for 15 minutes on each side. In an AirClean 600 PCR Workstation (AirClean Systems Inc., Creedmoor, NC), three carbon steel disks were inserted into each of three polypropylene coupon holders. Three of the coupon holders were inserted into each of the three bioreactors. The bioreactors were sampled weekly for three weeks by removing one of the polypropylene coupon holders and replacing it with a sterilized bioreactor blank coupon holder, allowing for three technical and three biological replicates. The coupons collected from each reactor were cleaned and weighed to determine mass loss, which was used to calculate corrosion rates (described below). The surface topology of each coupon was also determined to quantify the area and depth of any corrosion. The pH of the aqueous phase was determined at each sampling time, as was the viability of the isolates or sterility of controls. Viability measurements of the planktonic microorganisms were made by sampling medium from the bioreactors and conducting MPN/mL measurements for *Paecilomyces* AF001 and CFU/mL measurements for *Wickerhamomyces* SE3 using liquid or solid HS medium, accordingly. The population density of microorganisms attached to each coupon was determined by removing biomass with a sterile nylon swab and transferring it to sterile PBS. The biomass was suspended by vortexing and used to determine MPN or CFU/mL as described above. After removing the biomass with a swab, each coupon was cleaned using ASTM method G01-03 C3.5 and immediately weighed to determine mass loss. After being weighed, the coupons were stored in an anaerobic chamber to prevent further abiotic oxidation until surface analysis could be conducted. The technical replicates were averaged and used for data analysis.

The surface of each coupon was analyzed using white light profilometry (Nanovea PS50; Nanovea, Inc.; Irvine, CA). To ensure that the same area was being scanned on all coupons, a clip was used to align the coupons in the same location on the profilometer's stage (Supplemental information contains 3D files that can be 3D printed and examined; https://github.com/Jfloydo/3D-Printed-White-Light-Profilometer-Stage-Cover-for-Nanovea-PS50).

A 6 x 6 mm area was scanned on the coupon and visualized using Mountains Software version 6.3 (Digital Surf). Intensity and height maps were combined in the software and leveled using a least squares plane method by subtraction. Non-measured points were filled in using calculations of points from the nearest neighbors. Pits were defined as any points that were greater than 20 μm below the mean surface average. Maximum pit depth and total pitted area were calculated from the surface analyses.

Localizing Corrosion in Fuel, Interphase, and Aqueous Phases

Static corrosion experiments were set up with the intent of determining where corrosion was greatest, in the fuel, interphase, or aqueous phase of water-containing fuel systems. The static incubations were made by first filling test tubes (16 x 150 mm) with 3 mL of sterile ASW medium to mimic water present in the underground storage tanks from runoff or condensation within the tank (54). B20 biodiesel was filter sterilized into an autoclaved 1L Schott Bottle using a Steritop™ bottle top filter unit with a 40 cm^2 filter area and 0.22 μm nominal pore size (Millipore Sigma) and 3 mL of this biodiesel was aseptically added to the tubes, resulting in a 1:1 fuel to ASW ratio. Non-galvanized carbon steel brads (0.5 mm diameter x 19 mm length) were washed in acetone to remove any machine oil, weighed to obtain initial mass, and autoclaved anaerobically in Balch tubes with a N_2 headspace to prevent abiotic corrosion and

ensure sterility prior to the experiment. The brads were inserted into holes drilled into nylon bolts at three levels before the autoclave cycle. The holes were positioned so that the brads were exposed to either the fuel phase, the fuel-water interface, or the aqueous phase.

Five replicates of the static corrosion tubes described above were either inoculated with a final concentration of $1x10^4$ *Paecilomyces* sp. spores or *Wickerhamomyces* sp. cells per mL. An additional five tubes remained uninoculated as controls. The tubes were incubated for 21 days at room temperature in the dark. After 21 days, the pH of the aqueous phase was measured using an Oakton pH Spear waterproof Pocket pH Testr™. The viability of the organisms (or sterility of the controls) was assessed by growth on HS agar medium and direct microscopy. Viability of the *Wickerhamomyces* sp. was determined by CFU/mL on HS agar medium. Growth of the *Paecilomyces* sp. was confirmed by observation of hyphal growth under light microscopy by preparing a wet mount and examining at 100x magnification. Corrosion rates were calculated from mass loss using the approach described below (Calculating corrosion rates from mass loss measurements).

Additional static corrosion experiments were conducted with flat coupons that traversed the fuel, interphase, and aqueous phases in order to visualize the surface of the coupon across all phases with scanning electron microscopy and measure the area and depth of corrosion pits using the white light profilometry as described above. The coupons used for this experiment were composed of 1018 carbon steel, 76.2 cm long, 9.5 cm wide, and 1.6 mm thick, and finished by the manufacturer by sanding using a 120-grit belt (Alabama Specialty Products, Inc.; Munford, AL). Each coupon was placed in separate 250 mL Erlenmeyer flasks containing 25 mL of sterile B20 biodiesel and ASW for a 1:1 ratio. These flasks were either inoculated with $1x10^4$ spores of

the filamentous fungus *Paecilomyces* or kept uninoculated as controls, incubated at 25°C for 90 days, and used to quantify and characterize surface corrosion.

The surface of the coupons was analyzed using white light profilometry as described above. To ensure that the same area 20 x 8 mm area was being scanned on all coupons, a clip was used to align the coupons in the same location on the profilometer's stage (https://github.com/Jfloydo/3D-Printed-White-Light-Profilometer-Stage-Cover-for-Nanovea-PS50)

Intensity and height maps were combined using the Mountains Software version 6.3 (Digital Surf; Besançon, France) and leveled using a least squares plane method by subtraction. Within the software, non-measured points were filled in using calculations of points from the nearest neighbors. Pits were defined as any points that were less than 20 µm below the mean surface average. Maximum pit depth and total pitted area were calculated from the surface analyses.

Calculation of Corrosion Rates from Mass Loss Measurements

Following incubation, carbon steel brads and coupons were cleaned using ASTM method G01-03 C3.5 (55). The final mass was measured and used to determine the rates of corrosion in milli-inches per year (MPY) using the following equation:

Corrosion rate = $\frac{K*W}{(A*T*D)}$ where

K = Mils per year (MPY) rate [Constant]

T = Time of exposure in hours

A = Area in cm^2

W = Mass loss in grams (Initial coupon mass – final coupon mass)

D = Density of metal in g/cm^3

Quantification and Characterization of B20 Biodiesel Fuel Biodegradation.

Fungal biodegradation of B20 was evaluated by direct measure of fungal growth and consumption of the fuel compounds. Fungal growth and ability to degrade B20 biodiesel was measured every 7 days for 21 days. All biodegradation experiments were incubated aerobically at 25 °C and non-shaking (i.e. static) conditions. For all experiments, negative controls (un-inoculated) were included to evaluate contamination risks and assess abiotic degradation. Un-amended controls (inoculated but with no B20) were also included to evaluate nutrient carryover from the initial inocula. Test tubes (16 x 150 mm) were filled with a total volume of 5 mL filter sterilized B20 as the sole carbon and energy source and ASW liquid medium in a 1:10 (0.5 mL B20:4.5 mL ASW) fuel to ASW ratio. *Wickerhamomyces* and *Paecilomyces* were initially grown on HS broth and spun down at 10,000 x RCF to pellet cell mass. This pellet was resuspended in PBS by vortex, centrifuged and resuspended a total of 3 times to remove any potential nutrient carry over before inoculation. Finally, the cell/spore density was determined using a hemocytometer, allowing the B20 and ASW to be inoculated to a final concentration of $1x10^4$ cells/mL or spores/mL respectfully. The fuel phase of these cultures was separated using a 10 mL separatory funnel and diluted 1:10 in hexane ≥97.0% (GC) and analyzed by Gas Chromatography/Mass Spectrometry (GC/MS). The chemical composition of the B20 biodiesel samples prior to degradation was determined by GC/MS using a Shimadzu QP 2010 SE (Shimadzu Corporation, USA). Each sample was diluted 1:10 with hexane prior to injection. A volume of 1 µL was injected via autosampler with a split ratio of 1:10 for a final dilution of 1:100. Injection started at 300 °C, the oven was at 40°C with a 1.5 min hold, which increased to 320°C at a rate of 10°C min^{-1}. Chemical components were separated with a Restek Column Rxi 5Sil with dimensions: 30 m, 0.25 mm ID, 0.25 µm. High purity helium was used as a carrier gas

at a linear velocity of 36.8 cm s^{-1}. Mass spectra were analyzed in scan mode with the following parameters: interface at 320 °C, ion source 200 °C, solvent cut of 2.75 min, event time of 0.25 sec and scan speed of 2000. Each Total Ion Chromatogram (TIC) was processed using the software LabSolutions version 4.20 (Shimadzu Corporation, USA). Peaks were identified using the mass spectra library NIST version 14 and verified and quantified using reference standards for FAME (Supelco® 37 Component FAME Mix, Sigma Aldrich, USA) and saturated alkanes (C7-C40 Saturated Alkanes Standard, Sigma Aldrich, USA). Major alkane and FAME peaks were identified by the NIST library replicates and underwent destructive sampling of quintuplicates at each time point. The degradation of fuel compounds was measured by determining the amount (%) of the remaining fuel components relative to a non-exposed control.

Statistical Analysis and Data Visualization

Statistical analysis and figure generation was carried out in R version 3.3.3 and GraphPad Prism 8.3.0. Significant differences were calculated using two-way ANOVA with a Tukey's HSD to determine significant differences in corrosion rates, maximum pit depths, total pitted areas, and pH between the isolates and uninoculated controls.

Acknowledgements

We acknowledge the men and women of the US Air Force and Civilian Personnel at US Air Force bases; their cooperation and assistance were critical to this research. Additionally, we would like to thank Emily Junkins for insightful comments during the development of this manuscript. This work was supported by the Air Force Research Laboratory Biological Materials and Processing Research Team, Materials and Manufacturing Directorate and the U.S. Department of Defense Office of Corrosion Policy & Oversight Technical Corrosion Collaboration (Grant # FA7000-15-2-0001).

Works Cited

1. Singleton L, Weller CE. 2001. Prosperity Wasn't Just Around the Corner. Economic Policy Institute 166.

2. John V. 2001. Economic Impact of the Terrorist Attacks of September 11, 2001. Atl Econ J 29:353–357.

3. U.S. Energy Information Administration. 2020. Biofuels Explained Use of Biomass-Based Diesel Fuel.

4. U.S. Energy Information Administration. 2019. Biodiesel and Other Renewable Fuels Overview.

5. Environmental Protection Agency. 2018. Renewable Fuel Standard Program: Standards for 2019 and Biomass Based Diesel Volume for 2020. 83 FR 63704

6. Ogunkunle O, Noor AA. 2019. A Review of Global Current Scenario of Biodiesel Adoption and Combustion in Vehicular Diesel Engines. Energy Reports 5:1560–1579.

7. Department of Defense. 2016. Department of Defense 2016 Operational Energy Strategy.

8. Özener O, Yüksek L, Ergenç AT, Özkan Muammer. 2014. Effects of Soybean Biodiesel on a DI Diesel Engine Performance, Emission and Combustion Characteristics. Fuel 115:875-883.

9. Meher LC, Sagar DV, Naik SN. 2006. Technical Aspects of Biodiesel Production by Transesterification—a Review. Renew Sust Energ Rev 10:248-268

10. Zuleta EC, Baena L, Rios LA, Calderón JA. 2012. The Oxidative Stability of Biodiesel and its Impact on the Deterioration of Metallic and Polymeric Materials: A Review. J Braz Chem Soc 23:2159-2175.

11. Demirbaş A. 2008. Biodegradability of Biodiesel and Petrodiesel Fuels. Energy Sources, Part A: Recovery, Utilization, and Environmental Effects. 31:169-174

12. Prince RC, Haitmanek C, Lee CC. 2008. The Primary Aerobic Biodegradation of Biodiesel B20. Chemosphere 71:1446-1451.

13. Aktas DF, Lee JS, Little BJ, Ray RI, Davidova IA, Lyles CN, Suflita JM. 2010. Anaerobic Metabolism of Biodiesel and its Impact on Metal Corrosion. Fuels 24:2924–2928.

14. Thomas AO, Leahy MC, Smith JWN, Spence MJ. 2017. Natural Attenuation of Fatty Acid Methyl Esters (FAME) in Soil and Groundwater. Q R Eng Geol Hydroge 50:301-317.

15. Houten SM, Wanders RJA. 2010. A General Introduction to the Biochemistry of Mitochondrial Fatty Acid β-oxidation. J Inherit Metab Dis 33:469-477.

16. Morawe M, Hoeke H, Wissenbach DK, Lentendu G, Wubet T, Kröber E, Kolb S. 2017. Acidotolerant Bacteria and Fungi as a Sink of Methanol-Derived Carbon in a Deciduous Forest Soil. Front Microbiol 8:1361.

17. Abbasian F, Lockington R, Mallavarapu M, Naidu R. 2015. A Comprehensive Review of Aliphatic Hydrocarbon Biodegradation by Bacteria. Appl Biochem Biotech 176:670-699.

18. Colombo JC, Cabello M, Arambarri AM. 1996. Biodegradation of Aliphatic and Aromatic Hydrocarbons by Natural Soil Microflora and Pure Cultures of Imperfect and Lignolitic Fungi. Environ Pollut 94:355-362.

19. Rojo F. 2010. Enzymes for Aerobic Degradation of Alkanes, p 781-797. *In* Timmis KN (eds), Handbook of Hydrocarbon and Lipid Microbiology, Springer, Berlin, Heidelberg.

20. Skovhus T, Eckert RB, Rodrigues E. 2017. Management and Control of Microbiologically Influenced Corrosion (MIC) in the Oil and Gas Industry—Overview and a North Sea Case Study. J Biotechnol 256:31–45.

21. Amy PS, Jones DA. 2002. A Thermodynamic Interpretation of Microbiologically Influenced Corrosion. Corrosion 58:638-645.

22. Stewart PS, Franklin MJ. 2008. Physiological Heterogeneity in Biofilms. Nat Rev Microbiol 6:199-210.

23. Usher KM, Kaksonen AH, Cole I, Marney D. 2014. Critical Review: Microbially Influenced Corrosion of Buried Carbon Steel Pipes. Int Biodeterior Biodegradation 93:84-106.

24. Bento FM, Beech IB, Gaylarde CC, Englert GE, Muller IL. 2005. Degradation and Corrosive Activities of Fungi in a Diesel–Mild Steel–Aqueous System. World J Microbiol Biotechnol 21:135-142.

25. Bücker F, Santestevan NA, Roesch LF, Jacques RJS, Peralba MCR, Camargo FAOC, Bento FM. 2011. Impact of Biodiesel on Biodeterioration of Stored Brazilian Diesel Oil. Int Biodeterior Biodegradation 65:172-178.

26. Mohanan S, Rajasekar A, Muthukumar N, Maruthamuthu S, Palaniswamy N. 2005. The Role of Fungi on Diesel Degradation, and Their Influence on Corrosion of APl 5LX Steel. Corrosion Prevention and Control 4:123–130.

27. United States Air Force. Air Force Energy Plan 2010.

28. Stamps BW, Bojanowski CL, Drake CA, Nunn HS, Lloyd PF, Floyd JG, Emmerich KA, Neal AR, Crookes-Goodson WJ, Stevenson BS. 2020. In situ Linkage of Fungal and Bacterial Proliferation to Microbiologically Influenced Corrosion in B20 Biodiesel Storage Tanks. Front Microbiol 11:167.

29. NACE. 2013. Preparation, Installation, Analysis, and Interpretation of Corrosion Coupons in Oilfield Operations. SP0775.

30. Suflita JM, Lyles CN, Aktas DF, Sunner J. 2014. Biocorrosion Issues Associated with the Use of Ultra-low Sulfur Diesel and Biofuel Blends in the Energy infrastructure, p 313-328. *In* Liengen T, Basseguy R, Féron D, Birrien V, Understanding Biocorrosion: Fundamentals and Applications, Netherlands, Elsevier Science.

31. American Society for Testing and Materials. Standard Specification for Diesel Fuel Oils. ASTM International.

32. European Union for Standardization. 2009. Automotive fuels - Diesel - Requirements and Test Methods. EN 590.

33. Andrade O. 2016. Master Thesis. Characterization of Fungal Contaminants in B20 Biodiesel Storage Tanks and Their Effect on Fuel Composition. University of Oklahoma, Norman, OK.

34. Liebenberg JJ, Skinner W. 1993. Corrosion Characteristics of Carbon Steel in Organic Solvent Containing Fatty Acids. Brit Corros J 2:130-132.

35. Little BJ, Lee JS. 2014. Microbiologically Influenced Corrosion: an Update. Int Mater Rev 59:384–393.

36. Papanikolaou S, Chevalot I, Komaitis M, Aggelis G, Marc I. 2001. Kinetic Profile of the Cellular Lipid Composition in an Oleaginous *Yarrowia lipolytica* Capable of Producing a Cocoa-Butter Substitute from Industrial Fats. A Van Leeuw J Microb 80:215–224.

37. Tzirita M, Papanikolaou S, Chatzifragkou A, Quilty B. 2018. Waste Fat Biodegradation and Biomodification by *Yarrowia lipolytica* and a Bacterial Consortium Composed of *Bacillus* spp. and *Pseudomonas putida*. Eng Life Sci 18:932–942.

38. Szatmari I, Tudosie L, Cojocaru A, Lingvay M, Prioteasa P, Vişan T. 2015. Studies on Biocorrosion of Stainless Steel and Copper in Czapek Dox Medium with *Aspergillus niger* Filamentous Fungus. UPB Scientific Bulletin, Series B: Chemistry and Materials Science 77:91-102.

39. Kruger J. 1989. The Nature of the Passive Film on Iron and Ferrous Alloys. Corrosion Science 29:149-162.

40. Rahner D. 1996. Fe3O4 as Part of the Passive Layer on Iron. Solid State Ion 86-88:865-871.

41. Little BJ, Lee JS, Ray RI. The Influence of Marine Biofilms on Corrosion: a Concise Review. Electrochim Acta 54:2-7.

42. Speidel H, Lightner R, Ahmed I. 2000. Biodegradability of New Engineered Fuels Compared to Conventional Petroleum Fuels and Alternative Fuels in Current Use. Appl Biochem Biotechnol 84-86:879-897.

43. Videla H, Herrera LK. 2005. Microbiologically Influenced Corrosion: Looking to the Future. Int Microbiol 8:169-80.

44. Lee JS, Ray RI, Little BJ. 2010. An Assessment of Alternative Diesel Fuels: Microbiological Contamination and Corrosion Under Storage Conditions. Biofouling 26:623-635.

45. Kaul S, Saxena RC, Kumar A, Negi MS, Bhatnagar AK, Goyal HB, Gupta AK. 2007. Corrosion Behavior of Biodiesel from Seed Oils of Indian Origin on Diesel Engine Parts. Fuel Process Technol 88:303–307.

46. Meira M, Santana PB, Araújo AS, Silva CL, Filho J, Ferreira HT. 2014. Oxidative Degradation and Corrosiveness of Biodiesel. Corrosion Reviews 32:143–161.

47. Cavalcanti E de, Zimmer A, Bento F, Ferrão M. 2019. Chemical and Microbial Storage Stability Studies and Shelf Life Determinations of Commercial Brazilian Biodiesels Stored in Carbon Steel Containers in Subtropical Conditions. Fuel 993–1007.

48. Meyer DD, Beker SA, Bücker F, Peralba MCRP, Frazzon APG, Osti JF, Andreazza R, Camargo FAO, Bento FM. 2014. Bioremediation Strategies for Diesel and Biodiesel in Oxisol from Southern Brazil. Int Biodeterior Biodegradation 95:356-363.

49. Hestrin S, Schramm M. 1954. Synthesis of Cellulose by *Acetobacter xylinum*. 2. Preparation of Freeze-Dried Cells Capable of Polymerizing Glucose to Cellulose. Biochem J 58:345-352.

50. White TJ, Bruns T, Lee S, Taylor J. 1990. Amplification and Direct Sequencing of Fungal Ribosomal RNA Genes for Phylogenetics, p 315-322. *In* PCR Protocols A Guide to Methods and Applications, Academic Press.

51. Gardes M, Bruns TD. 1993. ITS Primers with Enhanced Specificity for Basidiomycetes-Application to the Identification of Mycorrhizae and Rusts. Mol Ecol 2:113-118.

52. Huang X, Madan A. 1999. CAP3: A DNA Sequence Assembly Program. Genome Res 9:868-877.

53. Kumar S, Nei M, Dudley J, Tamura K. 2008. MEGA: a Biologist-centric Software for Evolutionary Analysis of DNA and Protein Sequences. Brief Bioinform 9:299-306.

54. McNamara CJ, Thomas PD, Leard R, Bearce K, Dante J, Mitchell R. 2006. Corrosion of Aluminum Alloy 2024 by Microorganisms Isolated from Aircraft Fuel Tanks. Biofouling 21:257–265.

55. American Society for Testing and Materials. 2011. Practice for Preparing, Cleaning, and Evaluating Corrosion Test Specimens. ASTM International.

56. B. Stevenson, B. Stamps. 2021. It's Complicated: Rapid Publication of Genomes in Microbiology Resource Announcements Can be Both Part of the Problem and the Solution to Fungal Taxonomic Resolution. Microbiological Resource Announcements.

Chapter 3. Connection Between Fuel Composition and the Microbiological Communities Contaminating Fuel Storage Tanks

James G. Floyd[1], Blake W. Stamps[2,3], Caitlin L. Bojanowski[4], Wendy J. Goodson[4], Bradley S. Stevenson[1]

1 – University of Oklahoma, Department of Microbiology and Plant Biology, Norman OK

2 – 711th Human Performance Wing, Airman Systems Directorate, Air Force Research Laboratory, Wright-Patterson AFB, OH, United States

3 – UES Inc., Integrative Health and Performance Sciences Division, Dayton, OH, United States

4 – Soft Matter Material Branch, Materials and Manufacturing Directorate, Air Force Research Laboratory, Wright-Patterson AFB, OH

Key Words: Biofouling, Diesel, Biodiesel, Redundancy Analysis

Foreword

Microbial community analysis and fuel collection has been an ongoing project from the Stevenson lab dating back to 2013. For this study I performed the fuel composition analyses, extracted DNA from fuels and prepared libraries for sequencing, analyzed sequence data, performed statistical analyses, generated figures, made Redundancy Analysis Models, and wrote the manuscript. Dr. Blake Stamps was involved in collecting fuel samples, extracting DNA and prepared libraries for sequencing, and aided in the writing and editing of this manuscript. Dr. Caitlin Bojanowski at AFRL helped with the collection of fuel samples and aided us in obtaining access to fuel tanks on military installations. Dr. Wendy Goodson assisted with the collection of fuel samples and additionally aided obtaining access to fuel tanks on military installations. Bradley Stevenson helped with the experimental design, helped with the collection of fuel samples, and aided in the writing and editing of the manuscript.

Abstract

Contamination of diesel storage tanks by microorganisms is a widespread and under realized problem. These microorganisms can degrade components of the fuel, leading to fouling and corrosion. To better understand the connection between the microorganisms that are responsible for this contamination, the composition of affected fuels, and the resulting impact on fuel quality, we conducted a survey of 106 fuel tanks at 17 military bases across the continental United States. Fuel was sampled from the bottom of each tank, where microbial contamination is most prevalent, and the resident microbial communities were characterized using high throughput sequencing of small subunit ribosomal RNA (SSU rRNA) gene libraries. Fatty acid methyl esters (FAME, i.e. biodiesel) and n-alkanes from contaminated fuels were characterized and quantified using GC-MS to determine how components of the fuels might be correlated with the presence of microbial taxa. Redundancy Analysis Modeling (RDA) was used to determine which microbial taxa, especially those known to increase carbon steel corrosion, were more prominent in contaminated fuels based on the fuel's chemical composition. Members of the fungal family Trichomaceae were found to be prominent in fuels containing more FAME. Members of the yeast family Debaryomycetaceae were found to be prominent in fuels containing more pentadecanoic and oleic acid methyl esters, which both contain one degree of unsaturation. Fuels with higher concentrations of pentadecanoic acid methyl ester were found to have a positive correlation with Debaryomycetaceae and no correlation with Trichomaceae, while fuels with a higher concentration of palmitoleic acid methyl ester had a positive correlation with Trichocomaceae and no correlation with Debaryomycetaceae. These relationships between fungal taxa and fuel components were directly tested in growth experiments with representative isolates of the Trichocomaceae (*Paecilomyces* AF001) and Debaryomycetaceae

(*Wickerhamomyces* SE3) families. Each isolate was inoculated into cultures containing pentadecanoic acid and linoleic acid methyl esters as sole carbon and energy sources. *Paecilomyces* was capable of growth on linoleic acid methyl ester but unable to grow on pentadecanoic acid methyl ester. *Wickerhamomyces* was able to grow using both substrates. While fuel composition provides some understanding of which microorganisms can proliferate, other factors like competition and symbiosis between these microbial populations will need to be considered to better understand the ecological drivers of microbial proliferation, fouling, degradation, and corrosion in diesel fuels.

Importance

Biodiesel, widely used as an additive or extender of ultra-low sulfur diesel, can increase the potential for microorganisms to proliferate in storage tanks. It is important to know how the composition of diesel fuels can influence the growth of organisms linked to fuel degradation and microbiologically influenced corrosion. This research describes how certain populations of fungi and bacteria can prevail in fuels of different composition, which can be helpful in formulating fuels less susceptible to the growth of problematic organisms.

Introduction

Diesel that has been amended with biodiesel is the primary transportation fuel for heavy trucks and buses. In recent years, the U.S. Department of Energy has incentivized the use of biodiesel through December 2022 in efforts to offset carbon emissions (1). The U.S. Energy Information Administration predicts that petroleum and other fuel consumption can be expected to rise from the current consumption of 16 million barrels per day to just under 25 million barrels per day by the year 2050 (2). Biodiesel has been used in various blends with petroleum ultra-low sulfur diesel (ULSD; less than 15 ppm sulfur), commonly containing 20% biodiesel and 80%

petroleum diesel (B20 Biodiesel) since it represents a balance of costs, emissions, cold-weather performance, and engine material compatibility (3). Additionally, biodiesel has been readily added to ULSD at up to 5% v/v to compensate for the loss of lubricity from the desulfurization process (4). Biodiesel is also more easily bio-remediated if spilled in the environment and has a much higher flash point when compared to ULSD, making it much safer for the environment and those handling the fuel (4–6). However, this biodegradability also proves problematic for operators that store their biodiesel and diesel fuels long term (7).

Biodiesel is composed of fatty acid methyl esters (FAME) that can be produced through a transesterification reaction with feedstocks of animal, plant, or microbial lipids (8). These FAME compounds in biodiesel make the fuel more susceptible to microbial contamination since FAME compounds exist naturally in the environment and readily degraded by many different microorganisms (9, 10). Additionally, hydrocarbons in diesel fuel can also be used as an oxidizable substrate for many microorganisms (11). Microbiological degradation can prove to be problematic for operators to store biodiesel and biodiesel blends for long term periods as their fuels can become contaminated. Microbial contamination of biodiesel and biodiesel blends not only leads to increased operating costs through mechanical cleaning of storage tanks, but also increases the risk of corrosion as microbial populations produce acidic byproducts from the metabolism of the fuel as well as generating oxygen corrosion cells in aerobic environments (12). Previous work has demonstrated the fungi and bacteria grown on B20 biodiesel can not only degrade FAME and hydrocarbons, but also increase corrosion rates and pitting corrosion of carbon steel (12–14).

When different feedstocks are used to produce biodiesel, they can result in different FAME profiles with variations in fatty acid chain lengths and degrees of saturation (15).

Microorganisms tend to preferentially oxidize unsaturated FAME (9), using lipases to first hydrolyze the ester bond, converting the FAME to methanol and the corresponding fatty acid (16). Different microorganisms have different capabilities of fatty acid metabolism that depends on fatty acid chain length (17). Microorganisms have different affinities for the metabolism of FAME so niches could be established in fuel systems where some organisms have access to oxidizable substrates while others would not. Not all organisms that contaminate fuel storage tanks can metabolize all the FAME compounds. Due to this, metabolic selectivity of FAME components can play a role on the community's composition by selecting for those that can gain a competitive edge by metabolizing substrates other organisms cannot.

Variability in fuel composition can also be driven by the types of hydrocarbons in petroleum-based diesel, which is affected by the provenance of the crude oil and the distillation processes (18). Diesel fuel primarily consists of hydrocarbons between 7 and 24 carbon atoms and is typically comprised of 64% alkanes (including n-, iso-, and cyclo-alkanes), 1-2% alkenes and 34% aromatic hydrocarbons (19, 20). In general, microorganisms preferentially oxidize smaller chained hydrocarbons (21), although there are some exceptions of microorganisms preferentially metabolizing longer chain alkanes (C20+) (22). The combination of compositional differences in diesel fuels and differential metabolic capabilities among microorganisms would represent a selective framework that could partially explain the structure of microbial communities in contaminated fuel.

Microbial community assemblies can shift based on the available carbon substrates that are available in the environment (23–26). To determine the relationship between fuel composition and microbial communities in contaminated fuels, we conducted a survey of diesel fuels (ULSD and biodiesel blends) from military bases across the continental United States.

Microbial communities were analyzed via SSU rRNA library analyses to determine community composition and fuel composition was analyzed with GC-MS. Previous work has linked certain taxa of fungi and bacteria to higher risks of corrosion when grown on biodiesel and diesel fuels (12, 13, 27). Correlations between substrates and taxa from the RDA analyses were tested using the fungal isolates *Paecilomyces* AF001 (Family - Trichocomaceae) and *Wickerhamomyces* SE3 (Family -Debaryomycetaceae), which have both been previously linked to corrosion risks when grown using biodiesel as a sole carbon and energy source (Chapter 2). With a better understanding of the relationships between fuel composition and their contaminating microbial communities, we can alert operators to the potential risks associated with fouling and microbiologically influenced corrosion for diesel fuel with based on its composition. Based on the preferential and specialized oxidation of some FAME and hydrocarbon compounds it is critical to understand how the composition of FAME and hydrocarbons of a particular fuel can impact microbial community structures.

Results

Characterization of n-Alkanes and FAME Components in Fuels

Biodiesel and diesel fuels were found to have different abundances of n-alkanes and FAME components. Differences of the alkane components are more geographically based instead of dependent upon the fuel type being diesel or biodiesel. The largest drivers of alkane variability in the collected fuels were from C9-C20 alkanes and were responsible for much of the separation of samples in the PCA (FIG 3.1).

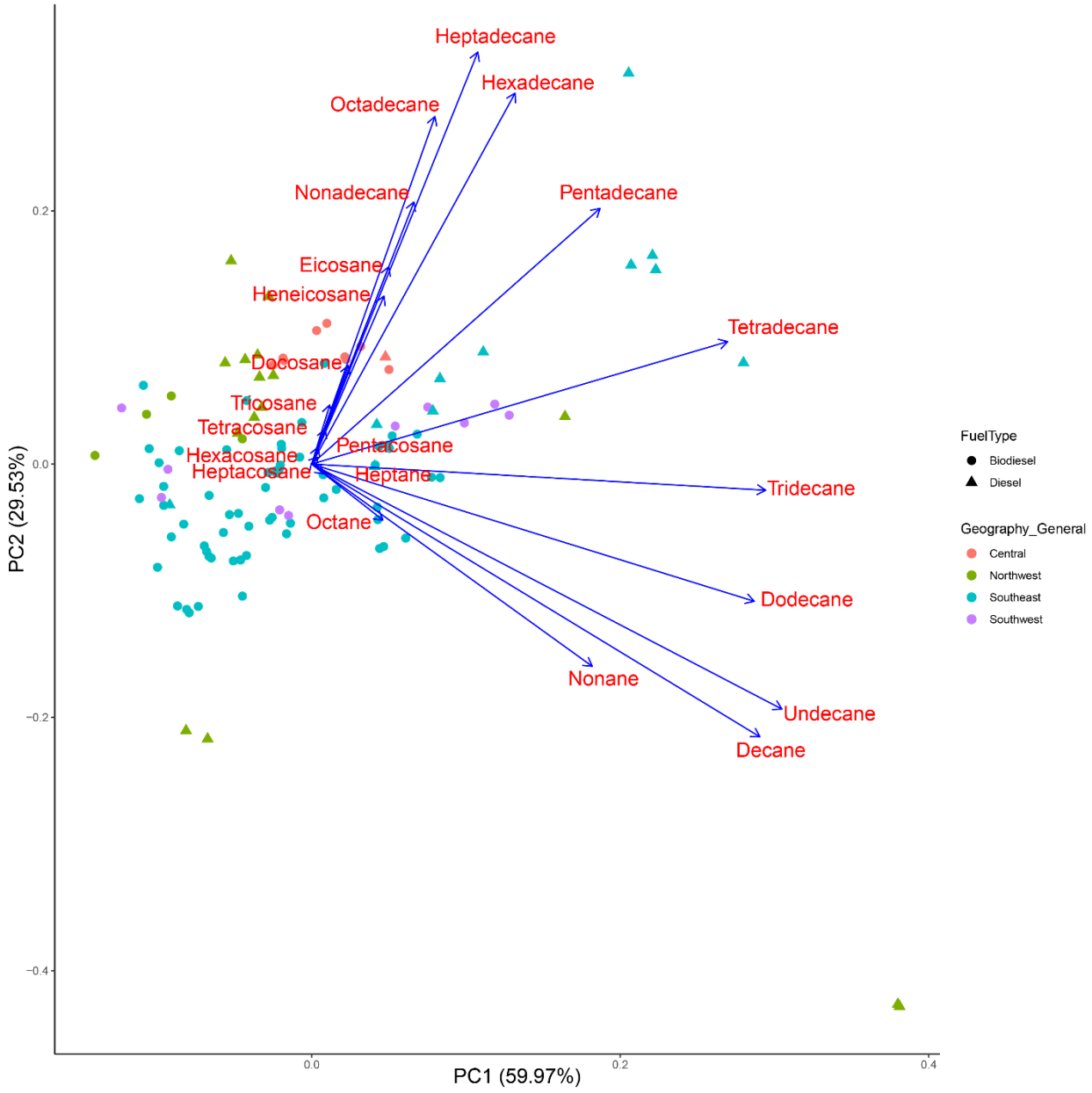

FIG 3.1. PCA ordination of fuel samples based on n-alkane composition. Biodiesel (circles) and diesel (triangles) fuel samples from different geographical areas in the continental U.S. are represented with different colors with Central (Orange), Northwest (Green), Southeast (Blue), and Southwest (Purple). Blue vectors represent the different n-alkanes and their contribution to the separation of the fuel samples in this ordination space.

Additionally, fuel samples were analyzed to determine differences in FAME composition. Unlike the n-alkanes, fuel type did impact the clustering of the samples, with diesel

fuels clustering together. The biggest drivers of FAME variability were due to linoleic, oleic, and palmitic acid methyl esters and to a lesser extent steric and linoleic acid methyl esters (FIG 3.2).

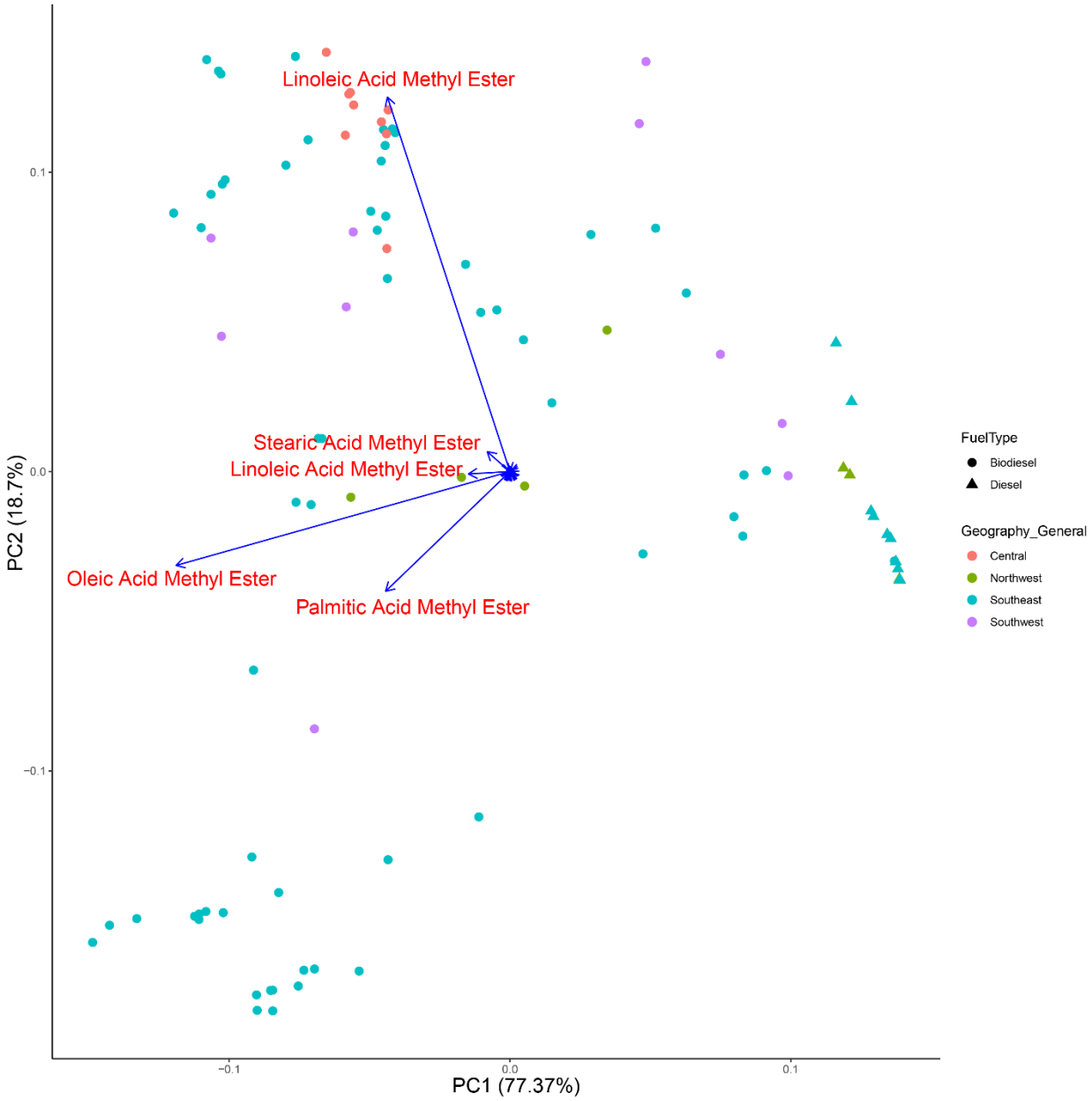

FIG 3.2. PCA ordination of fuel samples based on FAME composition. Biodiesel (circles) and diesel (triangles) fuel samples were from different bases are represented with different colors and the corresponding geographical location is indicated by Northwest, Southeast, Central, or Southwest. Blue vectors represent the different FAME components and their contribution to the separation of the fuel samples in this ordination space. Many FAME components had low

eigenvectors in this PCA, and their chemical names are excluded for simplicity; however, their vectors remain in this PCA to give a better overview of how fuel samples are separated.

Taxonomic Analysis of Contaminated Fuels

The bacterial populations in each microbial community were more diverse than the fungal populations in contaminated fuels, with some exceptions where the fuel sample contained more than 80% relative abundance of one bacterial family (FIG 3.3). When these the bacterial communities had lower diversity, members of the bacterial families Acetobacteriaceae and Moraxellaceae were mostly responsible. Fuels contaminated with Acetobacteriaceae did not appear to be constrained by geography as these contamination events occurred in both the Northwest and Southeast U.S. Moraxcellaceae were the most abundant population were only observed fuels from the Southeast U.S., but they were scattered across different locations in the Southeast.

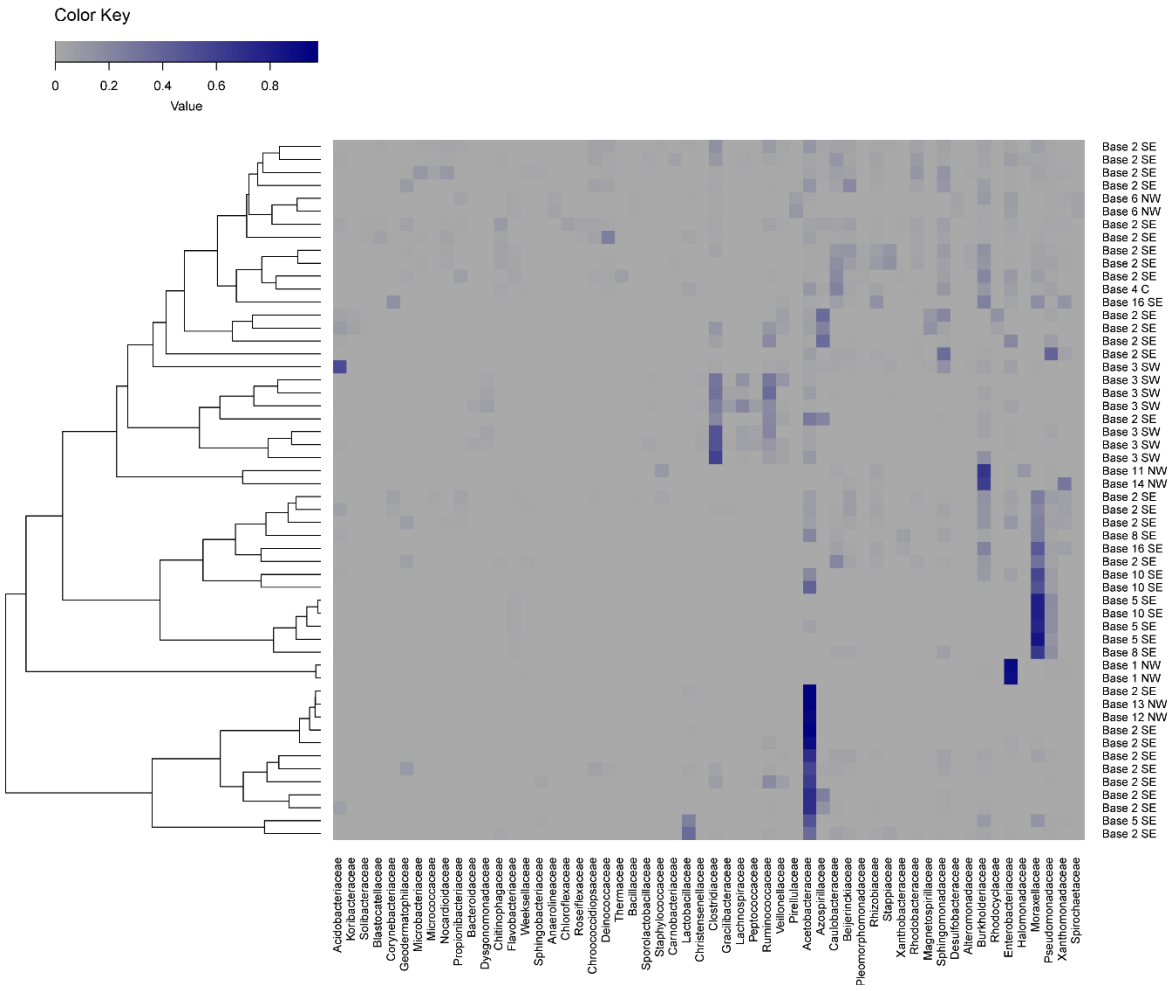

FIG 3.3. Heatmap representing the relative abundance of bacterial populations in microbial communities from contaminated fuels. Relative abundance of 100% is represented by dark blue, while gray represents 0% of the reads. Samples are sorted by the dendrogram on the left y-axis, which was based on bacterial population similarity. Bacterial families are denoted along the x-axis and sample names are denoted on the right y-axis. Bacterial families with less than 5 sequences remaining after rarefication were removed from this heatmap for simplicity.

Unlike the bacterial populations, the fungal populations present in microbial communities from contaminated fuels were primarily comprised of the fungal family Trichocomaceae. While the Trichocomaceae were usually the dominant family in contaminated diesel and biodiesel, several other fuels primarily contained members of the fungal family Debaryomycetaceae. These fungi were the more prominent fungal contaminant Southeast region of the U.S.

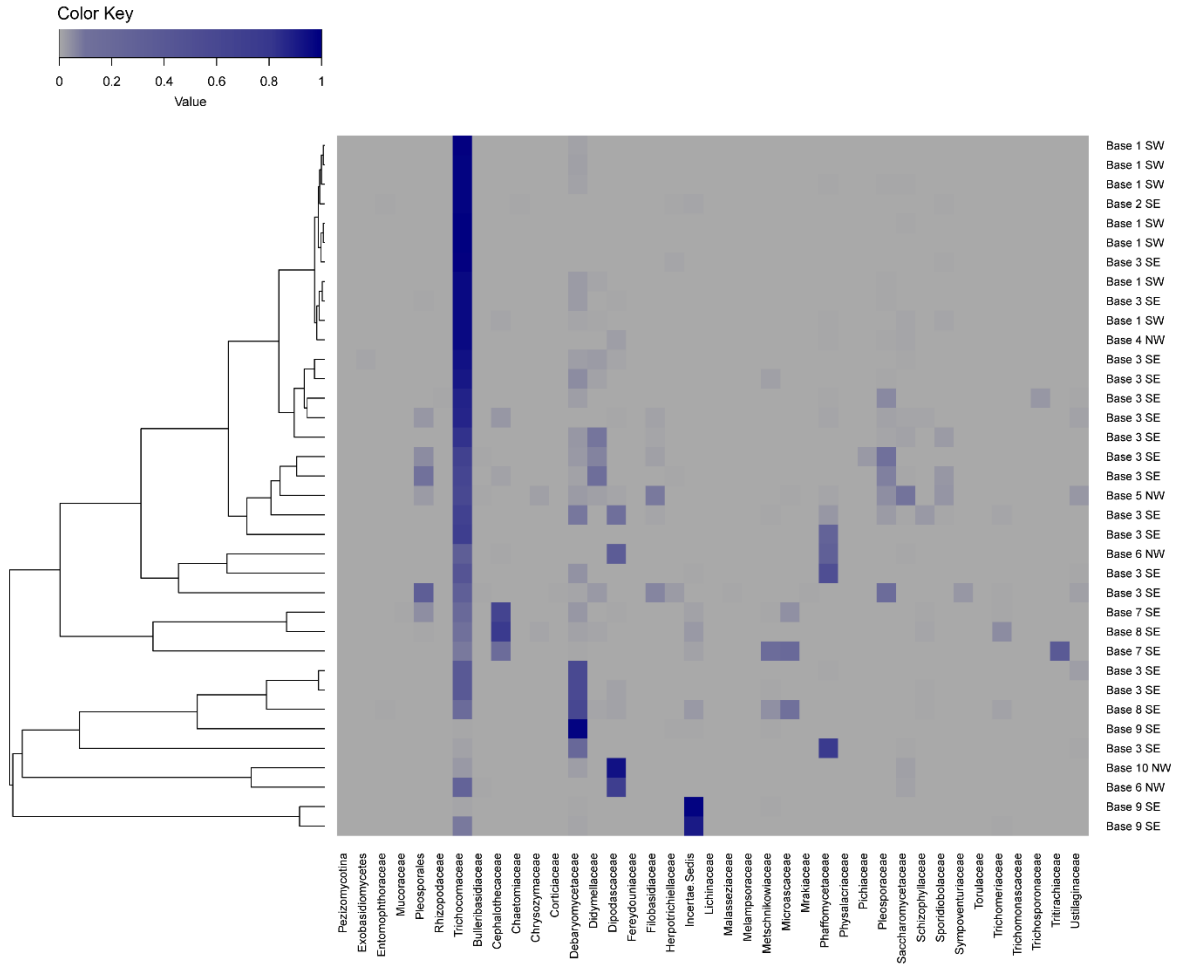

FIG 3.4. Heatmap representing the relative abundance of fungal populations in microbial communities from contaminated fuels. Relative abundance of 100% is represented by dark blue, while gray represents 0% of the reads. Samples are sorted by the dendrogram on the left y-axis, which was based on fungal population similarity. Fungal families are denoted along the x-axis and sample names are denoted on the right y-axis. Fungal families with less than 5 sequences remaining after rarefication were removed from this heatmap for simplicity.

Redundancy Analysis Correlating Fuel Components to Taxonomy

Redundancy analyses were conducted to extract and summarize the variation in the microbial taxonomic data and how it correlated with the fuel components. Redundancy analyses were performed for both the bacterial and fungal populations and used to determine correlations between taxa and fuel composition. If a vector is pointing towards a bacterial family a positive

correlation exists, if a vector is perpendicular no correlation exists, and if a vector is pointing away from a bacterial family a negative correlation exists. Certain bacterial families were found the be correlated with the increased abundances of n-alkanes and FAME (FIG 3.5). The bacterial family Acetobacteriaceae were found to be positively correlated to fuels containing more long chain alkanes such as eicosane, tricosane, and tetracosane. The Acetobacteriaceae were also positively correlated with increases in linoleic acid methyl ester. In contrast, the bacterial family Moraxellaceae was positively correlated with fuels containing shorter alkanes and higher concentrations of myrisoleic acid methyl ester. The RDA model from the bacterial taxa and fuel composition had a R^2 value of 0.33 with p=0.003. Forward selection of fuel compounds used in the bacterial RDA using an adonis test on the Hellinger transformed taxonomic data can be seen in Table 3.1 and correlation values for RDA axes can be seen in Table 3.2.

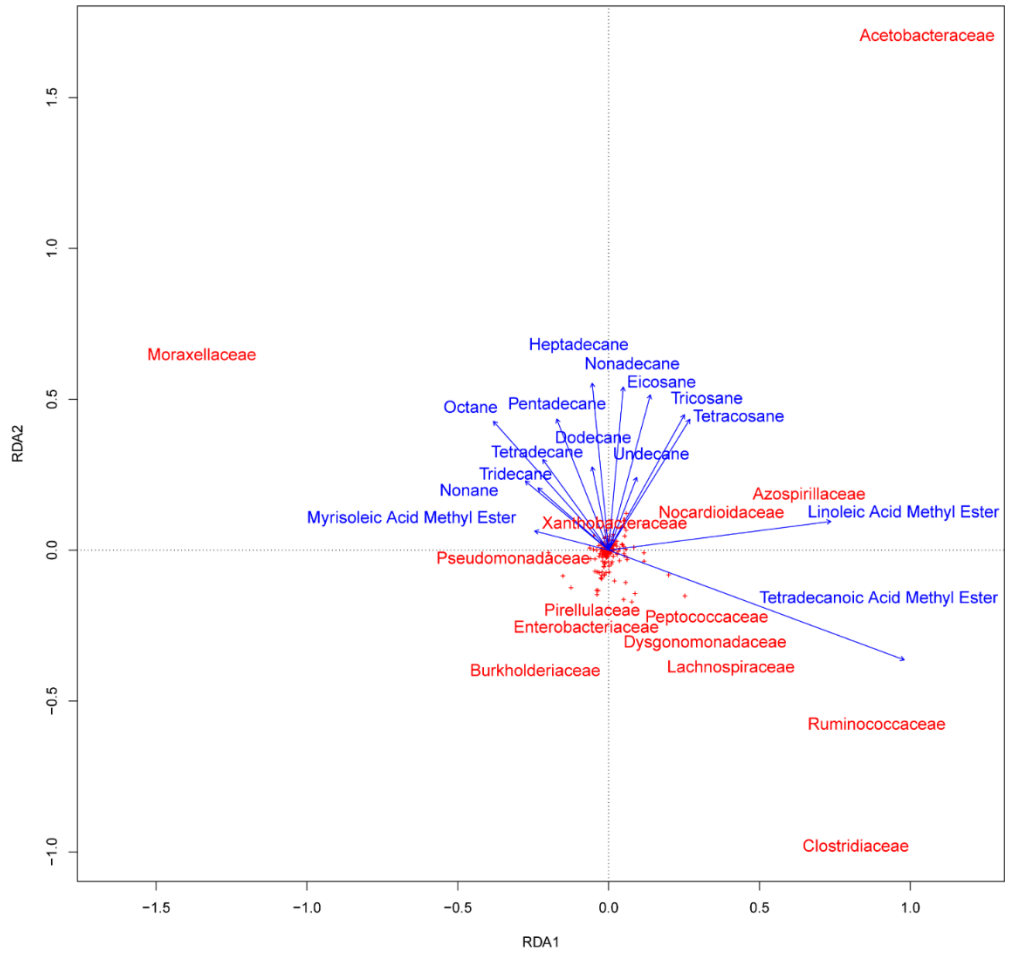

FIG 3.5. Redundancy analysis (RDA) of the Hellinger-transformed bacterial populations constrained by the fuel composition. Bacterial families are denoted as red text. In this RDA the red crosses are bacterial families that still contribute to this ordination space, but not specifically named due to their central clustering indicating a low correlation coefficient. Fuel component variables are represented by blue vectors. Blue vectors lengths indicate the relative weight of a fuel component in the ordination.

Table 3.1. Forward selection of significant ($p \leq 0.05$) fuel variables based on an adonis permutational multivariate analysis of variance on the bacterial Hellinger transformed taxonomic data.

Fuel Component	Mean Squares	F. Model	R^2	Pr(>F)
Heptane	0.190	1.177	0.012	0.300
Octane	0.656	4.076	0.042	0.001
Nonane	0.505	3.137	0.032	0.003
Decane	0.297	1.849	0.019	0.045
Undecane	0.142	0.879	0.009	0.523
Dodecane	0.307	1.907	0.020	0.044
Tridecane	0.342	2.121	0.021	0.041
Tetradecane	0.617	3.835	0.040	0.001
Pentadecane	0.313	1.946	0.020	0.050
Hexadecane	0.389	2.415	0.025	0.019
Heptadecane	0.283	1.757	0.018	0.080
Octadecane	0.154	0.955	0.009	0.484
Nonadecane	0.296	1.840	0.019	0.058
Eicosane	0.145	0.902	0.009	0.508
Heneicosane	0.213	0.213	0.014	0.188
Docosane	0.466	2.896	0.030	0.005
Tricosane	0.293	1.817	0.019	0.051
Tetracosane	0.329	2.040	0.021	0.039
Pentacosane	0.366	2.274	0.024	0.020
Hexacosane	0.489	3.033	0.031	0.004

Heptacosane	0.149	0.921	0.010	0.493
Undecanoic Acid ME	0.238	1.475	0.015	0.126
Dodecanoic Acid ME	0.276	1.715	0.018	0.080
Myrisoleic Acid ME	0.328	2.035	0.021	0.025
Tetradecanoic Acid ME	0.365	2.264	0.023	0.018
Pentadecenoic Acid ME	0.234	1.451	0.015	0.157
Palmitoleic Acid ME	0.233	1.447	0.015	0.133
Palmitic Acid ME	0.101	0.631	0.007	0.817
Heptadecenoic Acid ME	0.235	1.461	0.015	0.147
Linoleic Acid ME	0.519	3.222	0.033	0.002
Oleic Acid ME	.0165	1.022	0.011	0.403
Stearic Acid ME	0.148	0.917	0.009	0.486
Arachidonic Acid ME	0.226	1.401	0.145	0.164
Eicosapentaenoic Acid ME	0.204	1.264	0.013	0.246
Eicosadienoic Acid ME	0.176	1.090	0.011	0.356
Eicosadenoic Acid ME	0.219	1.363	0.014	0.161
Eicosanoic Acid ME	0.260	1.615	0.017	0.098
Arachidic Acid ME	0.207	1.284	0.013	0.224

Heneicosanoic Acid ME	0.126	0.781	0.008	0.648
Docosahexaenoic Acid ME	0.117	0.727	0.008	0.675
Docosadienoic Acid ME	0.218	1.346	0.014	0.175
Tricosanoic Acid ME	0.117	0.725	0.007	0.666
Tetracosenoic Acid ME	0.189	1.175	0.012	0.302
Tetracosanoic Acid ME	0.127	0.788	0.008	0.624

Table 3.2. Correlation coefficients for fuel compounds for RDA1 and RDA2 axes for the bacterial RDA plot.

Fuel Component	RDA1	RDA2
Heptane	0.077	0.005
Octane	-0.102	0.230
Nonane	-0.018	0.178
Decane	0.052	0.076
Undecane	0.030	0.050
Dodecane	-0.049	0.094
Tridecane	-0.141	0.127
Tetradecane	-0.137	0.205
Pentadecane	-0.148	0.286
Hexadecane	-0.183	0.370
Heptadecane	-0.153	0.375
Octadecane	-0.148	0.384
Nonadecane	-0.128	0.375
Eicosane	-0.077	0.373
Heneicosane	0.192	-0.010
Docosane	-0.017	0.367
Tricosane	0.030	0.362
Tetracosane	0.069	0.384
Pentacosane	0.200	0.347
Hexacosane	0.389	0.119
Heptacosane	0.294	0.107

Undecanoic Acid ME	0.052	-0.231
Dodecanoic Acid ME	0.107	-0.120
Myrisoleic Acid ME	-0.148	0.180
Tetradecanoic Acid ME	0.492	-0.202
Pentadecenoic Acid ME	0.383	-0.228
Palmitoleic Acid ME	0.047	0.076
Palmitic Acid ME	0.420	-0.146
Heptadecenoic Acid ME	-0.321	0.244
Linoleic Acid ME	0.447	-0.155
Oleic Acid ME	0.177	-0.170
Stearic Acid ME	0.451	-0.239
Arachidonic Acid ME	-0.002	-0.035
Eicosapentaenoic Acid ME	0.075	-0.025
Eicosadienoic Acid ME	0.242	-0.129
Eicosadenoic Acid ME	-0.839	-0.275
Eicosanoic Acid ME	0.306	0.078
Arachidic Acid ME	0.313	-0.211
Heneicosanoic Acid ME	0.123	-0.032
Docosahexaenoic Acid ME	0.019	-0.042
Docosadienoic Acid ME	0.100	-0.130
Tricosanoic Acid ME	0.100	-0.149
Tetracosenoic Acid ME	0.124	0.023
Tetracosanoic Acid ME	0.268	-0.158

The fungal taxonomic data was also used to determine correlations between the fungal populations and fuel composition (FIG 3.6). The prominent fungal taxa, Trichocomaceae, was found to be positively correlated with fuels containing higher concentrations of FAME. Debaryomycetaceae was found to be prominent in fuels containing higher concentrations of pentadecanoic and oleic acid methyl acids. The Debaryomycetaceae were also found in fuels containing more mid-chain n-alkanes pentadecane and hexadecane. The RDA of the fungal taxa based on fuel composition had a R^2 value of 0.45 with $p = 0.005$. Based on this RDA, the fungal family Trichocomaceae had no correlation with the FAME pentadecanoic acid methyl ester.

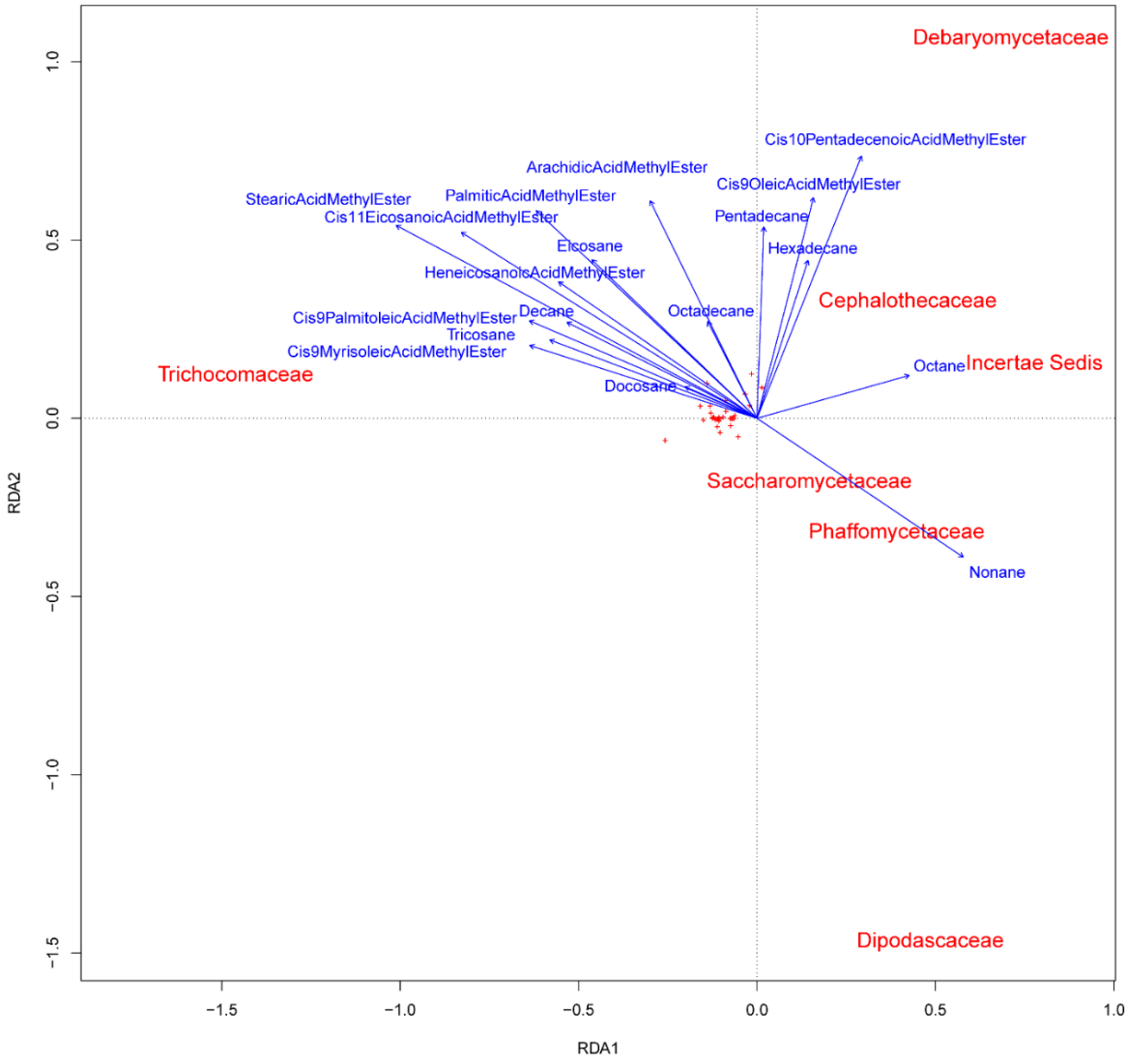

FIG 3.6. Redundancy analysis (RDA) of the Hellinger-transformed fungal communities constrained by the fuel composition. Fungal families are denoted as red text. In this RDA the red crosses are fungal families that still contribute to this ordination space, but not specifically named due to their central clustering indicating a low correlation coefficient. Fuel component variables are represented by blue vectors. Blue vectors lengths indicate the relative weight of a fuel component in the ordination.

Table 3.3. Forward selection of significant ($p \leq 0.05$) fuel variables based on an adonis permutational multivariate analysis of variance on the fungal Hellinger transformed taxonomic data.

Fuel Component	Mean Squares	F. Model	R^2	Pr(>F)
Heptane	0.162	1.774	0.017	0.125
Octane	0.389	4.269	0.040	0.003
Nonane	0.257	2.819	0.026	0.019
Decane	0.258	2.823	0.027	0.025
Undecane	0.100	1.092	0.010	0.377
Dodecane	0.091	0.993	0.009	0.449
Tridecane	0.176	1.932	0.018	0.101
Tetradecane	0.082	0.895	0.008	0.504
Pentadecane	0.223	2.438	0.023	0.049
Hexadecane	0.276	3.031	0.029	0.018
Heptadecane	0.092	1.009	0.009	0.441
Octadecane	0.458	5.019	0.047	0.002
Nonadecane	0.189	2.071	0.195	0.083
Eicosane	0.544	5.963	0.056	0.001
Heneicosane	0.190	2.087	0.020	0.064
Docosane	0.309	3.384	0.032	0.012
Tricosane	0.337	3.698	0.035	0.005
Tetracosane	0.131	1.437	0.014	0.211
Pentacosane	0.193	2.118	0.020	0.084
Hexacosane	0.111	1.219	0.015	0.300

Heptacosane	0.082	0.898	0.008	0.501
Undecanoic Acid ME	0.050	0.549	0.005	0.754
Dodecanoic Acid ME	0.030	0.331	0.003	0.928
Myrisoleic Acid ME	0.543	5.962	0.056	0.001
Tetradecanoic Acid ME	0.099	1.089	0.102	0.385
Pentadecenoic Acid ME	0.059	4.132	0.038	0.006
Palmitoleic Acid ME	0.295	3.236	0.030	0.011
Palmitic Acid ME	0.240	2.982	0.027	0.046
Heptadecenoic Acid ME	0.162	1.774	0.017	0.120
Linoleic Acid ME	0.134	1.473	0.014	0.199
Oleic Acid ME	0.345	3.782	0.036	0.010
Stearic Acid ME	0.262	2.877	0.027	0.020
Arachidonic Acid ME	0.056	0.610	0.006	0.748
Eicosapentaenoic Acid ME	0.184	2.018	0.019	0.092
Eicosadienoic Acid ME	0.114	1.245	0.012	0.307
Eicosadenoic Acid ME	0.306	3.354	0.032	0.006
Eicosanoic Acid ME	0.101	1.108	0.010	0.367
Arachidic Acid ME	0.224	2.460	0.023	0.041

Heneicosanoic Acid ME	0.231	2.530	0.024	0.044
Docosahexaenoic Acid ME	0.038	0.412	0.004	0.877
Docosadienoic Acid ME	0.089	0.976	0.009	0.441
Tricosanoic Acid ME	0.069	0.760	0.007	0.603
Tetracosenoic Acid ME	0.091	1.000	0.009	0.433
Tetracosanoic Acid ME	0.097	1.067	0.010	0.418

Table 3.4. Correlation coefficients for fuel compounds for RDA1 and RDA2 axes for the fungal RDA plot.

Fuel Component	RDA1	RDA2
Heptane	0.184	0.030
Octane	0.047	-0.115
Nonane	0.004	-0.178
Decane	-0.011	-0.067
Undecane	-0.036	-0.035
Dodecane	-0.046	-0.073
Tridecane	-0.068	-0.106
Tetradecane	-0.030	-0.153
Pentadecane	-0.020	-0.214
Hexadecane	-0.042	-0.247
Heptadecane	-0.020	-0.256
Octadecane	0.001	-0.228
Nonadecane	0.009	-0.230
Eicosane	0.084	-0.220
Heneicosane	-0.007	-0.207
Docosane	0.169	-0.232
Tricosane	0.192	-0.251
Tetracosane	0.188	-0.258
Pentacosane	0.227	-0.217
Hexacosane	0.290	-0.200
Heptacosane	0.265	-0.027

Undecanoic Acid ME	0.093	0.146
Dodecanoic Acid ME	-0.062	0.121
Myrisoleic Acid ME	0.080	-0.081
Tetradecanoic Acid ME	0.170	0.114
Pentadecenoic Acid ME	-0.172	-0.297
Palmitoleic Acid ME	0.022	0.122
Palmitic Acid ME	0.168	0.050
Heptadecenoic Acid ME	-0.012	-0.165
Linoleic Acid ME	0.180	0.005
Oleic Acid ME	-0.035	0.121
Stearic Acid ME	0.127	0.026
Arachidonic Acid ME	-0.097	0.177
Eicosapentaenoic Acid ME	-0.051	0.179
Eicosadienoic Acid ME	0.249	-0.089
Eicosadenoic Acid ME	-0.312	0.352
Eicosanoic Acid ME	0.332	-0.162
Arachidic Acid ME	0.125	-0.079
Heneicosanoic Acid ME	0.118	-0.044
Docosahexaenoic Acid ME	-0.004	0.215
Docosadienoic Acid ME	0.287	-0.024
Tricosanoic Acid ME	0.173	-0.078
Tetracosenoic Acid ME	0.228	-0.127
Tetracosanoic Acid ME	0.195	-0.145

Physiological Characterization of Isolates to Test Correlations Predicted from Fungal RDA

After performing RDA many correlations were discovered between both bacterial and fungal communities and fuel composition. Prior work in this lab has yielded representative fungal isolates from contaminated fuels and were used to test some of the predicted correlations from the fungal RDA (Chapter 2). The filamentous fungus *Paecilomyces* was found to be able to grow successfully on palmitoleic acid methyl ester as a sole carbon and energy source; however, it was unable to grow using pentadecanoic acid methyl ester as a sole carbon source. Additionally, *Wickerhamomyces* was able to grow using both palmitoleic and pentadecanoic acid methyl esters as sole carbon and energy sources (Fig 3.7).

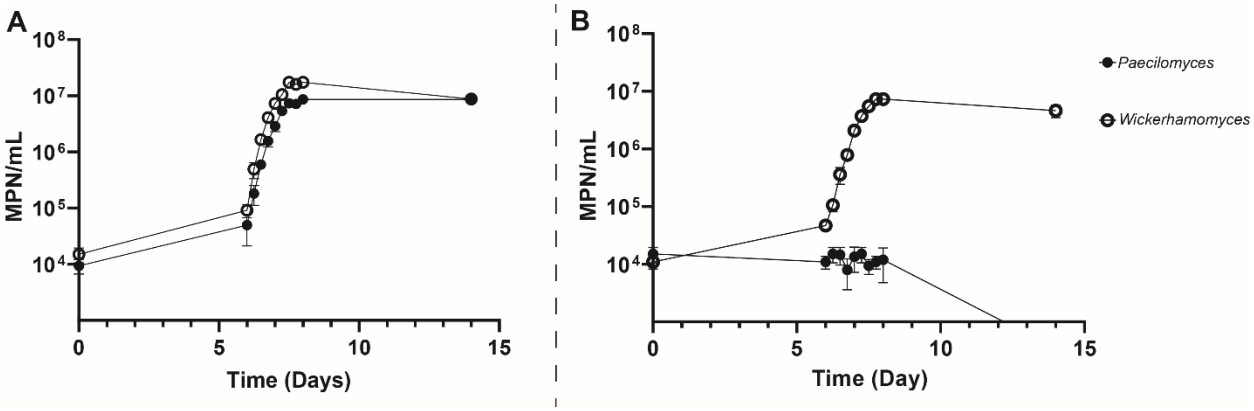

FIG 3. 7. Growth curve of the fungal isolates *Paecilomyces* AF001 (Filled circles; Trichocomaceae) and *Wickerhamomyces* SE3 (Open circles; Debaryomycetaceae) when grown on palmitoleic acid methyl ester as a sole carbon and energy source. Error bars represent standard deviation for mean *Paecilomyces* AF001 or *Wickerhamomyces* SE3 (n=3). **B:** Growth curve of the fungal isolates *Paecilomyces* AF001 (Filled circles; Trichocomaceae) and *Wickerhamomyces* SE3 (Open circles; Debaryomycetaceae) when grown on pentadecanoic acid methyl ester as a sole carbon and energy source. Error bars represent standard deviation for mean *Paecilomyces* AF001 or *Wickerhamomyces* SE3 (biological replicates n=3).

Discussion

Microbial communities in any environment can be influenced by numerous factors including the availability of different oxidizable substrates (28). Relationships between the composition of both B20 biodiesel and diesel fuel compositions were used to determine the correlation between specific fuel compounds and microbial community composition. Two of the positive correlations predicted by the redundancy models were between members of the fungal families Trichocomaceae and Debaryomycetaceae and palmitoleic and pentadecanoic acid methyl esters, respectively. These were confirmed by growth studies with the representative isolates *Paecilomyces* AF001 and *Wickerhamomyces* SE3 and palmitoleic and pentadecanoic acid methyl esters as a sole carbon and energy source.

Fuel compositions of biodiesel and diesel fuels were analyzed with GC-MS to identify FAME and n-alkane species and their concentrations. Most of the differences in n-alkanes of biodiesel and diesel fuels can be attributed to the presence of higher chain alkanes (C15-24) vs. lower chain alkanes (C9-C14) (FIG 3.1.). Most of the biodiesel fuel samples clustered in the middle of this PCA due to their low eigenvalues indicating that differences in their n-alkane composition were smaller compared to the diesel fuels. Diesel fuels had more similar FAME profiles, likely because FAME was in much lower abundance when compared to the B20 biodiesel blends. The variation in FAME composition in B20 biodiesel fuels was largely based on the concentration of linoleic, palmitic, oleic, stearic, and linolelaidic acid methyl esters. Different feedstocks used to make biodiesel result in different total percent weights of these FAME (15). The fuels analyzed in this study were chemically diverse, which are also correlated with the microbial community composition of contaminated fuels.

The bacterial populations found in contaminated fuels were much more diverse than the fungal populations (FIG 3.3 & 3.4). However, there were some exceptions as some contaminated fuels contained higher relative abundances of bacteria from the families Acetobacteriaceae and Moraxellaceae. Both bacterial families have been implicated in diesel and biodiesel contamination and some representatives have been linked to increased risks of corrosion as the can produce organic acids that pose a risk to infrastructure as they metabolize fuel (12, 29).

Fungal populations were not as diverse as the bacteria even though contamination in the fuels was primarily attributed to fungi. Fungal contamination in sampled fuels was largely comprised of members of the family Trichocomaceae. Although the Trichocomaceae are ubiquitous in nature and normally associated with the decay of fruit juices and foods, they have also been linked to biodiesel degradation and increasing the risk of MIC (13, 30). Members of the fungal family Debaryomycetaceae were also a primary contaminant in fuels and had blooming events, although to a lower extent than Trichocomaceae. This yeast family has previously been used in fermentation processes in the food industry but has also been recently linked to fuel degradation and increases in microbiologically influenced corrosion when degrading fuel components (12, 13, 31).

Different microbial populations in fuels can have different fouling properties, different metabolic processes, and pose different risks to infrastructure as they metabolize fuels (32, 33). To determine how fuel composition can lead to different microbial communities in contaminated fuels correlations were examined between fuel components and bacterial or fungal populations. To address these questions redundancy analysis (RDA) was performed to determine if there were any correlations between the microbial taxa and fuel components present in the fuels. Members of the bacterial family Acetobacteraceae were positively correlated to fuels that contained higher

alkane chain lengths than others as well as with linoleic acid methyl ester. Some bacteria, such as *Pseudomonas* and *Acinetobacter*, tend to primarily degrade alkanes with higher chain lengths (C19+) substrates (22, 34). Although it is still not clearly understood what hydrocarbon substrates Acetobacteriaceae utilize, they have been readily found in contaminated diesel and biodiesel fuels (12, 35, 36). This could indicate that these bacteria can potentially degrade higher chain alkanes (C19-24) potentially providing them a niche in fuels containing more long chain alkanes. Additionally, the bacterial family Moraxellaceae was found to be positively correlated with smaller alkane chains (C8-14) and myrisoleic acid methyl ester (FIG 3.5). Members of this bacterial family have also been observed in contaminated fuels; however, like the Acetobacteraceae, little is known about which compounds they specifically metabolize in fuels (37, 38). The correlation between their abundance in fuels containing with alkanes could be indicative of a preference for mid to long alkanes.

The same approach was used to test for correlations between the abundance of fungal populations and fuel components. Trichocomaceae was the prominent fungal population in contaminated fuels and correlated with fuels containing more fatty acid methyl esters including palmitoleic acid methyl ester. Members of the yeast family Debaryomycetaceae were more abundant in fuels containing more Cis-10-Pentadecenoic Acid Methyl Esters and Cis-9-Oleic Acid Methyl Esters (FIG 3.6). The ordination of these two fungal families in our RDA suggest that they may have differences in which fuel components they can or prefer to metabolize. This is of interest here because members of the Trichocomaceae and Debaryomycetaceae have been implicated in contamination of diesel and biodiesel fuels and appear to be a common fuel contaminant across the continental U.S. when fungal contamination is a problem (12, 39).

Representative organisms from both fungal families have recently been implicated in increased corrosion risks when they metabolize B20 biodiesel as a sole carbon and energy source (13).

The potential differences in fuel component utilization between the fungal families Trichocomaceae and Debaryomycetaceae predicted by our RDA were directly tested in culture studies using two representative taxa, *Paecilomyces* AF001 and *Wickerhamomyces* SE3, isolated from contaminated B20 biodiesel (13). These studies were corroborated with the predictions of the RDA. *Wickerhamomyces* SE3 grew well on both palmitoleic and pentadecanoic acid methyl ester, but *Paecilomyces* could only grow on palmitoleic acid methyl ester. Both FAME compounds contain one degree of unsaturation, but palmitoleic acid methyl ester has an even number carbon chain (C16) while pentadecanoic acid methyl ester has an odd number carbon chain (C15). Additionally, even though both have one degree of saturation, the double bond in palmitoleic acid methyl ester is at C9, while pentadecanoic acid methyl ester has a double bond at C10, an odd and an even numbered carbon in the fatty acid chains. Not all organisms are able to metabolize odd numbered fatty acids and more enzymes are needed to metabolize the double bonds in the fatty acid chain (40). Odd numbered bonds are typically activated by isomerases while the double bonds on even numbered chains must be activated by isomerases and reductases which *Paecilomyces* may not have and could explain why it was never able to reach log phase during the growth curve.

Availability of different carbon substrates can influence microbial community composition (41–43). Correlations between both bacterial and fungal populations in contaminated fuels and the composition of FAME and alkanes in those fuels were investigated and tested to determine the validity of some of the correlations. While carbon substrates in an environment can drive community structure, it is important to note that this is not the only driver.

Biotic and abiotic factors such as symbiotic relationships between microorganisms can also dictate the community or the amount of water present in a contaminated fuel tank. Other factors can also influence communities such as what material fuel storage tanks are made from and availability of nutrients such as phosphorous and nitrogen. This work describes how fuel can impact microbial contamination in storage tanks, more work will need to be done to fully understand the microbial ecology in contaminated biodiesel and diesel storage tanks. Unveiling the factors that contribute to microbial communities in contaminated fuels provides insights that can be used to dictate which biofuel feedstocks can be used to generate biodiesel and ULSD fuels. This in turn can lead to renewable biodiesel fuel sources that are less prone to contamination from organisms known to contribute to microbiologically influenced corrosion.

Materials and Methods

Fuel Tank Sampling Protocol

Fuel from storage tanks was collected using a stainless-steel Bacon Bomb (Koehler™ Instrument Petroleum Bacon Bomb Sampler, Fisher Scientific) that was field disinfected using 100% isopropanol prior to insertion into the tanks. Once disinfected the Bacon Bomb was inserted into the fuel storage tanks and 500 mL of fuel was collected from the bottom of the tanks and transferred into a sterile 1L Schott Bottle. Immediately after collection another sterile 1L Schott Bottle was fixed with a polyether sulfone Steritop Filter Unit™ with a pore size of 0.45 μm and the fuel was filtered through. Fuel was collected from across the continental U.S. and was contingent on obtaining access to contaminated fuel storage tanks. A map containing an overview of our fuel samples from across the U.S. is described below (FIG 3.8). Fuel descriptions and fuel component characterizations are in the APPENDIX.

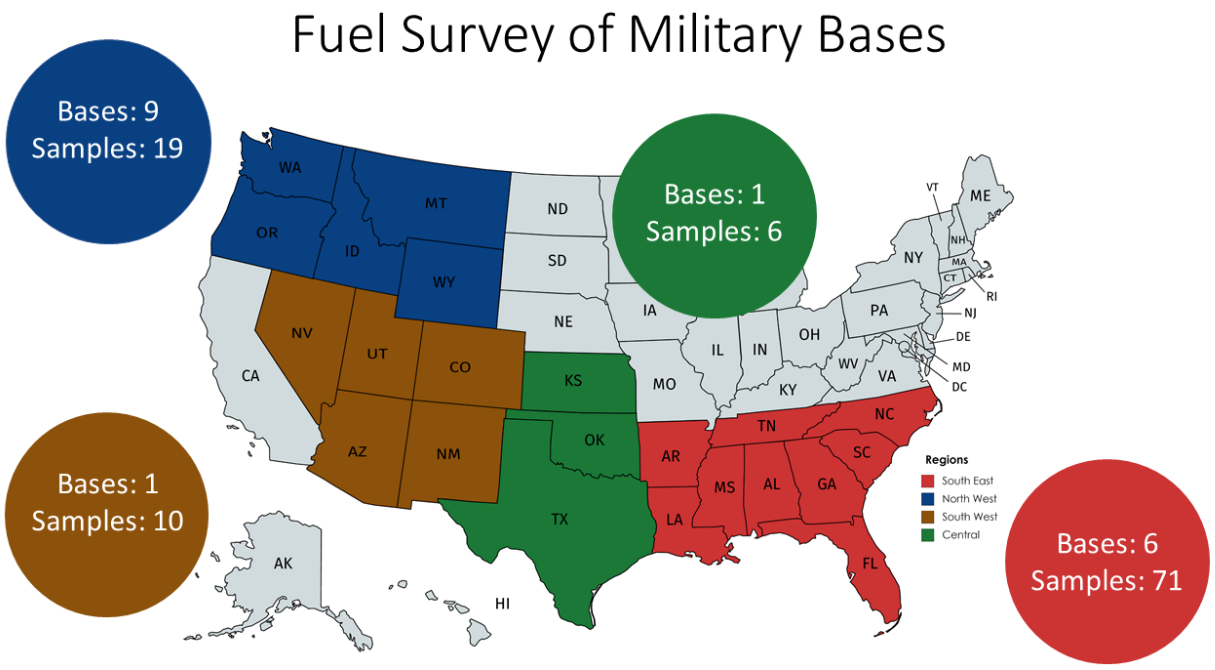

FIG 3.8. A map on the U.S where fuel samples were obtained for this analysis. Due to DoD confidentiality a rough overview of where the fuel samples are shown representing different regions in the U.S. from the Southeast (Red), Northwest (Blue), Southwest (Brown), and Central (Green). Map generated from https://mapchart.net/usa.html.

DNA Extraction, SSU rRNA Gene Library Preparation, and Sequencing

Following filtration of the fuel the polyether sulfone Steritop Filter Unit™ filter was removed using sterile disposable scalpels. This filter was then cut into four quarters using sterile disposable scalpels and 3 of those quarters were individually placed into Zymo Quick-DNA Fecal/Soil Microbe ZR BashingBead™ Lysis Tube with DNA/RNA Shield™ and Lysis/Stabilization solution (Zymo Research Co, Irvine, CA, United States) creating three technical replicates for extraction and sequencing. The fourth quarter of the filter was used to quantify contamination through MPN analysis and isolated representative isolates from the fuel. The biomass in the BashingBead™ tubes were then physically lysed in the field using a custom designed reciprocating saw in the field and sent back to the University of Oklahoma for further

processing. Samples were shipped at ambient temperature in the BashingBead™ tubes with the DNA/RNA shield and typically took 2-3 days to arrive in the lab via ground shipping. Samples shipped back to the lab were immediately extracted once they arrived in the lab and DNA extraction proceeded via the Zymo Quick-DNA Fecal/Soil Microbe kits manufacturer protocol.

Small subunit (SSU) rRNA libraries were generated by amplifying the extracted DNA using PCR primers that spanned the V4 and V5 hypervariable regions of the 16S ribosomal RNA gene between position 515 and 926 (*Escherichia coli* numbering), which produced a ~400 bp fragment for Bacteria and Archaea and ~600 bp fragments for the Eukarya 18S rRNA gene. These primers were chosen due to them being able to amplify a broad distribution of SSU rRNA genes from all three domains of life (44). The forward primer 515F-Y (5'-**GTA AAA CGA CGG CCA GC**CG TGY CAG CMG CCG CGG TAA-3') contains the M13 forward primer (in bold) fused to the gene-specific forward primer (non-bold). The reverse primer 926R (5'-CCG YCA ATT YMT TTR AGT TT-3') was unmodified from Parada et al. (44). 5 PRIME HotMasterMix (Quanta Biosciences, Beverly, MA, United States) was used for all library prep PCR reactions with a final reaction volume of 50 µL. Thermocycler conditions included a 3 min heating step at 95°C followed by 30 cycles of 95°C for 45 s, 50°C for 45 s, 68°C for 90 s, and a final extension of 68°C for 5 min. Reactions were then purified with Sera-Mag™ paramagnetic beads (MilliporeSigma, St. Louis, MO) at a final concentration of 0.8x. Following purification 4 µL of PCR product was used in a barcoding reaction affixing a unique 12 bp barcode to each library in 50 µL reactions. Unique barcode primers were obtained from Integrated DNA Technology (Coralville, Iowa, U.S.) that affixed to the M13 forward primer sequence on the amplicons. During a PCR reaction with the following conditions: with a 3-minute heating step at 95°C for 3 min followed by 6 cycles of 95°C for 45 s, 50°C for 45 s, 68°C for 90 s, and a final

extension of 68°C for 5 min. Once barcoded these reactions were again purified using Sera-Mag™ beads in a final volume of 50 µL. DNA of these purified samples were than quantified using QuBit™ dsDNA HS assay kit (Thermo Fisher Scientific Inc., Waltham, MA, United States) and pooled in equimolar amounts before concentrated using an Amicon® Ultra 0.5 mL centrifugal filter with Ultracel-30K membrane (Millipore Sigma, Billerica, MA, United States) to a final volume of 80 µL. To mitigate the effects of reagent contamination triplicate extraction blanks (DNA extraction with no sample addition) and negative PCR controls (PCR with no template DNA added) were sequenced as well. The pooled prepared libraries were than submitted for sequencing on the Illumina MiSeq (Illumina Inc., San Diego, CA, United States) using V2 PE250 chemistry at the University of Oklahoma Consolidated Core Lab.

Quantification and Characterization of FAME and Alkanes in Fuels

Biodiesel and diesel fuels that were collected from fuel storage tanks were analyzed to determine the amount of FAME and n-alkanes in the fuel. Following filtration of the fuel collected from the field the fuel was sent back to the University of Oklahoma for analysis using a Shimadzu GCMS-QP2010 (Shimadzu, Kyoto, Japan). Fuel was initially diluted using GC grade hexane in a 1:10 ratio which was then analyzed via GC-MS. These fuel sample were run in triplicates on the GC-MS producing technical replicates for each fuel sample using an AOC-20i autosampler. Briefly, the autosampler injection syringe was rinsed after each 1µL injection with 100% ethanol three times. Once the injection syringe was rinsed with the ethanol it rinsed itself once with the diluted fuel sample prior to the actual injection into the GCMS. A split injection was used on the GC-MS with a split ratio of 10 making the final dilution of the fuels 1:100.

A Rtx-5MS column (Restek) was used in the GC with a length of 30.0 m, thickness of 0.25 µm and a diameter of 0.25 µm. The injection temperature was set at 300°C while the initial

column temperature was 40.0°C. The column temperature was held at this temperature for 1.5 minutes upon injection. After the initial hold the temperature of the column increased by 10°C per minute to a final temperature of 300°C. Once it reached 300°C the column was held at this temperature for 2.75 minutes. The carrier gas used for this analysis was high purity helium at a linear velocity of 36.8 cm per second. Mass spectra were analyzed in scan mode with a solvent cut time of 2.75 min, an ion source temperature of 200°C and an interface temperature of 300°C. Scans from the MS were performed with event times of 0.25 seconds with a scan speed of 2000. Spectra between m/z 35 and 500 were used for this analysis.

To quantify the concentration of fuel components in the samples, external standards were obtained for FAME (Supelco 37 FAME Mix) and n-alkane (C7-C40 Saturated Alkanes Standard) to generate standard curves of the fuel components to quantify parts per million. These standards were diluted in hexane in ratios of 1:50, 1:25, and 1:10 to generate a three-point standard curve of these fuel components. The limit of detection of these alkane and FAME compounds were 0.2 PPM. Once these standard curves were generated for each of these fuel components the unknown fuel samples ion intensities were compared to the known standard curves to generate parts per million of FAME and n-alkane components.

Analysis of SSU rRNA Gene Sequencing Libraries

Small subunit rRNA gene analyses were carried out in QIIME2 version 2019.10.0 (45). Briefly, barcodes from the sequences were extracted, and samples were demultiplexed prior to operational taxonomic unit (OTU) clustering. Chimera sequences and singletons were filtered out prior to clustering using the USEARCH64 reference database. Representative sequences for each OTU was assigned a taxonomic identity with the QIIME2 sklearn classifier against the Silva 132 database clustered to a 97% identity (46, 47). Following this, sequences were separated

to generate feature tables that contained separated 16S and 18S rRNA data. For 16S rRNA and 18S rRNA phylogenetic trees were generated with Fasttree 2 (48). Datasets were rarefied to 1000 sequences per sample for Bacteria and 250 sequences per sample for Eukarya. Rarefaction was done due to the many samples varying library sizes to better compare the fuel communities over this longitudinal study (52). These data were then converted to biom files and exported for further analyses in R. (49)

Redundancy Analyses (RDA)

The fuel and taxonomic relative abundance data were used to generate redundancy analyses to determine how fuel components correlate to microbial community composition. Initial the taxonomic data was imported in R and underwent a Hellinger transformation to give low weights to rare taxa in the biom files. Once this was done a forward selection of fuel variables was done using an adonis test in R to determine which fuel components had a significant ($p<0.05$) impact on community composition. Once this was done an RDA was generated by using the transformed community data and the significant fuel components determined by the adonis test to correlate how microbial communities correlate with fuel components in diesel and biodiesel.

Validation of the Fungal Redundancy Analysis Model

Following the generation of the redundancy analyses FAME components that were found to have strong correlations with Trichocomaceae and Debaryomycetaceae were used to determine how well representative organisms isolated from contaminated fuels could grow on these FAME as the sole carbon and energy sources. Prior work from our lab has yielded the fungal isolate *Paecilomyces* AF001 and *Wickerhamomyces* SE3 which are representative of the fungal families Trichocomaceae and Debaryomycetaceae respectively. A spore suspension of the

filamentous fungus *Paecilomyces* AF001 and a cell suspension of the yeast *Wickerhamomyces* SE3 were used to inoculate a 1:20 FAME substrate in artificial sump water (ASW, per L: 0.015g NaCl, 0.035g NaF, 0.02g $CaCl_2$, 0.018g KNO_3, 0.01g Na_2SO_4, 0.015g $(NH_4)_2SO_4$, and 0.017g K_2HPO_4) (50).

To prepare a spore suspension, a glycerol stock of this isolate was struck onto a Hestrin Schramm (HS) agar medium (per L: 20g glucose, 5g yeast extract, 5g peptone, 2.7g Na_2HPO_4, 1.15g citric acid, 7.5g Agar; pH adjusted to 6.0 with diluted HCl or NaOH) and incubated at 25°C for 7 days (51) After growth 5mL of phosphate buffered saline was added overtop the HS agar containing hyphael growth of *Paecilomyces* AF001 and an inoculating loop was used to scrape off the fungal growth. This PBS solution was then collected from the agar plate and filtered through a 10 µm pore size polyether sulfone filter to separate the spores from the hyphael biomass. The filtrate containing spores was then centrifuged at 10,000 x RCF for 1 minute. The supernatant was decanted, and sterile PBS was added back to the spore pellet and vortexed to resuspend the spores. This wash step was repeated for a total of three washes. Spore concentrations were determined using a Petroff-Hausser counting chamber then diluted to adjust the inoculum concentration to $1x10^4$ spores/mL.

To produce a suspension of yeast cells *Wickerhamomyces* SE3 was grown in HS broth for 48 hours and centrifuged at 10,000 RCF to pellet cell mass. Following this the supernatant was decanted and sterile PBS was added to the cell pellet and vortexed to resuspend the cells. This was step was repeated for a total of three washes. Cell concentrations were again determined using a Petroff-Hausser counting chamber and diluted to adjust the initial inoculum concentration to $1x10^4$ cells/mL.

These isolates were grown on palmitoleic and pentadecanoic acid methyl esters (Fisher Scientific, Waltham, MA) to determine their capacity on using these substrates for growth. A total volume of 5 mL 1:20 FAME and artificial sump water mixture was made and inoculated with 10^4 spores or cells per mL for T=0. Growth was measured by destructively sampling triplicate test tubes at time points 0, 6, 6.25, 6.5, 6.75, 7, 7.25, 7.5, 7.75, 8, and 14 days at room temperature and generating MPNs.

Statistical Analyses and Data Visualization

Statistical analyses and figure generation was carried out in R version 3.3.3 and GraphPad Prism 8.3.0. Significant differences from fuel components that contributed to microbial community structure were detemined by using an adonis test on the Hellinger transformed taxonomic data.

Acknowledgements

We acknowledge the men and women of the US Air Force and Civilian Personnel at US Air Force bases; their cooperation and assistance were critical to this research. Additionally, we would like to thank Emily Junkins for insightful comments during the development of this manuscript. This work was supported by the Air Force Research Laboratory Biological Materials and Processing Research Team, Materials and Manufacturing Directorate and the U.S. Department of Defense Office of Corrosion Policy & Oversight Technical Corrosion Collaboration (Grant # FA7000-15-2-0001).

Works Cited

1. U.S. Department of Energy. 2021. Biodiesel Income Tax Credit.

2. U.S. Energy Information Administration. 2021. Annual Energy Outlook 2021 Petroleum PDF.

3. U.S. Department of Energy. 2021. Alternative Fuels Data Center.

4. U.S. Department of Energy. 2021. Biodiesel Benefits and Considerations.

5. Demirbaş A. 2008. Biodegradability of Biodiesel and Petrodiesel Fuels, Energy Sources, Part A: Recovery, Utilization, and Environmental Effects, 31:169-174.

6. Mariano A, Tomasella R, Oliveira L, Angelis D. 2008. Biodegradability of Diesel and Biodiesel Blends. Afr J Biotechnol 7:1323-1328.

7. Dodos GS, Zannikos F. 2013. Microbiological Growth Study of Biodiesel Fuel. Sae Int J Fuels Lubr 6:419–429.

8. Moser B. 2009. Biodiesel Production, Properties, and Feedstocks. In Vitro Cell Dev-Pl 45:229-266.

9. Fuller S, Spikmans V, Vaughan G, Guo C. 2013. Effects of Weathering on Sterol, Fatty Acid Methyl Ester (FAME), and Hydrocarbon Profiles of Biodiesel and Biodiesel/Diesel Blends. Environ Forensics 14:42–49.

10. Owsianiak M, Chrzanowski Lukasz, Szulc A, Staniewski J, Olszanowski A, Olejnik-Schmidt AK, Heipieper HJ. Biodegradation of Diesel/Biodiesel Blends by a Consortium of Hydrocarbon

Degraders: Effect of the Type of Blend and the Addition of Biosurfactants. Bioresource Technol 100:1497-1500.

11. Rojo F. 2010. Enzymes for Aerobic Degradation of Alkanes, p 781-797. In Timmis KN (eds), Handbook of Hydrocarbon and Lipid Microbiology, Springer, Berlin, Heidelberg.

12. Stamps BW, Bojanowski CL, Drake CA, Nunn HS, Lloyd PF, Floyd JG, Emmerich KA, Neal AR, Crookes-Goodson WJ, Stevenson BS. 2020. In situ Linkage of Fungal and Bacterial Proliferation to Microbiologically Influenced Corrosion in B20 Biodiesel Storage Tanks. Front Microbiol 11:197.

13. Floyd JG, Stamps BW, Goodson WJ, Stevenson BS. 2021. Locating and Quantifying Carbon Steel Corrosion Rates Linked to Fungal B20 Biodiesel Degradation. Appl Environ Microb AEM0117721.

14. Lee J, Ray R, Little BJ. 2010. An Assessment of Alternative Diesel Fuels: Microbiological Contamination and Corrosion Under Storage Conditions. Biofouling 6:623-635.

15. Hoekman KS, Broch A, Robbins C, Ceniceros E, Natarajan M. 2012. Review of Biodiesel Composition, Properties, and Specifications. Renew Sustain Energy Rev 16:143–169.

16. Peraza-Reyes L, Berteaux-Lecellier V. 2013. Peroxisomes and Sexual Development in Fungi. Front Physiol 4:244.

17. Sousa DZ, Balk M, Alves M, Schink B, McInerney MJ, Smidt H, Plugge CM, Stams AJM. 2010. Handbook of Hydrocarbon and Lipid Microbiology 963–980.

18. National Academies of Sciences, Engineering, and Medicine. 2016. Spills of Diluted Bitumen from Pipelines: A Comparative Study of Environmental Fate, Effects, and Response, p. 21–33. *In* Chemical and Physical Properties of Crude Oils. The National Academies Press, Washington, DC.

19. Demirbas A. 2008. Distillation Properties of Various Diesel Oils. Energy Sources, Part A: Recovery, Utilization, and Environmental Effects 30:1484–1490.

20. Pitz WJ, Mueller CJ. 2011. Recent Progress in the Development of Diesel Surrogate Fuels. Prog Energ Combust 37:330–350.

21. Hasinger M, Scherr K, Lundaa T, Brauer L, Zach C, Loibner A. 2012. Changes in iso-and n-Alkane Distribution During Biodegradation of Crude Oil Under Nitrate and Sulphate Reducing Conditions. J Biotechnol 157:490-498.

22. Ciric L, Philp J, Whiteley AS. 2010. Hydrocarbon Utilization Within a Diesel-Degrading Bacterial Consortium. FEMS Microbiol Lett 2:116-122.

23. Konopka A, Oliver L, Turco, Jr. RF. 1998. The Use of Carbon Substrate Utilization Patterns in Environmental and Ecological Microbiology. Microbial Ecol 35:103–115.

24. Rinnan R, Bååth E. 2009. Differential Utilization of Carbon Substrates by Bacteria and Fungi in Tundra Soil. Appl Environ Microb 75:3611–3620.

25. Xing W, Lu X, Xu F, Ying J, Chen D, Bai Y. 2019. Linking Microbial Community Structure to Carbon Substrate Chemistry in Soils Following Aboveground and Belowground Litter Additions. Appl Soil Ecol 141:18–25.

26. Liu Q, Tang J, Gao K, Gurav R, Giesy JP. 2017. Aerobic Degradation of Crude Oil by Microorganisms in Soils from Four Geographic Regions of China. Scientific Reports 7:14856.

27. Jia R, Unsal T, Xu D, Lekbach Y, Gu T. 2019. Microbiologically influenced corrosion and current mitigation strategies: A state of the art review. Int Biodeter Biodegr 137:42–58.

28. Goldfarb KC, Karaoz U, Hanson CA, Santee CA, Bradford MA, Treseder KK, Wallenstein MD, Brodie EL. 2011. Differential Growth Responses of Soil Bacterial Taxa to Carbon Substrates of Varying Chemical Recalcitrance. Front Microbiol 2:94.

29. Williamson CHD, Jain LA, Mishra B, Olson DL, Spear JR. 2015. Microbially Influenced Corrosion Communities Associated with Fuel-Grade Ethanol Environments. Appl Microbiol Biot 99:6945–6957.

30. Kotzekidou P. 2014. *Paecilomyces*. *In* Batt C and Tortorello ML (eds) Encyclopedia of Food Microbiology (Second Edition). Article Titles: B 344–350.

31. Wang W, Fan G, Li X, Fu Z, Liang X, Sun B. 2020. Application of *Wickerhamomyces anomalus* in Simulated Solid-State Fermentation for Baijiu Production: Changes of Microbial Community Structure and Flavor Metabolism. Front Microbiol 11:598758.

32. Passman FJ. 2013. Microbial Contamination and its Control in Fuels and Fuel Systems Since 1980 – A Review. Int Biodeter Biodegr 81:88–104.

33. Thomas AO, Leahy MC, Smith JWN, Spence MJ. 2017. Natural Attenuation of Fatty Acid Methyl Esters (FAME) in Soil and Groundwater. Q R Eng Geol Hydroge 50:301-317.

34. Xu X, Liu W, Tian S, Wang W, Qi Q, Jiang P, Gao X, Li F, Li H, Yu H. 2018. Petroleum Hydrocarbon-Degrading Bacteria for the Remediation of Oil Pollution Under Aerobic Conditions: A Perspective Analysis. Front Microbiol 9:2885.

35. U.S. Environmental Protection Agency. 2016. Investigation of Corrosion-Influencing Factors in Underground Storage Tanks with Diesel Service.

36. Xue J, Wu Y, Liu Z, Li M, Sun X, Wang H, Liu B. 2017. Characteristic Assessment of Diesel-degrading Bacteria Immobilized on Natural Organic Carriers in Marine Environment: The Degradation Activity and Nutrient. Sci Rep-uk 7:8635.

37. Révész F, Figueroa-Gonzalez PA, Probst AJ, Kriszt B, Banerjee S, Szoboszlay S, Maróti G, Táncsics A. 2020. Microaerobic Conditions Caused the Overwhelming Dominance of *Acinetobacter* spp. and the Marginalization of *Rhodococcus* spp. in Diesel Fuel/Crude Oil Mixture-amended Enrichment Cultures. Arch Microbiol 202:329–342.

38. Fuentes S, Barra B, Caporaso JG, Seeger M. 2016. From Rare to Dominant: A Fine-Tuned Soil Bacterial Bloom during Petroleum Hydrocarbon Bioremediation. Appl Environ Microb 82:888–896.

39. Ye C, Ching TH, Yoza B, Masutani S, Li Q. 2017. Cometabolic Degradation of Blended Biodiesel by *Moniliella wahieum* Y12T and *Paecilomyces nivea* M1. Int Biodeter Biodegr 125:166-169.

40. Berg JM, Tymoczko JL, Stryer L. 2002. Certain Fatty Acids Require Additional Steps for Degradation. *In* Biochemistry 5th edition. 22.3.

41. Poret-Peterson AT, Albu S, McClean AE, Kluepfel DA. 2019. Shifts in Soil Bacterial Communities as a Function of Carbon Source Used During Anaerobic Soil Disinfestation. Frontiers Environ Sci 6:160.

42. Ghimire R, Norton JB, Stahl PD, Norton U. 2014. Soil Microbial Substrate Properties and Microbial Community Responses under Irrigated Organic and Reduced-Tillage Crop and Forage Production Systems. Plos One 9:103901.

43. Liu M, Sui X, Hu Y, Feng F. 2019. Microbial Community Structure and the Relationship with Soil Carbon and Nitrogen in an Original Korean Pine Forest of Changbai Mountain, China. Bmc Microbiol 19:218.

44. Parada A, Needham DM, Fuhrman JA. 2016. Every Base Matters: Assessing Small Subunit rRNA Primers for Marine Microbiomes with Mock Communities, Time Series and Global Field Samples. Environ Microbiol 5:1403-1414.

45. Bolyen E, Rideout JR, Dillon MR, Bokulich NA, Abnet CC, Al-Ghalith GA, Alexander H, Alm EJ, Arumugam M, Asnicar F, Bai Y, Bisanz JE, Bittinger K, Brejnrod A, Brislawn CJ, Brown CT, Callahan BJ, Caraballo-Rodríguez AM, Chase J, Cope EK, Silva RD, Diener C, Dorrestein PC, Douglas GM, Durall DM, Duvallet C, Edwardson CF, Ernst M, Estaki M, Fouquier J, Gauglitz JM, Gibbons SM, Gibson DL, Gonzalez A, Gorlick K, Guo J, Hillmann B, Holmes S, Holste H, Huttenhower C, Huttley GA, Janssen S, Jarmusch AK, Jiang L, Kaehler BD, Kang KB, Keefe CR, Keim P, Kelley ST, Knights D, Koester I, Kosciolek T, Kreps J, Langille MGI, Lee J, Ley R, Liu Y-X, Loftfield E, Lozupone C, Maher M, Marotz C, Martin BD, McDonald D, McIver LJ, Melnik AV, Metcalf JL, Morgan SC, Morton JT, Naimey AT,

Navas-Molina JA, Nothias LF, Orchanian SB, Pearson T, Peoples SL, Petras D, Preuss ML, Pruesse E, Rasmussen LB, Rivers A, Robeson MS, Rosenthal P, Segata N, Shaffer M, Shiffer A, Sinha R, Song SJ, Spear JR, Swafford AD, Thompson LR, Torres PJ, Trinh P, Tripathi A, Turnbaugh PJ, Ul-Hasan S, Hooft JJJ van der, Vargas F, Vázquez-Baeza Y, Vogtmann E, Hippel M von, Walters W, Wan Y, Wang M, Warren J, Weber KC, Williamson CHD, Willis AD, Xu ZZ, Zaneveld JR, Zhang Y, Zhu Q, Knight R, Caporaso JG. 2019. Reproducible, Interactive, Scalable and Extensible Microbiome Data Science Using QIIME 2. Nat Biotechnol 37:852–857.

46. Edgar RC. 2013. uParse: Highly Accurate OTU Sequences from Microbial Amplicon Reads. Nature Methods 10:996-998.

47. Yilmaz P, Parfrey L, Yarza P, Gerken J, Pruesse E, Quast C, Schweer T, Peplies J, Ludwig W, Glockner F. 2013. The SILVA Ribosomal RNA Gene Database Project: Improved Data Processing and Web-based Tools. Nucl. Acids Res. 41:590-596.

48. Price MN, Dehal PS, Arkin AP. 2010. FastTree 2 – Approximately Maximum-Likelihood Trees for Large Alignments. Plos One 5:9490.

49. R Core Team. 2018. A Language and Environment for Statistical Computing. R Foundation for Statistical Computing. Vienna, Austria.

50. McNamara CJ, Thomas PD, Leard R, Bearce K, Dante J, Mitchell R. 2006. Corrosion of Aluminum Alloy 2024 by Microorganisms Isolated from Aircraft Fuel Tanks. Biofouling 21:257–265.

51. Hestrin S, Schramm M. 1954. Synthesis of Cellulose by *Acetobacter xylinum*. 2. Preparation of Freeze-Dried Cells Capable of Polymerizing Glucose to Cellulose. Biochem J 58:345-352.

52. Cameron E, Schmidt P, Trmblay B, Emelko M, Muller K. 2020. To Rarefy or not to Rarefy: Enhancing Diversity Analysis of Microbial Communities Through Next-generation Sequencing and Rarefying Repeatedly. bioRxiv 2020.09.09.290049.

Chapter 4. Transcriptomic Analysis of *Paecilomyces* AF001 Grown on B20 Biodiesel and Ultra-Low Sulfur Diesel

James G. Floyd[1], Blake W. Stamps[2,3], Bradley S. Stevenson[1]

1 – University of Oklahoma, Department of Microbiology and Plant Biology, Norman OK

2 – 711th Human Performance Wing, Airman Systems Directorate, Air Force Research Laboratory, Wright-Patterson AFB, OH, United States

3 – UES Inc., Integrative Health and Performance Sciences Division, Dayton, OH, United States

Key Words: Transcriptome, Lipase Assay, Fungi, Biodiesel, Ultra-low Sulfur Diesel

Foreword

The research discussed in this chapter was a collaborative effort between Dr. Bradley Stevenson's lab and the Air Force Research Labs. In this study, I performed growth curves in the fuels, conducted lipase assays, extracted RNA, prepared it for sequencing, assisted in the bioinformatics associated with these transcriptomes, generated figures, and wrote the manuscript. Dr. Blake Stamps helped analyze the transcriptomes, generated figures, and assisted in writing and editing this manuscript. Dr. Bradley Stevenson assisted with the experimental design, assisted in the data analysis, and helped write and edit this manuscript.

Abstract

B20 biodiesel is widely used as an alternative to Ultra-Low Sulfur Diesel (ULSD) and contains up to 20% FAME. However, ULSD also can contain up to 5% FAME (B5) and not be labeled as biodiesel. Microbial contamination in B20 biodiesel and B5 ULSD fuels is becoming more prominent as more fatty acid methyl esters (FAME) are added to these fuels. *Paecilomyces* AF001 has been described as a prominent fungus that has fouled biofuel and B5 ULSD fuels across the U.S, but little is known how this organism grows in these different fuels. To gain a better understanding of the metabolic capabilities of this organism, a transcriptomic analysis was conducted using *Paecilomyces* grown on B20 biodiesel and B5 ULSD. Gene expression and lipase activity were measured from multiple time points that correspond to lag, logarithmic, and stationary growth phases. It was found when *Paecilomyces* AF001 was grown on B5 it expressed more of the genes encoding to mono and dioxygenases as compared to growth on B20 biodiesel. When *Paecilomyces* AF001 was grown on B5 it expressed lipase genes; however, expression was higher when it was grown on B20 biodiesel. Understanding the different metabolic activities this organism undergoes when growing on B20 biodiesel and B5 ULSD not only provides insights into how this organism lives in these fuels but can potentially be used to develop early detection methods such as biosensors by focusing extracellular enzymes that are produced.

Importance

Biodiesel and diesel storage tanks are susceptible to greater microbial contamination with the addition of FAME to the fuels. Controlling microbial activity in fuel storage tanks is a primary concern to limit the loss of fuel and decrease corrosion associated with biofouling. Current practices for detecting microbiological contamination in fuel storage tanks is lacking, and most operators are oblivious to fouling until biofilms have already established themselves in

storage tanks. It is therefore critical to have a better understanding of how the prominent fungal contaminant *Paecilomyces* AF001 establishes itself in fuels. This research provides the groundwork for understanding potential biomonitoring targets using enzymatic assays and transcriptomic analyses from *Paecilomyces* AF001 when grown on B20 biodiesel and B5 ULSD.

Introduction

Members of the genus *Paecilomyces* are ubiquitous in nature and have a wide range of ecological niches including soils, fruits, vegetables, and in B20 biodiesel and B5 ULSD fuels (1, 2). Proliferation of *Paecilomyces* in fuels has been shown to lead to degradation of fuel components as well as increase the potential to compromise equipment performance by biofouling and microbiologically influenced corrosion (2, 3). Growth of *Paecilomyces* in storage tanks produces thick biofilms, and biofilm attachment can hinder the ability of the automatic tank gauge (ATG) to report water intrusion into tanks (4). Operators of these tanks are therefore left assuming that their tanks are operating normally; however, thick biofilms may be establishing (3). It is important to better understand how *Paecilomyces* grows in both B20 biodiesel and B5 ULSD and elucidate the metabolic pathways that are involved with its growth in both fuels. This information can be used to develop molecular based biosensors that can aid operators in diagnosing contamination in their storage tanks.

Microbial contamination of B20 biodiesel and B5 ULSD fuels has been frequently reported by the scientific community and microbial community analyses of contaminated fuels often demonstrate that there can be numerous microbes in the fuels with low diversity indicating that contaminated fuels are dominated by one organism (5, 6). Investigations have primarily focused on studying the bacterial genera commonly found in contaminated fuels including *Bacillus*, *Pseudomonas*, *Serratia*, *Flavobacterium*, and *Sphingomonas* as well as a few fungal

genera including *Aspergillus*, *Hormoconis*, and recently *Paecilomyces* (2, 7–10). *Paecilomyces* has previously been implicated in the spoiling of foods due to its ability to produce ascospores and resist heat treatment (1). However, a gap exists in understanding how this organism survives in contaminated fuel samples and presents an opportunity to explore how these organisms can degrade fuels. Due to the lack of diversity in contaminated fuel systems, investigations on prominent members known to contaminate these tanks provide insights the overall performance of the fuel tank system.

Fungal oxidation and degradation of FAME, alkanes, alkenes, and aromatic hydrocarbons are mediated by different enzymes such as lipases, monooxygenases, dioxygenases, cytochrome P450, and peroxidases (8, 11, 12). B20 biodiesel and B5 ULSD consists of hydrocarbons with different chain lengths, aromatic hydrocarbons, and fatty acid methyl esters with different degrees of saturation and fatty acid chain length (13–15). Under aerobic conditions, metabolism of FAME and hydrocarbons in biodiesel and ULSD results in the production of organic acids, which can be corrosive to metals (16, 17). While there is a general understanding of how fungi can grow in fuels by metabolizing hydrocarbons and FAME, exactly which genes are expressed in different fuel compositions and in different stages of growth is unknown.

In this study, we aimed to better understand how the prominent fuel contaminating fungus *Paecilomyces* grows in both B20 biodiesel and B5 ULSD. Traditional wet lab techniques and transcriptomics were employed to better understand how this fungus grew on the fuels and what enzymes were expressed during different stages of growth. *Paecilomyces* AF001 growth was monitored on B20 and B5 ULSD to determine the lag, log, and stationary phases of this organism so that sampling for lipase activity and transcriptomic analyses can be done at these time points since different growth stages tend to have dynamic changes in different genes

expression (18). Specific genes were analyzed related to hydrocarbon and FAME degradation including those encoding lipase activity, beta-oxidation, and mono and dioxygenases. Having a better understanding of how *Paecilomyces* metabolizes both B20 biodiesel and B5 ULSD can be used in future studies to develop tools for rapid detection of contamination in fuel storage tanks.

Results

Fuel Sterilization and Selection

B20 biodiesel and B5 ULSD fuels were screened for potential contamination left over from filter sterilization. Filters were cut out of the Steritop™ bottle top filter and used to extract nucleic acids from any microorganisms that were entrapped on them after filtration. After extraction, TaqMan qPCR was conducted on the extract using both BactQuant and FungiQuant primers and probes to determine if there were any 16S or 18S SSU genes in the samples. TaqMan qPCR did not detect any quantifiable transcripts for either condition in either of the fuel types.

Additionally, both B20 biodiesel and B5 ULSD after filtration were used as a sole inoculation and carbon substrate and was placed into sterile artificial sump water (ASW). This fuel was allowed to sit for 2 weeks to allow any potential contamination in the fuels to proliferate and grow. After 2 weeks elapsed the fuels and ASW were extracted and TaqMan qPCR using BactQuant and FungiQuant primers and probes to again determine if there were any 16S or 18S SSU genes in the samples. TaqMan qPCR did not detect any quantifiable transcripts again for either condition of the fuel types.

Determining *Paecilomyces* AF001 Growth Stages on Fuels

Paecilomyces AF001 growth on both B20 biodiesel and B5 ULSD was found to have similar lag, logarithmic, and stationary phase times; however, there were greater MPNs in the B20 biodiesel fuels at all growth phases. It was determined that *Paecilomyces* AF001 had lag phases in the fuels that lasted from initial inoculation until around day 6 (FIG 4.1). After the lag phase lasting for 6 days, an exponential growth phase was observed from days 6-8, following a stationary phase a few days before day 14. Based on these data, sampling points for lipase activity and transcriptomic analysis was selected to be on day 6 for lag phase, day 8 for logarithmic growth, and day 14 for stationary phase. The chemical composition of n-alkanes and FAME in the B20 biodiesel (fuel sample 33) and B5 ULSD (fuel sample 46) fuel used for these experiments can be found in the APPENDIX.

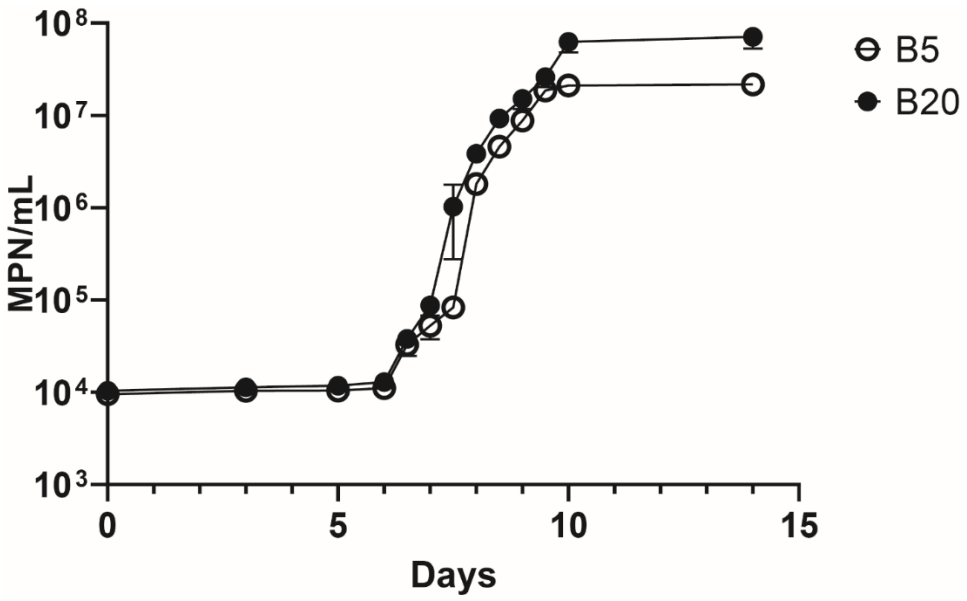

FIG 4.1. Growth of *Paecilomyces* AF001 with on B5 ULSD (open circle) and B20 biodiesel (closed circle) as the sole carbon and energy source. Error bars represent standard deviation of mean MPNs (n=3).

Biomass-based Growth Measurements and Lipase Assay

Biomass was measured by determining dry mass on a 0.45µm filter during this experiment to normalize lipase activity and verify *Paecilomyces* AF001 was in the different growth phases determined by MPN. Biomass increased proportionally to the growth curve in FIG 4.1 (FIG 4.2).

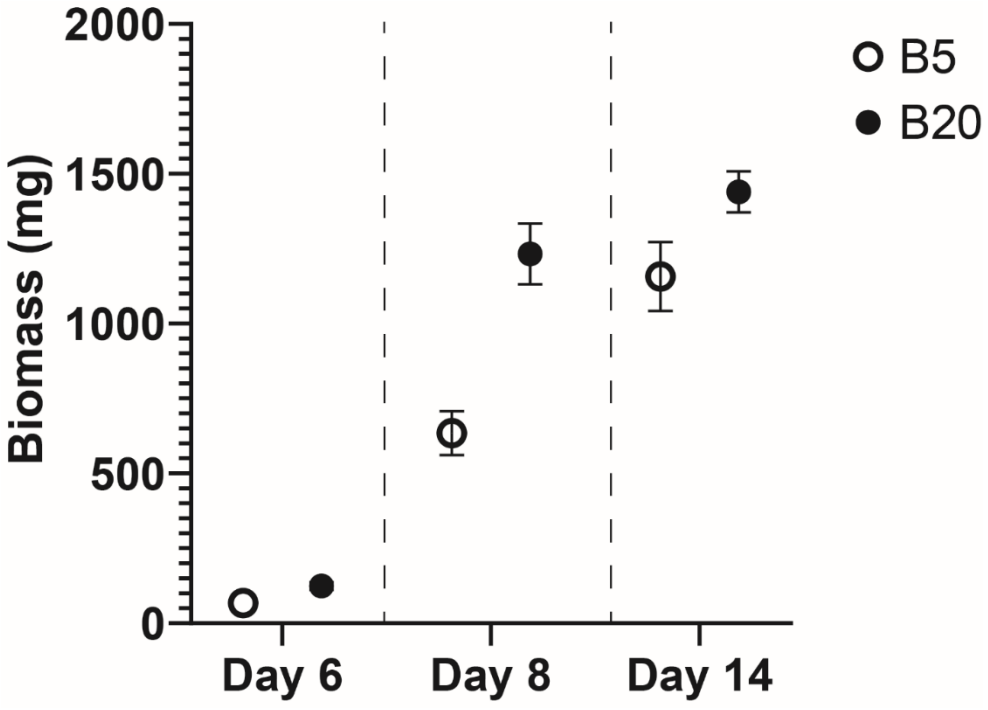

FIG 4.2. Total biomass as dry weight of *Paecilomyces* AF001 during growth with B5 (open circle) or B20 (closed circle) as the sole carbon and energy source. The total volume filtered was 10 mL ASW and 40 mL fuel for a total volume of 50 mL with most of the biomass being localized at the interface. Error bars represent standard deviation of the mean of the biomass (mg) (n=3).

At each of the timepoints in the biomass sampling, lipase activity was also determined colorimetrically using a plate reader and normalized to the dry biomass that was found on the filters (FIG 4.3). Lipase activity was found to be significantly higher in B20 biodiesel samples when compared to the B5 ULSD at all time points ($p \leq 0.05$). However, there was no significant

changes to lipase activity for *Paecilomyces* AF001 across the time points for each growth condition.

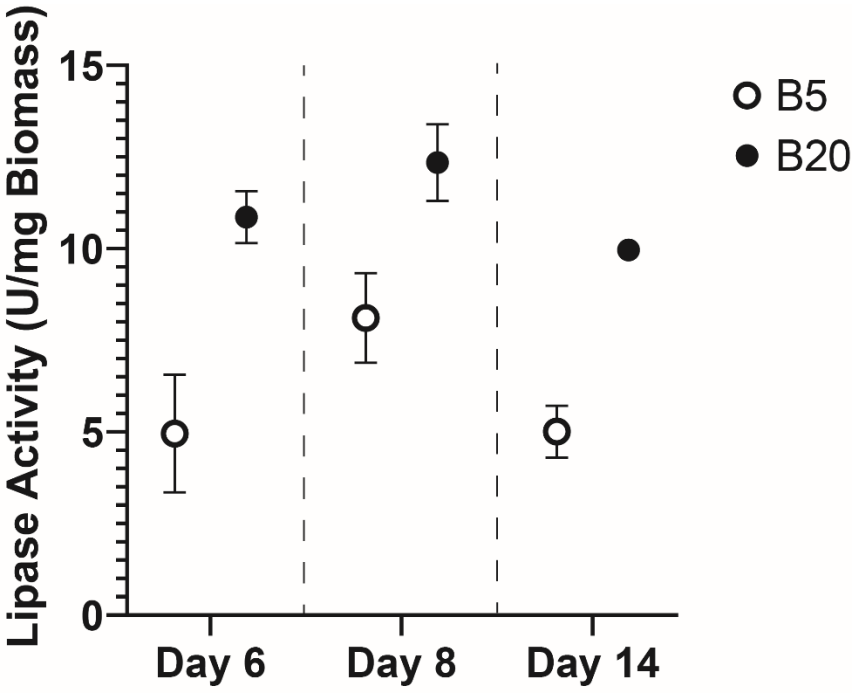

FIG 4.3. Lipase activity of *Paecilomyces* AF001 when grown on B5 (open circle) or B20 (closed circle) normalized to biomass collected at each timepoint. Data is presented as units of lipase per mg of dry biomass. Error bars represent standard deviations for each mean (biological replicates n=3).

Transcriptome Analysis

RNA recovery was too low to detect in day 6 samples for when *Paecilomyces* AF001 was grown on both B20 biodiesel and B5 ULSD; therefore, samples were excluded from the lag phase of the transcriptomic analysis. Sufficient RNA was recovered from cultures grown on B20 biodiesel and B5 ULSD on days 8 and 14. Transcript differences between conditions were visualized with a principal component analysis (PCA) to compare *Paecilomyces* AF001 grown on B20 biodiesel and B5 ULSD, showing clear separation between the two fuel types (FIG 4.4).

However, there was little separation between gene expression profiles grown on the same fuel but at different time points. The outlier separation between the B5 ULSD for both timepoints was due to less transcripts being detected, and those samples had less biomass compared to the other B5 samples. Sequenced cDNA transcripts were ~150 base pairs in length with Phred scores of X >35 for all base pair positions. The total reads for all the conditions used in this analysis were B20 biodiesel D8 conditions had an average of 27 million reads per replicate, B20 biodiesel D14 had an average of 30 million reads per replicate, B5 ULSD D8 had an average of 10 million reads per replicate, and B5 ULSD D14 had an average of 12 million reads per replicate.

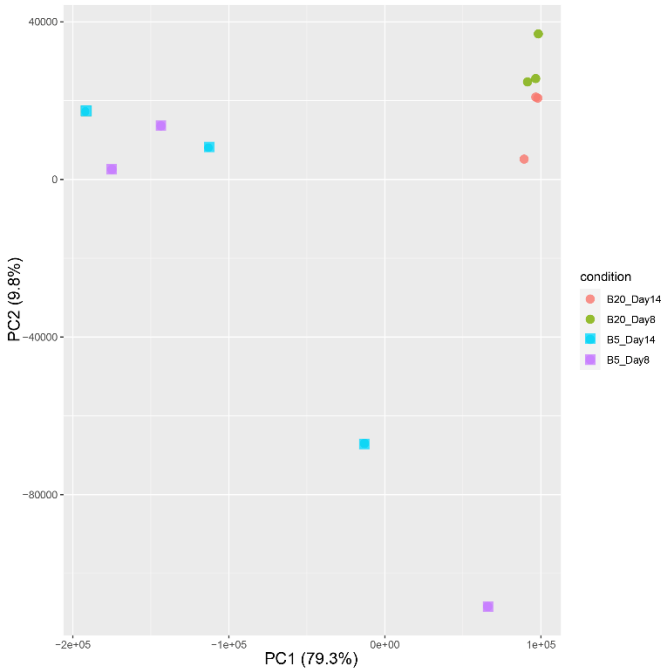

FIG 4.4. Principal component analysis (PCA) of transcripts produced by *Paecilomyces* AF001 grown on B20 biodiesel or B5 ULSD. B20 samples are represented by circles. The day 14 B20 samples are represented by orange while the day 8 B20 samples are represented by green. B5 samples are represented by squares. The day 14 B5 samples are teal while the day 8 B5 samples are purple.

Genes known to be involved in the degradation of hydrocarbons and FAME were analyzed to determine if there were any differences in expression when grown on B20 biodiesel

or B5 ULSD. Significant differences were found by using the sleuth package in RStudio after transcript abundances were quantified using kallisto (19, 20). A monooxygenase (GO:0016705) with oxidoreductase activity involved in incorporating a molecular oxygen into a donor was not detected when *Paecilomyces* AF001 was grown in B20 biodiesel but was when grown in B5 ULSD (FIG 4.5; $p \leq 0.001$). There were not significant differences between this level of monooxygenase expression by *Paecilomyces* AF001 when grown on B5 ULSD between days 8 and 14.

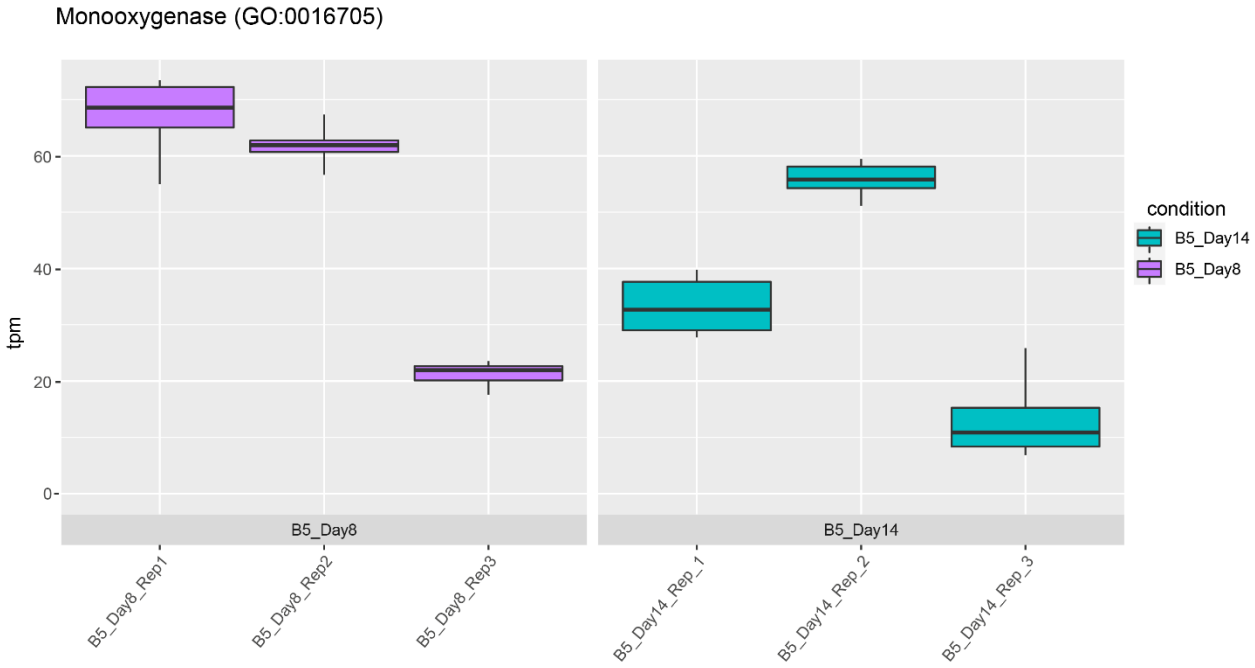

FIG 4.5. Quantification of transcripts per million (TPM) mapped to a monooxygenase (GO:0016705) with oxidoreductase activity that incorporates molecular oxygen into reduced donors. Boxplots represent bootstrap values (n=3) from each replicate's transcripts per million that map to the genome of *Paecilomyces* AF001.

Additionally, transcripts found to be related to dioxygenase (GO:0051213) that are involved in redox reactions that incorporate both O_2 atoms into reduced products were examined. Similar to the monooxygenase case, *Paecilomyces* AF001 did not produce detectable transcripts

for dioxygenases when grown on B20 and produced significantly higher transcripts for this enzyme when grown in B5 ULSD (FIG 4.6; $p \leq 0.001$).

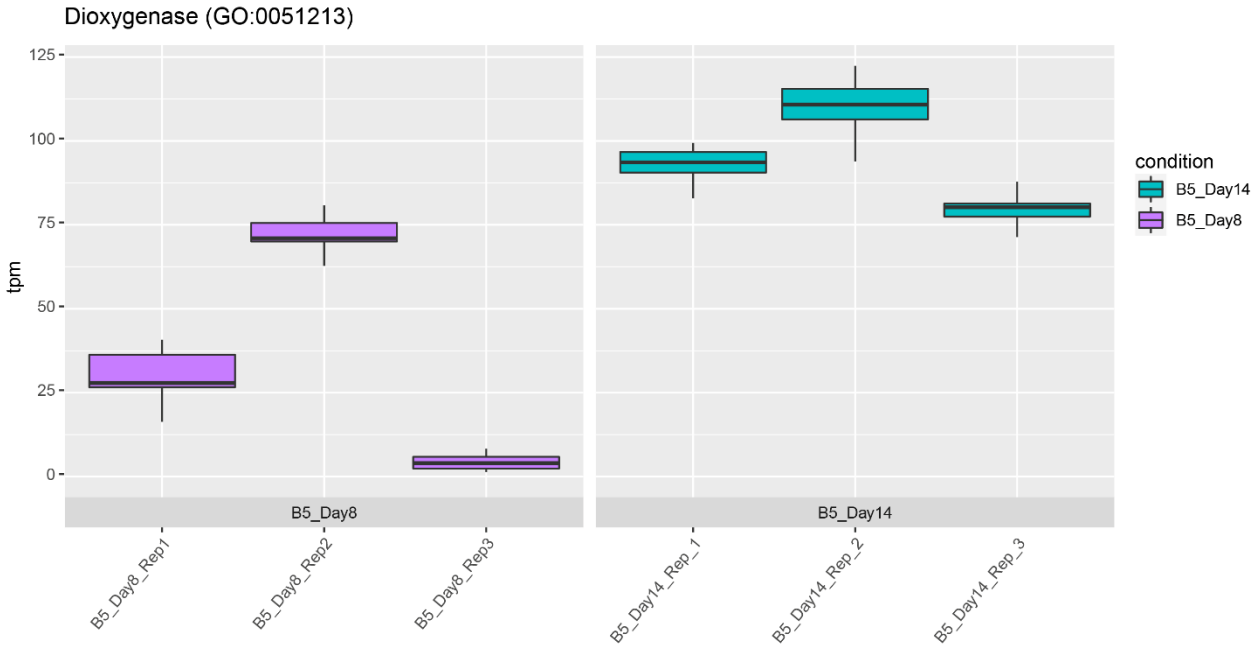

FIG 4.6. Quantification of transcripts per million (TPM) mapped to a dioxygenase (GO:0051213) with oxidoreductase activity that incorporates both atoms of molecular oxygen into reduced donors. Boxplots represent bootstrap values (n=3) from each replicate's transcripts per million that map to the genome of *Paecilomyces* AF001.

Transcripts were found to be related to a lipase (GO:0052689) known to be important in the activation of FAME by catalyzing the hydrolysis of the ester bonds (FIG 4.7). Transcripts were significantly higher and roughly twice as abundant in conditions where *Paecilomyces* AF001 was grown on B20 biodiesel when compared to B5 ULSD for both day 8 and day 14 ($p \leq 0.05$).

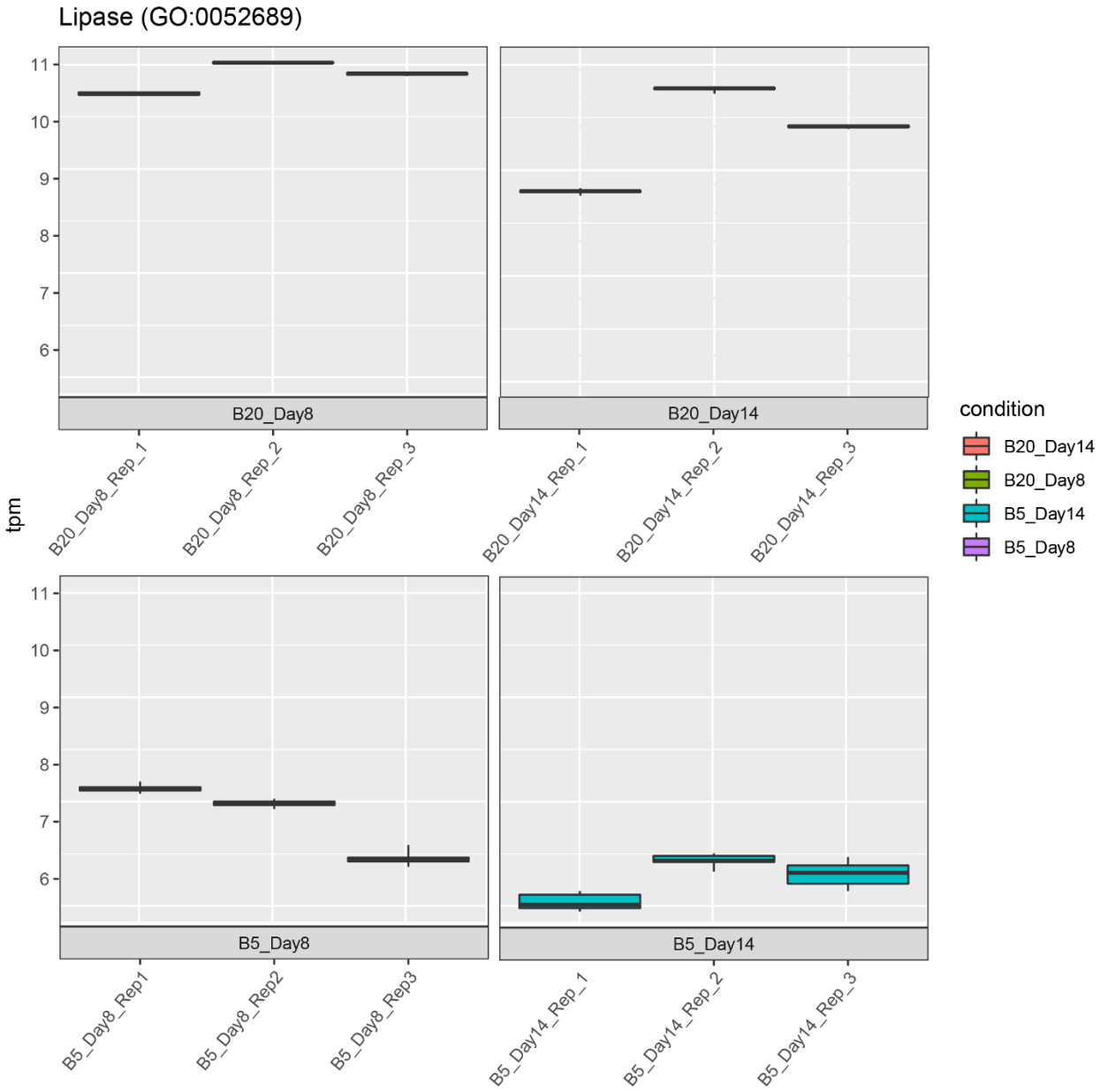

FIG 4.7. Quantification of transcripts per million (TPM) mapped to a lipase (GO:0052689) that is known to be involved with the catalysis of the hydrolysis of carboxylic ester bonds. Cultures grown in B20 (top) and B5 ULSD (B5, bottom) for 8 and 14 days. Boxplots represent bootstrap values (n=3) from each replicate's transcripts per million that map to the genome of *Paecilomyces* AF001.

Finally, transcripts found to be related to an acyl-CoA dehydrogenase (GO: 0006635) that acts on CoA derivatives of fatty acids with chain lengths from 8-18 (FIG 4.8). Additionally,

this enzyme is involved in the first step of the peroxisomal beta-oxidation of fatty acids and is rate-limiting. Transcripts were significantly higher in conditions where *Paecilomyces* AF001 was grown on B20 biodiesel when compared to B5 ULSD for day 14 ($p \leq 0.05$). These transcripts were not observed in either condition at day 8.

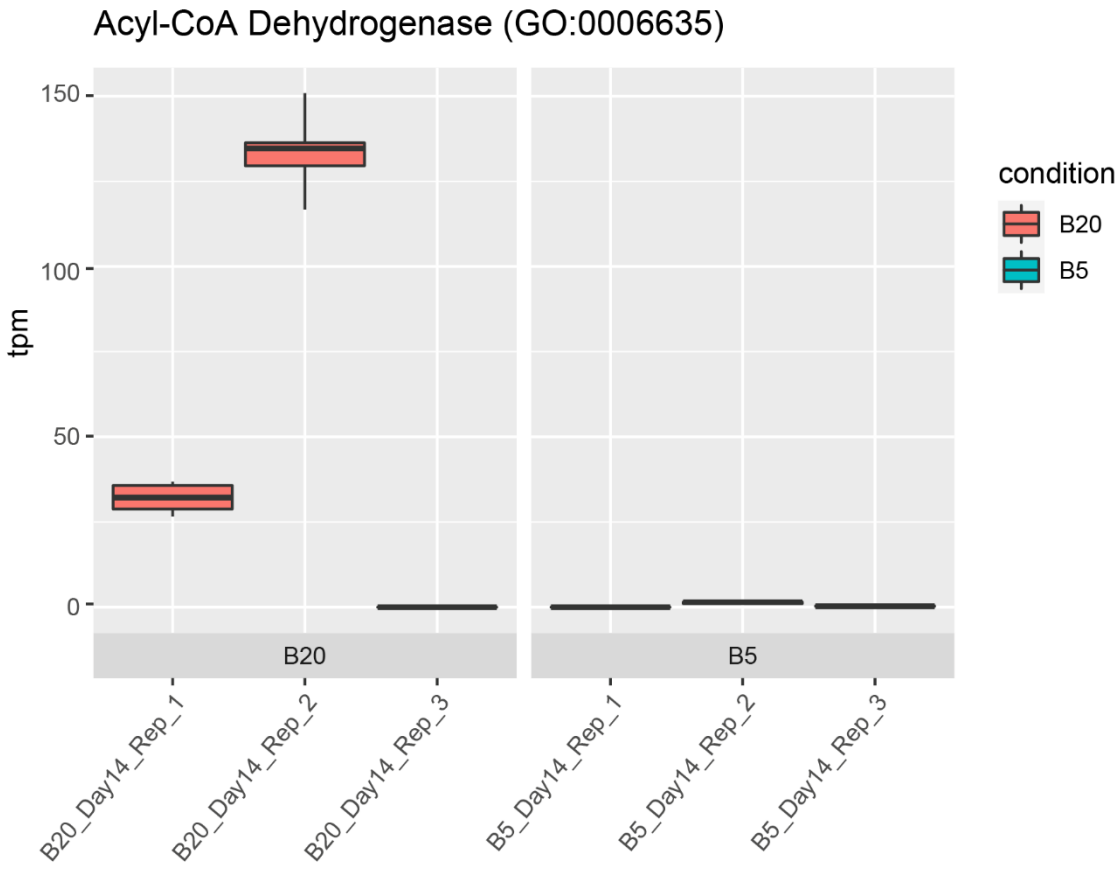

FIG 4.8. Quantification of transcripts per million (TPM) that mapped to an acetyl transferase (GO:0006635) used in the beta-oxidation pathway of fatty acid. Samples are normalized to transcripts per million (TPM) reads for each sample. Boxplots represent bootstrap values (n=3) from each replicate transcripts per million that map to the genome of *Paecilomyces* AF001.

Discussion

Transcriptomics identified the metabolic and functional processes of *Paecilomyces* AF001 expresses when growing on B20 biodiesel or B5 ULSD. However, it fails to address if

these organisms are translating transcripts into functional proteins as eukaryotic organisms are known for post-transcriptional modifications and epigenetic modulators of gene expression (21). It is therefore important to use traditional microbiological techniques such as enzyme assays to verify their expression and utilization. In this study *Paecilomyces* AF001 was grown in both B20 biodiesel and B5 ULSD to identify any metabolic differences. Significant differences in the abundance of transcripts were found between transcripts that are involved in the degradation of hydrocarbons and FAME compounds in B20 and B5 fuels. The monooxygenase (GO:0016705), dioxygenase (GO:0051213), lipase (GO:0052689), and acyl-CoA dehydrogenase (GO: 0006635) transcripts that were examined showed differential expression depending on which fuel was used as the sole carbon and energy source. Additionally, differences in lipase gene expression were supported by corresponding differences in lipase activity under both conditions (FIG 4.7).

Paecilomyces AF001 was grown on both B20 biodiesel and B5 ULSD to determine the lag, logarithmic, and stationary phases of this organism to act as targets for screening. B20 biodiesel and B5 ULSD both have FAME compounds as well as different hydrocarbons found in diesel fuels, but B20 fuels contain more FAME than B5 ULSD, likely resulting in the higher biomass that was observed (FIG 4.1). *Paecilomyces* AF001 appeared to have similar time points for these phases when grown on both fuel types at room temperature. *Paecilomyces* AF001 produced lipases in both fuels, but more lipase activity and gene expression were observed in the B20 samples compared to the B5 ULSD (FIG 4.3 & FIG 4.7). Additionally, an acyl-CoA dehydrogenase transcript related to the beta oxidation of FAME was only detected when *Paecilomyces* AF001 was grown on B20 fuels as the sole carbon and energy source. Rhizospheric fungal isolates exposed to increasing crude oil concentrations produce more peroxidases involved in hydrocarbon degradation (22). This could also be true of *Paecilomyces*

AF001 as there is more FAME in B20 biodiesel compared to B5 ULSD leading to more expression of lipases involved in the oxidation of these compounds. Likewise, when this fungus was grown in B20 biodiesel there was no observed expression of genes involved in the metabolism of hydrocarbons like there was when grown on B5 ULSD (FIG 4.5 &4.6). This can be an example of the underlying gene expression resulting from substrate preference (11, 23, 24).

FAME will continue to be added to diesel fuels to offset carbon emissions, reduce dependency on non-renewable fuels, and to improve lubricity of the fuels for engine use (25, 26). Since FAME is more readily oxidizable than the hydrocarbons in petroleum based ULSD, instances of biofouling and biocontamination of fuels are becoming more common (27–29). There is still a lot of work to be done in addressing how to prevent contamination of these fuels as well as how to detect fouled fuels. The total extent of contamination across the U.S and world is largely misunderstood due to lack of detection methods except measuring water entrapment in storage tanks (9). In 2016, the U.S. EPA described particulates and biofouling in 42 underground storage tanks across the U.S., with 27 of the storage tanks owners being unaware of any potential corrosion and contamination risks associated with fouling of these fuels (30). Additionally, our research group has observed that many B20 biodiesel and B5 ULSD tank operators were unaware of their tanks being contaminated (3). There is therefore a critical global need to determine ways that stored fuels are at risk of contamination. This work has provided foundational data to develop a biosensor that can be used to detect metabolites from the oxidation of FAME or target exoenzymes associated with fuel degradation. Biosensors are becoming more common to detect contamination and largely depend on the detection of enzymes, cells, nucleic acids, antibodies, or metabolites (31). This work has identified that *Paecilomyces* AF001 produced lipases in both B20 biodiesel and B5 ULSD that can be used as

target for biosensors to warn operators of contamination problems in their systems. *Paecilomyces* is a good target to study for this due to its prevalence in contaminated tanks (Chapter 3). More work is needed to examine how *Paecilomyces* AF001 alters its gene expression profile when in the presence of other microorganisms found in fouled tanks.

Materials and Methods

Fuel Sterilization and Selection

B20 biodiesel and B5 ultra-low sulfur diesel was collected from a military base in the southeastern U.S. The B20 biodiesel was collected from a delivery truck and was never stored in an underground storage tank. B5 ULSD was collected from an underground storage tank in operation using a stainless-steel Bacon Bomb that was disinfected with 100% isopropanol prior to insertion into the tank. Approximately 1L of fuels were collected and sterilized by filtration into a 1L sterile Schott bottle using a Millipore Steritop™ bottle top filter with a pore size of 0.45 µm (Millipore; Burlington, MA, USA). Both fuels were then stored in a dark container void of any light to prevent UV degradation prior to use.

Due to the inability to autoclave these fuel samples, the fuel was screened for any potential contamination using TaqMan qPCR to detect bacterial and fungal rRNA genes. When the field sterilized fuels arrived at the lab, the fuels were again filtered into a 1L sterilized Schott Bottle using a Millipore Steritop™ bottle top filter with a pore size of 0.45 µm. Each filter was then cut out and placed into a Zymo Quick-DNA Fecal/Soil Microbe ZR BashingBead™ Lysis Tube with DNA/RNA Shield™. Any potential biomass that might have been on the filter was physically lysed using a custom designed reciprocating saw and DNA extraction proceed via the Zymo Quick-DNA Fecal/Soil Microbe kit manufacturer's protocol. Following this, TaqMan qPCR was conducted on the extracts using the BactQuant and FungiQuant primers and probes

(Table 4.1) to determine if there were any potential contaminants in the fuels prior to use in experiments by targeting the 16S/18S small sub-unit gene for bacteria and fungi respectively (32, 33).

Table 4.1. Primers and probes used to quantify potential bacterial contamination in B20 biodiesel and B5 ULSD.

BactQuant	Sequence	Tm(°C)	*E. coli* Region
Forward Primer	5'-CCTACGGGDGGCWGCA-3'	55.9-58.4	341-356
Reverse Primer	5'-GSWCTATCCCCAKCACGA-3'	57.5-63.3	786-806
Probe	(6FAM) 5'-CAGCAGCCGCGGTA-3' (MGBNFQ)	68.0	519-532

Table 4.2. Primers and probes used to quantify potential fungal contamination in B20 biodiesel and B5 ULSD

FungiQuant	Sequence	Tm(°C)	*S. cerevisiae* Region
Forward Primer	5'-GGRAAACTCACCAGGTCCAG-3'	60.5-62.5	1199-1218
Reverse Primer	5'-GSWCTATCCCCAKCACGA-3'	57.5-63.3	786-806
Probe	(6FAM) 5'-TGGTGCATGGCCGTT-3' (MGBNFQ)	68.0	519-532

BactQuant and FungiQuant qPCR was done using 10 µL reactions with the final reaction concentrations containing 1.8 µM of each respective forward and reverse primer, 225 nM of the TaqMan™ probe, 1X Platinum Quantitative PCR Supermix-UDG w/ROX (Invitrogen Corp.) and nuclease free water. The experiments included an in-run standard curve (10^1-10^6 in ten-fold dilutions) and no template controls. BactQuant amplification of real-time fluorescence was performed on the Step-One™ Real-Time PCR System with the following PCR conditions: 3 min at 50°C, 10 min at 95°C for *Taq* activation, 15 s at 95°C for denaturation and 1 min at 60°C for annealing and extension for 40 cycles. FungiQuant was additionally performed on a Step-One™

Real-Time PCR system using the following PCR conditions: 3 min at 50°C, 10 min at 95°C for *Taq* activation, 15 s at 95°C for denaturing, and 1 min at 65°C for annealing and extension for 50 cycles. No detectable 16S or 18S SSU copies were detected in either the B20 or B5.

Determining *Paecilomyces* AF001 Growth Stages on Fuels

To determine sampling time points of *Paecilomyces* AF001 growing on B20 biodiesel and B5 ULSD, physiological characterization was conducted with this organism grown on each of the fuels as the sole carbon and energy source. Initially, *Paecilomyces* was grown on Hestrin Schramm (HS) agar medium (per L: 20 g glucose, 5 g yeast extract, 2.7 g Na_2HPO_4, 1.15 g citric acid, 7.5 g agar; pH adjusted to 6.0 with diluted HCl or NaOH) and incubated at 25°C for 7 days (34). Phosphate Buffered Saline (4 mL, PBS) was then spread over the surface of the HS agar plate and the biomass was scraped using a sterile inoculating loop. The suspension was then collected and placed into a sterile Eppendorf Tube and centrifuged at 10,000 x RCF for 1 minute. The supernatant was decanted, and sterile PBS was added back to the biomass and vortexed to resuspend the fungus. This was repeated for a total of three washes with PBS to reduce any potential nutrient carry over. This biomass was then inoculated into autoclaved artificial sump water (ASW) (per L: 0.015 g NaCl, 0.035 g NaF, 0.02 g $CaCl_2$, 0.018 g KNO_3, 0.01 g Na_2SO_4, 0.015 g $(NH_4)_2SO_4$, and 0.017 g K_2HPO_4) and filter sterilized B20 biodiesel or B5 ULSD was added as the sole carbon and energy source in a 1:5 ASW:Fuel ratio at ambient temperature statically. This was done to acclimate the fungus to growing on these fuels for a week.

Following initial growth on the fuels, the cultures were filter sterilized using a Steritop™ bottle top filter with 0.45 µm pore size into a sterile 1L Schott Bottle. Each filter was cut out of the filter housing using sterile disposable scalpels and placed into a 50 mL sterile Falcon tube containing 10 mL PBS. The Falcon tube was then vortexed to resuspend the biomass that was

collected on the filter into the PBS solution. A spore suspension was then prepared using this solution to normalize the inoculations of the experiments described below. To prepare the spore suspension, the resuspended fungal biomass was filtered into a sterile vacuum flask using a 10 µm pore size polyether sulfone filter to separate spores from hyphal biomass. The spores that were collected in the flow through were then centrifuged at 10,000 RCF for 1 minute. The supernatant was decanted, and 1 mL of sterilized PBS was added back to the spore pellet and vortexed to resuspend the spores. This wash was repeated three times. Spore concentrations were then determined using a Petroff-Hausser counting chamber and diluted to adjust the inoculum concentrations for the growth curves to $1x10^4$ spores/mL.

To monitor the growth of *Paecilomyces* on B20 biodiesel and B5 ULSD, MPNs were conducted in 1:5 ASW:Fuel in test tubes (16 x 150mm) with 0.5 mL ASW and 2.0 mL fuel for a final volume of 2.5 mL. These cultures were destructively sampled to avoid any changes that could be caused due to the removal of volume. Incubations were done statically at ambient temperature. MPNs were conducted initially at time 0 after initial inoculation and on days 3, 5, 6, 6.5, 7, 7.5, 8, 8.5, 9, 9.5, 10, and 14. At each time point the triplicate test tubes for each time point were rigorously vortexed to form an emulsion of the fuel and water phases to homogenize the biomass present in the test tubes. Once homogenized, MPN/mL measurements were conducted using HS medium.

Biomass Growth Measurements and Lipase Assay

Paecilomyces was again grown on B20 biodiesel and B5 ULSD as described above and inoculated into 1:5 ASW:Fuel to a final concentration of $1x10^4$ spores/mL with biological triplicates. Initially 10 mL of ASW was autoclaved in 16 oz Mason jars. After autoclaving the ASW; 40 mL of filter sterilized B20 biodiesel or B5 ULSD was added aseptically to these Mason

Jars and inoculated with *Paecilomyces* spores to a final concentration of $1x10^4$ spores/mL. To allow oxygen and CO_2 to freely diffuse in and out of these jars, the tops were covered with Breath-Easy Sealing Membranes (Millipore Sigma, Burlington, MA, USA). *Paecilomyces* was then grown for up to 2 weeks on either the B20 or B5 fuel sources and destructively sampled at days 6, 8, and 14 to representing growth in lag, logarithmic, and stationary phase, respectively. At each time point, the Mason jars contents were filtered through a 0.45µM polyether sulfone filter. This filter was cut into three equal sections. To obtain a dry weight of *Paecilomyces* grown in the fuels One of the three sections was placed into a sterile Petri dish and dried in an oven at 60°C for 24 hours to remove any moisture from the biomass and filter. Since the filter was destroyed, a tare weight was determined by measuring 10 of the polyether sulfone filters total mass and taking an average of all of them to correspond to the tare weights of all filters.

Another section of the filter was used to conduct lipase assays using the Lipase Activity Assay Kit (MAK046 Sigma Aldrich) according to the manufacturer's recommentdations. The filter section was initially placed in1.5 mL Eppendorf Tubes containing 500 µL Lipase Assay Buffer that has been amended with 5 mM calcium chloride for calcium-dependent lipases and vortexed vigorously to resuspend the biomass from the filter. This suspension was then used to conduct lipase assays according to the manufacture's recommendations in 96 well plates and read with Agilent BioTech Synergy HTX plate reader. Glycerol standards were used to quantify colorimetric lipase activity in concentrations of 2, 4, 6, 8, and 10 nM. Additionally, a blank was used containing no glycerol to determine the background signals produced from the assay. The 96 well plate was incubated at 37°C for the duration of the assay. The initial absorbance at 570 nm was taken 3 minutes after the start of the assay. The assay was run for 1.5 hours, and total lipase activity was quantified by the following equations:

Calculate change of absorbance from $T_{initial}$ to T_{final}:

$$\Delta A_{570} = (A_{570})_{final} - (A_{570})_{initial}$$

Calculate lipase activity of a sample

$$\text{Lipase Activity} = \frac{B \; x \; Sample \; Dilution \; Factor}{\text{Reaction Time x Biomass}} \text{ where}$$

B = Amount (nmole) of glycerol generated between $T_{initial}$ and T_{final}

Reaction Time = $T_{final} - T_{initial}$ (minutes)

Biomass = Biomass added to wells

One unit of Lipase is the amount of enzyme that produces 1 µmole of glycerol from triglycerides per minute at 37°C.

RNA Extraction and Sequencing

The final section of the filter was taken and placed into a Zymo *Quick*-DNA/RNA BashingBead™ tube containing lysis buffer and DNA/RNA shield™. The biomass in the BashingBead™ tube was then physically lysed using a custom designed reciprocating saw. The extraction of the nucleic acids proceeded via the Zymo *Quick*-DNA/RNA kits manufacturer protocols. RNA was initially quantified using Qubit RNA HS (High Sensitivity) Assay Kit and analyzed using a Qubit 2.0 fluorometer. Samples were then ribodepleted using a RiboCop Lexogen™ rRNA depletion kit according to the manufacture's recommendations. Following depletion of rRNA library preparation was done using a swift rapid library kit and sequenced on a NovaSeq 6000 using a S4 Paired End 2 x 150 chemistry at the Oklahoma Medical Research Facility.

Transcriptome Analysis

Reads were screened to remove human contamination, mapping against the hg19 reference using bbmap (35, 36). After this, reads were then mapped against the Paecilomyces sp. AF001 reference genome (PNEM00000000) to remove any potential contaminating sequence that failed to map back to the reference genome using bbduk (35). Finally, reads were concatenated and assembled using Trinity within a singularity container (37). Post assembly transcripts were refined using TransDecoder (38). Peptide sequence predicted by TransDecoder was then annotated using both DIAMOND (39) searching against the uniref90 database as well as HMMER (40) searching against the PFAM database. These results were then integrated into a searchable database using Trinotate (41).

Statistical Analyses and Data Visualization

Statistical analyses and figure generation was carried out in R version 3.3.3 and GraphPad Prism 8.3.0. Differences between lipase activity was carried out using an ANOVA with a Tukey's HSD to determine significances between *Paecilomyces* AF001 when grown on B20 biodiesel and B5 ULSD. Significant differences between transcripts from *Paecilomyces* AF001 when grown on the different fuels were conducted in RStudio using a sleuth analysis of transcript counts determined by kallisto.

Acknowledgements

This work was supported by the Air Force Research Laboratory Biological Materials and Processing Research Team, Materials and Manufacturing Directorate and the U.S. Department of

Defense Office of Corrosion Policy & Oversight Technical Corrosion Collaboration (Grant # FA7000-15-2-0001).

Works Cited

1. Kotzekidou P. 2014. Encyclopedia of Food Microbiology (Second Edition). Article Titles: B 344–350.

2. Stamps BW, Bojanowski CL, Drake CA, Nunn HS, Lloyd PF, Floyd JG, Emmerich KA, Neal AR, Crookes-Goodson WJ, Stevenson BS. 2020. In situ Linkage of Fungal and Bacterial Proliferation to Microbiologically Influenced Corrosion in B20 Biodiesel Storage Tanks. Front Microbiol 11:167.

3. Stamps BW. 2016. Measuring the Impact of Microbial Communities and their Proliferation in Engineered Ecosystems. University of Oklahoma Graduate College Dissertation.

4. Passman F. 2003. Fuel and Fuel System Microbiology: Fundamentals, Diagnosis, and Contamination Control. American Society for Testing & Materials.

5. Gaylarde CC, Bento FM, Kelley J. 1999. Microbial Contamination of Stored Hydrocarbon Fuels and its Control. Rev Microbiol 30:01–10.

6. Yemashova NA, Murygina VP, Zhukov DV, Zakharyantz AA, Gladchenko MA, Appanna V, Kalyuzhnyi SV. 2007. Biodeterioration of Crude Oil and Oil Derived Products: a Review. Rev Environ Sci Bio Technology 6:315–337.

7. Beech IB, Sunner J. 2004. Biocorrosion: Towards Understanding Interactions Between Biofilms and Metals. Curr Opin Biotech 15:181–186.

8. Khan SR, Kumar JIN, Kumar RN, Patel J. 2014. Enzymatic Evaluation During Biodegradation of Kerosene and Diesel by Locally Isolated Fungi from Petroleum-Contaminated Soils of Western India. Soil Sediment Contam Int J 24:514–525.

9. Passman FJ. 2013. Microbial Contamination and its Control in Fuels and Fuel Systems Since 1980 – A Review. Int Biodeter Biodegr 81:88–104.

10. Beale DJ, Morrison PD, Key C, Palombo EA. 2014. Metabolic Profiling of Biofilm Bacteria Known to Cause Microbial Influenced Corrosion. Water Sci Technol 69:1–8.

11. Rojo F. 2010. Enzymes for Aerobic Degradation of Alkanes, p 781-797. In Timmis KN (eds), Handbook of Hydrocarbon and Lipid Microbiology, Springer, Berlin, Heidelberg.

12. Clemente AR, Anazawa TA, Durrant LR. 2001. Biodegradation of Polycyclic Aromatic Hydrocarbons by Soil Fungi. Braz J Microbiol 32:255–261.

13. ASTM D7467-20a. 2015. Specification for Diesel Fuel Oil, Biodiesel Blend (B6 to B20). https://doi.org/10.1520/D7467-15C.

14. Prince RC, Haitmanek C, Lee C. The primary aerobic biodegradation of biodiesel B20 71.

15. Hoekman KS, Broch A, Robbins C, Ceniceros E, Natarajan M. 2012. Review of Biodiesel Composition, Properties, and Specifications. Renewable and Sustainable Energy Reviews 16:143–169.

16. Skovhus TL, Eckert RB, Rodrigues E. 2017. Management and Control of Microbiologically Influenced Corrosion (MIC) in the Oil and Gas Industry—Overview and a North Sea Case Study. J Biotechnol 256:31–45.

17. Floyd JG, Stamps BW, Goodson WJ, Stevenson BS. 2021. Locating and Quantifying Carbon Steel Corrosion Rates Linked to Fungal B20 Biodiesel Degradation. Appl Environ Microb AEM0117721.

18. He B, Hu Z, Ma L, Li H, Ai M, Han J, Zeng B. 2018. Transcriptome Analysis of Different Growth Stages of *Aspergillus oryzae* Reveals Dynamic Changes of Distinct Classes of Genes During Growth. BMC Microbiol 18:12.

19. Pimentel H, Bray NL, Puente S, Melsted P, Pachter L. 2017. Differential Analysis of RNA-seq Incorporating Quantification Uncertainty. Nat Methods 14:687–690.

20. Bray NL, Pimentel H, Melsted P, Pachter L. 2016. Near-optimal Probabilistic RNA-seq Quantification. Nat Biotechnol 34:525–527.

21. Anderson P, Kedersha N. 2009. RNA Granules: Post-Transcriptional and Epigenetic Modulators of Gene Expression. Nat Rev Mol Cell Bio 10:430–436.

22. Al-Zaban MI, AlHarbi MA, Mahmoud MA. 2021. Hydrocarbon Biodegradation and Transcriptome Responses of Cellulase, Peroxidase, and Laccase Encoding Genes Inhabiting Rhizospheric Fungal Isolates. Saudi J Biol Sci 28:2083–2090.

23. Yassine MH, Wu S, Suidan MT, Venosa AD. Aerobic Biodegradation Kinetics and Mineralization of Six Petrodiesel/Soybean-Biodiesel Blends. Environ Sci Technol 47:4619-4627.

24. Thomas A, Leahy M, Smith JWN, Spence MJ. 2017. Natural Attenuation of Fatty Acid Methyl Esters (FAME) in Soil and Groundwater. Q J Eng Geol Hydroge 50:301-317.

25. Mello V e, Farias A de, Souza E do, Oliveira M de, Alves S. 2014. Effect of Desulfurization of Diesel and its Blends with Biodiesel on Metallic Contact. Mater Res 17:82–88.

26. U.S. Department of Energy. 2021 Alternative Fuels Data Center Biodiesel Blends.

27. DeMello JA, Carmichael CA, Peacock EE, Nelson RK, Arey SJ, Reddy CM. Biodegradation and Environmental Behavior of Biodiesel Mixtures in the Sea: An Initial Study. Mar Pollut Butt 54:897-904.

28. Meyer D, Beker S, Bücker F, Peralba M do, Frazzon A, Osti J, Andreazza R, Camargo F de, Bento F. Bioremediation Strategies for Diesel and Biodiesel in Oxisol from Southern Brazil. Int Biodeter Biodegr 95:356-363.

29. Zuleta E, Baena L, Rios LA, Calderon JA. 2012. The Oxidative Stability of Biodiesel and its Impact on the Deterioration of Metallic and Polymeric Materials: a Review. J. Braz Chem Soc 23:2159-2175.

30. United States Environmental Protection Agency. 2016. Investigation of Corrosion-Influencing Factors in Underground Storage Tanks with Diesel Service. https://www.epa.gov/ust/investigation-corrosion-influencing-factors-underground-storage-tanks-diesel-service

31. McGrath TF, Elliott CT, Fodey TL. 2012. Biosensors for the Analysis of Microbiological and Chemical Contaminants in Food. Anal Bioanal Chem 403:75–92.

32. Liu CM, Aziz M, Kachur S, Hsueh P-R, Huang Y-T, Keim P, Price LB. 2012. BactQuant: An Enhanced Broad-coverage Bacterial Quantitative Real-time PCR Assay. BMC Microbiol 12:56.

33. Liu CM, Kachur S, Aziz M, Hsueh P-R, Huang Y-T, Liu CM, Kachur S, Dwan MG, Keim P, Abraham AG, Price LB, Aziz M, Hsueh P-R, Huang Y-T, Busch JD, Lamit LJ, Gehring CA, Keim P, Price LB. 2012. FungiQuant: A Broad-coverage Fungal Quantitative Real-time PCR Assay BMC Microbiol 12:255.

34. Hestrin S, Journal SM. 1954. Synthesis of Cellulose by *Acetobacter xylinum*. 2. Preparation of Freeze-dried Cells Capable of Polymerizing Glucose to Cellulose. Biochem J 58:345-352.

35. Bushnell B. 2014. BBMap: A Fast, Accurate, Splice-Aware Aligner. https://www.osti.gov/biblio/1241166-bbmap-fast-accurate-splice-aware-aligner

36. Church DM, Schneider VA, Graves T, Auger K, Cunningham F, Bouk N, Chen H-C, Agarwala R, McLaren WM, Ritchie GRS, Albracht D, Kremitzki M, Rock S, Kotkiewicz H, Kremitzki C, Wollam A, Trani L, Fulton L, Fulton R, Matthews L, Whitehead S, Chow W, Torrance J, Dunn M, Harden G, Threadgold G, Wood J, Collins J, Heath P, Griffiths G, Pelan S, Grafham D, Eichler EE, Weinstock G, Mardis ER, Wilson RK, Howe K, Flicek P, Hubbard T. 2011. Modernizing Reference Genome Assemblies. Plos Biol 9:e1001091.

37. Grabherr MG, Haas BJ, Yassour M, Levin JZ, Thompson DA, Amit I, Adiconis X, Fan L, Raychowdhury R, Zeng Q, Chen Z, Mauceli E, Hacohen N, Gnirke A, Rhind N, Palma F di, Birren BW, Nusbaum C, Lindblad-Toh K, Friedman N, Regev A. 2011. Trinity: Reconstructing

a Full-length Transcriptome Without a Genome from RNA-Seq Data. Nat Biotechnol 29:644–652.

38. Haas B. 2021. TransDecoder (Find Coding Regions Within Transcripts).

39. Buchfink B, Reuter K, Drost H-G. 2021. Sensitive Protein Alignments at Tree-of-life Scale Using DIAMOND. Nat Methods 18:366–368.

40. Finn RD, Clements J, Eddy SR. 2011. HMMER Web Server: Interactive Sequence Similarity Searching. Nucleic Acids Res 39:W29–W37.

41. Bryant DM, Johnson K, DiTommaso T, Tickle T, Couger MB, Payzin-Dogru D, Lee TJ, Leigh ND, Kuo T-H, Davis FG, Bateman J, Bryant S, Guzikowski AR, Tsai SL, Coyne S, Ye WW, Freeman RM, Peshkin L, Tabin CJ, Regev A, Haas BJ, Whited JL. 2017. A Tissue-Mapped Axolotl De Novo Transcriptome Enables Identification of Limb Regeneration Factors. Cell Reports 18:762–776.

Chapter 5. Conclusions

In this dissertation I linked the representative fungal isolates *Paecilomyces* AF001 and *Wickerhamomyces* SE3 to biodegradation of B20 biodiesel corrosion and investigated the risk they posed to carbon steel corrosion when metabolizing biodiesel-containing diesel fuels. Additionally, I explored microbial communities that fouled B20 biodiesel and ultra-low sulfur diesel storage tanks from military bases across the U.S. and correlated how fuel composition impacts microbiological community structure. Finally, I examined how the prominent fungal contaminant *Paecilomyces* grows in B20 biodiesel and B5 ULSD. I combined areas of traditional microbiology with molecular techniques to gain a better understanding of fuel microbiology and identify prominent contaminants of fuels and their impact to existing infrastructure. My work highlights the power of marrying both cultivation and molecular analyses to obtain a better understanding of biologically induced fuel contamination and corrosion.

Locating and Quantifying Carbon Steel Corrosion Rates Linked to Fungal B20 Biodiesel Degradation

Microbial contamination and fouling of biofuels, ULSD, and biofuel blends is an ongoing problem costing billions of dollars annually due to fuel disposal and microbiologically influenced corrosion (1). Most of the current knowledge on MIC is focused on anaerobic bacteria leaving a gap in our knowledge of aerobic microorganisms including fungi (2–4). Two fungi representative of common contaminants of biodiesel, *Paecilomyces* AF001 and *Wickerhamomyces* SE3, were shown to be able to oxidize fuel components in B20 biodiesel and cause an increased risk of corrosion through the localized production of high concentrations of organic acids (5). *Paecilomyces* sp. are more commonly involved in the spoilage of canned foods due to their heat resistant ascospores and *Wickerhamomyces* is a common yeast used in

fermentation processes (6, 7) Both fungi were prominent in contaminated B20 biodiesel, but previous field studies which identified these microorganisms lacked the necessary controls to implicate them directly in biofuel degradation and corrosion risks (8, 9) Additionally, I show that the highest risk to carbon steel corrosion occurs at the interface between the organic fuel and aqueous phase. While this has been suggested by some researchers it has never been empirically verified until this research (10).

It is important to note that more can still be determined from investigating microbial communities in fuel systems and their effects on corrosion. Microorganisms are rarely, if ever, found as an individual population outside of lab-based experiments (11, 12). While it is important to understand populations on a reductionist scale to understand how isolates can exist in environments, it would be naïve to ignore the potential microbiological interactions that can occur in communities. This work has shown that there are potential populations of nitrogen-fixing bacteria including *Gluconacetobacter* and *Burkholderia* in contaminated fuel communities as well as other potential hydrocarbon degrading bacteria and fungi (Chapter 3). In fuel storage tanks there are ample concentrations of oxidizable hydrocarbon substrate; however, other nutrients such as nitrogen and phosphorus can limit microbial growth or even stimulate competition among community members (13). If fixed nitrogen were more readily available to communities that contaminate fuel, these communities could grow to a higher density, leading to greater risks for fouling of fuel lines and corrosion. Oxygen is a limited resource in the fuel storage tank ecosystem, as oxygen concentrations drop drastically and become anaerobic below biofilm formations at the interface of fuel and water at the bottom of a tank (10). Finally, competition between microorganisms can increase when resources are scarce, which can lead to the production secondary metabolite production such as antibiotics (14). *Paecilomyces* is known

to produce numerous antibiotics including cephalosporins that can give it a competitive edge against susceptible organisms (6, 15). Cefdinir, a penicillin-type cephalosporin antibiotic, adheres to mild steel surfaces and inhibits the corrosive potential of the metal and reduces the risk of pitting type corrosion (16). If *Paecilomyces* AF001 can produce cephalosporins, this could lead to a dynamic environment where organic acids produced by the metabolism of fuel can be offset by the production of cephalosporins. More investigations into how microbial communities impact corrosion risks are important and would be more analogous to contaminated fuel storage tanks. However, work with isolated microorganisms still provides the foundations for a better understanding of what microbial taxa are capable of and is easier to interpret than studying mixed communities. Evaluation of microbial community functions can be confounded by numerous populations of microbes capable of different metabolic activities making it difficult to link activities to any specific population. Community analyses and isolation of relevant taxa are both important for understanding fuel degradation and the risks associated with this degradation and storage systems.

The impacts of MIC must also be considered during the cleaning of contaminated tanks and tanks at risk for contamination. Current best practices for cleaning of contaminated fuel storage tanks involve draining of contaminated fuel, power washing tank walls to remove any attached biomass, and allowing the tank to dry before refilling with supposedly uncontaminated fuel (17). This does not fully sterilize the system and once fuel is added back to the storage tank contamination is inevitable (8). The physical removal of biomass may also remove the passivation layer of iron oxides/hydroxides on tank walls and potentially lead to even more damage of the fuel storage infrastructure (18). Another approach operators can use to prevent microbiological contamination in fuel tanks is to add biocides to the stored fuels that can inhibit

any microbial growth. While this seems like a clear solution, biocides are designed to concentrate in either aqueous or organic solutions, and not both, potentially allowing the propagation microorganisms in the untreated phase (10, 19). Additionally, the proper dosing of biocides is an important consideration. The biocide 3,3'-methylene bis (5-methyloxazolidine, MBO) was effective at limiting microbial growth in B10 fuels when dosed at 1000 ppm; however, when dosed with 500 ppm of this compound allowed for more growth of microbial organisms at the interface that were not as diverse as the negative controls (20). This indicates that some organisms are resistant to biocides and can still cause biofouling and impact corrosion risks. Additionally, it is important to know when to treat contaminated tanks and if biocide treatment will be effective if thick biofilms have already been established (21). Finally, biocides themselves can lead to increased abiotic corrosion risks, exacerbating the damage of storage infrastructure. Glutaraldehyde is a commonly used biocide in fuel industries and has been shown to increase corrosivity of carbon steel when dosed at 50 ppm when compared to controls without this biocide (22).

Rather than attempting to treat fuels or entrained water, coatings can also be applied to fuel storage tanks to passivate the metal surfaces and prevent corrosion from occurring (23). Coatings work to exclude corrosion substrates, such as iron, from interacting with electrolytes such as nitrogen or sulfur. Fuel system coatings that are used to provide corrosion resistance are composed of polyurethanes, polyimides, polyvinyl chlorides, epoxy resins, or silicones (24). Biocidal agents are also added to coatings such as toxic metal ions or biogenic compounds (24). However, biocides containing copper and tin ions have been banned due to the ecotoxicity and biomagnification in local food chains. While coatings can provide some protection from microbial contamination, microorganisms are also associated with the degradation of polymeric

coatings (25). Coatings can disbond or delaminate due to material failure or the introduction of mechanical disruption such as scratches on coating surfaces reducing their effectiveness and increasing maintenance costs (26). Coating debonding can itself enhance the risk of corrosion. Microbiologically influenced corrosion was previously identified at debonding sites on an iron pipeline attributed to sulfate reducing bacteria (26). It is critical to understand how microorganisms can impact both coated and uncoated surfaces, as well as how these surfaces influence microbial community structure.

Microbial Communities in Biodiesel Storage Tanks Correlate with Fuel Composition

Understanding how microbiological communities within storage tanks influence fuel composition, and how the initial composition of stored fuels influence microbial communities will provide operators with insights on how to mitigate microbiological growth in their systems There are numerous factors that can influence microbiological community composition within a fuel storage tank including nutrient availability, water, temperature, oxygen concentration, geographic location, and microbial species interactions within a community (27, 28). The most obvious oxidizable substrate within a storage tank is the fuel. The type of carbon present within each fuel, whether a biofuel, ULSD, or a blend can vary wildly. Blends of B20 biodiesel as well as ULSD with up to 5% biodiesel contain differing proportions of fatty acid methyl esters (FAME) which are more readily oxidizable by microorganisms (29). Biofuel feedstocks used also influence the abundance and composition of saturated and unsaturated FAMEs within each fuel (30). Unsaturated FAMEs abiotically degrade more quickly than saturated FAMEs in controlled fuel weathering experiments and longer fatty acid chain lengths are more stable than shorter fatty acid chain lengths indicating a preferential degradation pattern (31, 32).

Microorganisms preferentially degrade certain alkanes as well as FAMEs (31, 33). In Chapter 3, I demonstrated how typical FAME and alkane abundances in B20 biodiesel and B5 ULSD correlate to bacterial and fungal communities using redundancy analyses (RDA). Numerous correlations were found including the presence of Trichocomaceae in fuels with more palmitoleic acid methyl esters and Debaryomycetaceae in fuels with more pentadecanoic acid methyl esters. I provided support for the correlations identified by RDA and provided a causative link between fuel composition and microbial growth by testing a select set of positive correlations between FAME compounds and representative fungal isolates through a series of growth experiments.

The correlations identified by the RDA also provided clues to controlling the growth of microorganisms that can damage storage infrastructure or produce excessive fouling. For example, *Paecilomyces* AF001 was not correlated with the FAME pentadecanoic acid methyl ester and when grown on this FAME as the sole carbon and energy source it was unable to reach log phase by the conclusion of the experiment. These correlations are not infallible: even though there was no correlation with the yeast *Wickerhamomyces* SE3 and the amount of palmitoleic acid methyl ester it was still able to grow using this as a sole carbon and energy source. One possible explanation for the lack of some correlations to provide actionable information is that additional factors influence mixed microbial growth such as the cell type (*e.g. Paecilomyces* is filamentous, and *Wickerhamomyces* is a yeast) that may provide a competitive advantage through the exclusion of other organisms in physical space. As the filamentous fungus *Paecilomyces* grows, it can extend its hyphae into the fuel phase allowing it to obtain oxidizable substrates where other non-hyphal organisms cannot, such as *Wickerhamomyces* SE3 (34). This could mean that even though both fungi can grow on palmitoleic acid methyl ester, when *Paecilomyces* AF001 is present then it can outcompete *Wickerhamomyces* SE3 and many other

bacteria and fungi. Broadly, the correlations predicted using RDA provide *post hoc* hypotheses to investigate how fuels and microorganisms influence one another. While not all these correlations will prove to be significant, the use of tools such as RDA allow us to down select the most likely correlations to then test and provide final, causative, actionable information to fuel producers and storage tank operators and provide best operating practices to limit microbial contamination of fuels.

Transcriptomic Analysis of *Paecilomyces* AF001 Grown on B20 Biodiesel and Ultra-Low Sulfur Diesel

A *Paecilomyces* sp. was found to be prominent in fouled B20 biodiesel and B5 ULSD storage tanks across the continental U.S.; however, there was a critical lack of understanding of how it was growing in the different fuel types. To address this, a study examining lipase activity and transcriptomics was done to investigate how *Paecilomyces* AF001 grew on both fuel types at different stages of growth. It was found that in both fuels *Paecilomyces* AF001 produced lipases that were known to be involved in the oxidation of fatty acid methyl esters (35). Interestingly, mono and dioxygenase transcripts known to be involved in the oxidation of hydrocarbons were only expressed in B5 ULSD conditions and not in the B20 biodiesel fuel (36). This can be explained by *Paecilomyces* AF001 having more access to FAME molecules in B20 biodiesel compared to B5 ULSD. Additionally, metabolism of FAME produces more ATP when compared to the oxidation of hydrocarbons so it could indicate a preferential degradation of FAME when its in excess when compared to B5 ULSD (36, 37).

Microbial contamination in underground storage tanks largely goes unnoticed by storage tank operators because the biofilms that form can interfere with current detection methods (10, 38) Operators are currently informed of any ongoing problems in storage tanks by using an

automated tank gauge that monitors the level of water in these fuels. As water becomes entrained into these storage tanks the chance of microbial contamination increases and operators work to counteract this by removing as much water from the system as possible (10). However, biofilms can form in contaminated tanks and can grow on the automated tank gauge that is typically positioned between the organic fuel phase and the aqueous phase of water that has entered through runoff or atmospheric condensation. Since this tank gauge can no longer inform operators of any water entrapment contamination of the fuels can be left unchecked and lead to loss of fuel quality and increased risks of microbiologically influenced corrosion (39).

I investigated a prominent fungal organism that has been observed in fouled B20 biodiesel and B5 biodiesel tanks across the U.S. Lipase activity was measured, as was the expression of genes associated with degradation of FAME and hydrocarbons through transcriptomic analysis. Lipase activity and their respective transcripts were detected when *Paecilomyces* AF001 was grown in both B5 ULSD and B20 biodiesel. These lipases are exoenzymes, released into the surrounding environment by the fungus. Therefore, lipases or FAME metabolites may be a good potential target for the development of biosensors (40). A biosensor dedicated to detecting the presence of lipases or metabolites could be employed on the automated tank gauge (ATG), since biomass accumulates in storage tanks at the interface between the fuel and aqueous phases where the automated tank gauges are deployed in the systems (19, 41).

Final Conclusions

Prominent fungal organisms found in contaminated diesel and biodiesel fuels were shown to cause increased rates of carbon steel corrosion, which was greatest at the interface between fuel and water phases. Microbial communities in contaminated B20 biodiesel and B5 ULSD

storage tanks were correlated with fuel composition, which was supported by subsequent growth studies with representative isolates. The expression of genes used by *Paecilomyces* AF001 to grow on B20 biodiesel and B5 ULSD is now known, providing insight into the metabolic pathways involved and a potential target for biosensor development. There is still much more work to be done in the field of microbiologically influenced corrosion and fuel degradation including gaining better understanding of how to treat already contaminated fuels and to mitigate contamination of non-contaminated fuels. Contaminated fuels are typically dominated with microbial communities of low diversity, making it important to study the interactions between these prominent populations. The use of renewable fuels will continue to be used as ULSD is a finite resource. It is anticipated that as science advances new renewable energy sources will be established and new generations of biofuels will be developed. Understanding how contamination in these newer systems occurs will be important to secure responsible and reliable energy for future generations.

Works Cited

1. Skovhus T, Eckert RB, Rodrigues E. 2017. Management and Control of Microbiologically Influenced Corrosion (MIC) in the Oil and Gas Industry—Overview and a North Sea Case Study. Journal Biotechnol 256:31–45.

2. AlAbbas F, Williamson C, Bhola S, Spear JR, Olson DL, Mishra B, Kakpovbia AE. 2013. Influence of Sulfate Reducing Bacterial Biofilm on Corrosion Behavior of Low-alloy, High-strength steel (API-5L X80). Int Biodeter Biodegr 78:34-42.

3. Li Y, Xu D, Chen C, Li X, Jia R, Zhang D, Sand W, Wang F, Gu T. 2018. Anaerobic Microbiologically Influenced Corrosion Mechanisms Interpreted Using Bioenergetics and Bioelectrochemistry: A review. J Mater Sci Technol 34:1713–1718.

4. Little BJ, Hinks J, Blackwood DJ. 2020. Microbially Influenced Corrosion: Towards an Interdisciplinary Perspective on Mechanisms. Int Biodeter Biodegr 154:105062.

5. Floyd JG, Stamps BW, Goodson WJ, Stevenson BS. 2021. Locating and Quantifying Carbon Steel Corrosion Rates Linked to Fungal B20 Biodiesel Degradation. Appl Environ Microb AEM0117721.

6. Kotzekidou P. 2014. Encyclopedia of Food Microbiology (Second Edition). Article Titles: B 344–350.

7. Coda R, Cassone A, Rizzello C, Nionelli L, Cardinali G, Gobbetti M. Antifungal Activity of *Wickerhamomyces anomalus* and *Lactobacillus plantarum* during Sourdough Fermentation:

Identification of Novel Compounds and Long-Term Effect during Storage of Wheat Bread. Appl Environ Microbiol 77:3484-3492.

8. Stamps BW, Bojanowski CL, Drake CA, Nunn HS, Lloyd PF, Floyd JG, Emmerich KA, Neal AR, Crookes-Goodson WJ, Stevenson BS. 2020. In situ Linkage of Fungal and Bacterial Proliferation to Microbiologically Influenced Corrosion in B20 Biodiesel Storage Tanks. Front Microbiol 11:167.

9. Stamps BW, Andrade OC, Lyon WJ, Floyd JG, Nunn HS, Bojanowski CL, Crookes-Goodson WJ, Stevenson BS. 2018. Genome Sequence of a *Byssochlamys* sp. Strain Isolated from Fouled B20 Biodiesel. Genome Announcements 6:e00085-18.

10. Passman F. 2003. Fuel and Fuel System Microbiology: Fundamentals, Diagnosis, and Contamination Control. American Society for Testing & Materials. ASTM Manual.

11. Gibbons SM, Gilbert JA. 2015. Microbial Diversity—Exploration of Natural Ecosystems and Microbiomes. Curr Opin Genet Dev 35:66–72.

12. Kobayashi H, Endo K, Sakata S, Mayumi D, Kawaguchi H, Ikarashi M, Miyagawa Y, Maeda H, Sato K. 2012. Phylogenetic Diversity of Microbial Communities Associated with the Crude-oil, Large-insoluble-particle and Formation-water Components of the Reservoir Fluid from a Non-flooded high-temperature Petroleum Reservoir. J Biosci Bioeng 113:204–210.

13. Litchman E, Edwards KF, Klausmeier CA. 2015. Microbial Resource Utilization Traits and Trade-offs: Implications for Community Structure, Functioning, and Biogeochemical Impacts at Present and in the Future. Front Microbiol 06:254.

14. Künzler M. 2018. How Fungi Defend Themselves Against Microbial Competitors and Animal Predators. Plos Pathog 14:e1007184.

15. Pisano MA, Vellozzi EM. 1974. Production of Cephalosporin C by *Paecilomyces persicinus* P-10. Antimicrob Agents Ch 6:447–451.

16. Singh AK, Chugh B, Saha SKr, Banerjee P, Ebenso EE, Thakur S, Pani B. 2019. Evaluation of Anti-corrosion Performance of an Expired Semi Synthetic Antibiotic Cefdinir for Mild Steel in 1 M HCl Medium: An Experimental and Theoretical Study. Results Phys 14:102383.

17. Beyond the microbes: 2nd LRS, 2nd CES work together > Barksdale Air Force Base > News.

18. Haupt S, Strehblow HH. 1987. Corrosion, Layer Formation, and Oxide Reduction of Passive Iron in Alkaline Solution: A Combined Electrochemical and Surface Analytical Study. Langmuir 3:873–885.

19. Passman FJ. 2013. Microbial Contamination and its Control in Fuels and Fuel Systems Since 1980–A Review. Int Biodeter Biodegr 81:88-104.

20. Bücker F, Barbosa CS, Quadros PD, Bueno MK, Fiori P, Huang C te, Frazzon APG, Ferrão MF, Camargo FA de O, Bento FM. 2014. Fuel biodegradation and molecular characterization of microbial biofilms in stored diesel/biodiesel blend B10 and the effect of biocide. Int Biodeter Biodegr 95:346–355.

21. Bas S, Kramer M, Stopar D. 2017. Biofilm Surface Density Determines Biocide Effectiveness. Front Microbiol 8:2443.

22. Eid MM, Duncan KE, Tanner RS. 2018. A semi-continuous system for monitoring microbially influenced corrosion. J Microbiol Meth 150:55–60.

23. Montemor MF. 2014. Functional and smart coatings for corrosion protection: A review of recent advances. Surf Coat Technol 258:17-37.

24. Little BJ, Blackwood DJ, Hinks J, Lauro FM, Marsili E, Okamoto A, Rice SA, Wade SA, Flemming H-C. 2020. Microbially influenced corrosion – any progress?. Corros Sci 170:108641.

25. Gu J-D, Mitton DB, Ford TE, Mitchell R. 1998. Microbial degradation of polymeric coatings measured by electrochemical impedance spectroscopy. Biodegradation 9:39–45.

26. Ding Q, Fang L, Cui Y, Wang Y. 2017. Experimental study on the influence of sulfate reducing bacteria on the metallic corrosion behavior under disbonded coating. Int J Corros 2017:1–13.

27. Braga RM, Dourado MN, Araújo WL. 2016. Microbial interactions: ecology in a molecular perspective. Braz J Microbiol 47:86–98.

28. Cao H, Chen R, Wang L, Jiang L, Yang F, Zheng S, Wang G, Lin X. 2016. Soil pH, total phosphorus, climate and distance are the major factors influencing microbial activity at a regional spatial scale. Sci Rep-uk 6:25815.

29. Thomas A, Leahy M, Smith JWN, Spence MJ. 2017. Natural attenuation of fatty acid methyl esters (FAME) in soil and groundwater. Q J Eng Geol Hydroge 50:301-317.

30. Hoekman KS, Broch A, Robbins C, Ceniceros E, Natarajan M. 2012. Review of biodiesel composition, properties, and specifications. Renew Sustain Energy Rev 16:143–169.

31. Fuller S, Spikmans V, Vaughan G, Guo C. 2013. Effects of Weathering on Sterol, Fatty Acid Methyl Ester (FAME), and Hydrocarbon Profiles of Biodiesel and Biodiesel/Diesel Blends. Environmental Forensics 14:42–49.

32. Dahiya A. 2020. Biomass to biofuels and waste to energy. *In* Bioenergy 2nd Edition 649–670.

33. Ciric L, Philp J, Whiteley AS. 2010. Hydrocarbon utilization within a diesel-degrading bacterial consortium. FEMS Microbiol Lett 303:116-122.

34. Miller RB, Sadek A, Crouch AL, Floyd JG, Drake CA, Stevenson BS, Crookes-Goodson W, Monty CN, Senko JM. 2020. Novel Mechanism of Microbially Induced Carbon Steel Corrosion at an Aqueous/Non-aqueous Interface. Ind Eng Chem Res 59:15784–15790.

35. White, A., Handler, P. & Smith, E.L. 1968. Principles of Biochemistry, 4th edn. McGraw–Hill, New York.

36. Rojo F. 2010. Enzymes for aerobic degradation of alkanes, p 781-797. *In* Timmis KN (eds), Handbook of hydrocarbon and lipid microbiology, Springer, Berlin, Heidelberg.

37. Sørensen G, Pedersen D, Nørgaard A. 2011. Microbial growth studies in biodiesel blends. Bioresour. Technol. 102:5259-5264.

38. Passman FJ. 2013. Microbial Contamination and its Control in Fuels and Fuel Systems Since 1980 – A Review. Int Biodeter Biodegr 81:88–104.

39. Stevenson BS, Stamps BW, Floyd JF, Bojanowski CL, Goodson WJ. 2021. Failure analysis of Microbiologically Influenced Corrosion in Storage Tanks Containing B20 Biodiesel. *In* Failure Analysis of Microbiologically Influenced Corrosion 1st Ed.

40. Peraza-Reyes L, Berteaux-Lecellier V. 2013. Peroxisomes and Sexual Development in Fungi. Front Physiol 4:244.

41. Floyd JG, Stamps BW, Goodson WJ, Stevenson BS. 2021. Locating and Quantifying Carbon Steel Corrosion Rates Linked to Fungal B20 Biodiesel Degradation. Appl Environ Microb AEM0117721.

APPENDIX

Table A.1. Fuel sample descriptions used in Chapter 3 for the meta-analysis.

Sample #	Base #	Geography	Fuel Type	Date Collected
1	1	Northwest	B20 Biodiesel	Aug 2019
2	2	Northwest	B5 ULSD	Aug 2019
3	2	Northwest	B5 ULSD	Aug 2019
4	3	Southeast	B20 Biodiesel	Mar 2015
5	3	Southeast	B20 Biodiesel	Jun 2015
6	3	Southeast	B20 Biodiesel	Jul 2015
7	3	Southeast	B20 Biodiesel	Aug 2015
8	3	Southeast	B20 Biodiesel	Oct 2015
9	3	Southeast	B20 Biodiesel	May 2015
10	3	Southeast	B20 Biodiesel	Oct 2015
11	3	Southeast	B20 Biodiesel	Oct 2015
12	3	Southeast	B20 Biodiesel	Mar 2015
13	3	Southeast	B20 Biodiesel	May 2015
14	3	Southeast	B20Biodiesel	Nov 2014
15	3	Southeast	B20 Biodiesel	Aug 2015
16	3	Southeast	B20 Biodiesel	Oct 2015
17	3	Southeast	B20 Biodiesel	Oct 2015
18	3	Southeast	B20 Biodiesel	Oct 2015
19	3	Southeast	B20 Biodiesel	Jul 2015
20	3	Southeast	B20 Biodiesel	Aug 2015
21	3	Southeast	B20 Biodiesel	Nov 2014
22	3	Southeast	B20 Biodiesel	June 2015
23	3	Southeast	B20 Biodiesel	May 2015

24	3	Southeast	B20 Biodiesel	Oct 2015
25	3	Southeast	B20 Biodiesel	Sep 2015
26	3	Southeast	B20 Biodiesel	May 2015
27	3	Southeast	B20 Biodiesel	Sep 2015
28	3	Southeast	B20 Biodiesel	Oct 2015
29	3	Southeast	B20 Biodiesel	Nov 2015
30	3	Southeast	B20 Biodiesel	Nov 2015
31	3	Southeast	B20 Biodiesel	Nov 2015
32	3	Southeast	B20 Biodiesel	Aug 2014
33	3	Southeast	B20 Biodiesel	Feb 2016
34	3	Southeast	B20 Biodiesel	Feb 2016
35	3	Southeast	B20 Biodiesel	Feb 2016
36	3	Southeast	B20 Biodiesel	Nov 2015
37	3	Southeast	B20 Biodiesel	Nov 2015
38	3	Southeast	B20 Biodiesel	Nov 2015
39	3	Southeast	B20 Biodiesel	Aug 2014
40	3	Southeast	B20 Biodiesel	Feb 2016
41	3	Southeast	B20 Biodiesel	Feb 2016
42	3	Southeast	B20 Biodiesel	Feb 2016
43	3	Southeast	B20 Biodiesel	Nov 2015
44	3	Southeast	B20 Biodiesel	Nov 2015
45	3	Southeast	B20 Biodiesel	Nov 2015
46	3	Southeast	B5 ULSD	Sep 2017
47	3	Southeast	B5 ULSD	Sep 2017
48	3	Southeast	B5 ULSD	Sep 2017
49	3	Southeast	B5 ULSD	Sep 2017
50	3	Southeast	B20 Biodiesel	Feb 2016

51	3	Southeast	B20 Biodiesel	May 2016
52	3	Southeast	B20 Biodiesel	May 2016
53	3	Southeast	B20 Biodiesel	Feb 2016
54	3	Southeast	B20 Biodiesel	Sep 2015
55	3	Southeast	B20 Biodiesel	May 2016
56	3	Southeast	B20 Biodiesel	May 2016
57	3	Southeast	B20 Biodiesel	May 2016
58	3	Southeast	B20 Biodiesel	May 2016
59	4	Southwest	B20 Biodiesel	Apr 2015
60	4	Southwest	B20 Biodiesel	Apr 2015
61	4	Southwest	B20 Biodiesel	Apr 2015
62	4	Southwest	B20 Biodiesel	Sep 2014
63	4	Southwest	B20 Biodiesel	Oct 2015
64	4	Southwest	B20 Biodiesel	Oct 2015
65	4	Southwest	B20 Biodiesel	Oct 2015
66	4	Southwest	B20 Biodiesel	Oct 2015
67	4	Southwest	B20 Biodiesel	Oct 2015
68	4	Southwest	B20 Biodiesel	Oct 2015
69	5	Central	B20 Biodiesel	Jan 2016
70	5	Central	B20 Biodiesel	Feb 2016
71	5	Central	B20 Biodiesel	Feb 2016
72	5	Central	B20 Biodiesel	Feb 2016
73	5	Central	B20 Biodiesel	Feb 2016
74	5	Central	B20 Biodiesel	Feb 2016
75	5	Central	B20 Biodiesel	Feb 2016
76	5	Central	B20 Biodiesel	Jan 2016
77	5	Central	B20 Biodiesel	Feb 2016

78	5	Central	B5 ULSD	Feb 2016
79	6	Southeast	B20 Biodiesel	Jun 2017
80	6	Southeast	B20 Biodiesel	Jun 2017
81	6	Southeast	B20 Biodiesel	Jun 2017
82	6	Southeast	B5 ULSD	Jun 2017
83	7	Northwest	B20 Biodiesel	Apr 2018
84	7	Northwest	B5 ULSD	Apr 2018
85	7	Northwest	B5 ULSD	Apr 2018
86	8	Northwest	B20 Biodiesel	Aug 2018
87	8	Northwest	B5 ULSD	Aug 2018
88	8	Northwest	B5 ULSD	Aug 2018
89	9	Northwest	B5 ULSD	Apr 2018
90	10	Southeast	B5 ULSD	Jun 2017
91	10	Southeast	B5 ULSD	Jun 2017
92	11	Northwest	B20 Biodiesel	Aug 2018
93	11	Northwest	B5 ULSD	Oct 2015
94	12	Northwest	B5 ULSD	Aug 2018
95	13	Southeast	B20 Biodiesel	Jun 2017
96	13	Southeast	B5 ULSD	Jun 2017
97	13	Southeast	B5 ULSD	Jun 2017
98	14	Northwest	B5 ULSD	Apr 2018
99	14	Northwest	B5 ULSD	Apr 2018
100	15	Northwest	B5 ULSD	Aug 2018
101	15	Northwest	B5 ULSD	Aug 2018
102	16	Northwest	B5 ULSD	Aug 2018
103	16	Northwest	B5 ULSD	Aug 2018
104	17	Southeast	B20 Biodiesel	Jun 2017

105	17	Southeast	B5 ULSD	Jun 2017
106	17	Southeast	B5 ULSD	Jun 2017

Table A.2. n-Alkane composition of fuels in parts per million (PPM) used in the analyses from Chapter 3. Values provides are the average PPM from 3 technical replicates analyzed from the same fuel. Sample descriptions can be seen in table A.1.

Sample	C7	C8	C9	C10	C11	C12	C13	C14	C15	C16	C17	C18	C19	C20	C21	C22	C23	C24	C25	C26
1	170	567	1461	2785	3794	3945	4327	4943	5227	5292	5576	4645	3657	2904	3890	1637	1153	575	287	0
2	158	568	1635	3665	5011	5346	5326	5655	5553	5512	5575	4712	3463	2689	2119	1532	1006	573	269	0
3	190	559	1594	3408	5084	5588	5799	6149	5689	5457	5718	4609	3769	3074	2484	1859	1281	799	453	211
4	632	974	2520	4409	5808	5584	5583	5590	5046	4535	4293	3567	2960	2370	1917	1336	1029	519	269	159
5	587	887	1867	3116	4384	4346	4505	4923	4608	4323	4160	3418	2783	2216	1758	1162	809	409	216	132
6	542	888	2056	4347	5168	4848	5055	5321	4611	4158	3784	3466	2433	1988	1387	1075	787	435	233	51
7	562	913	2118	4463	5254	4870	5081	5271	4586	4077	3784	3396	2403	1959	1488	1048	778	421	213	92
8	300	882	2655	6271	7291	6460	6758	7086	6645	5998	5657	4571	3634	2948	5716	1729	1173	704	345	196
9	459	886	2390	4212	5527	5355	5129	5312	4765	4276	4135	3395	2835	2253	4790	1287	970	509	260	160
10	298	824	2143	5038	5927	5406	5571	6048	5742	5198	4937	4101	3300	2670	4855	1584	1178	664	356	202
11	356	951	2831	6663	7723	6915	7128	7648	7057	6388	5950	4766	3822	3076	5903	1818	1245	744	374	212
12	411	768	2352	5244	6956	6633	6367	6418	5698	4969	4692	3797	3248	2642	4791	1627	1174	730	392	212
13	337	674	2128	4427	5851	5124	4986	5217	4733	4231	3936	3144	2635	2154	4120	1197	828	486	239	92
14	420	885	3194	5722	7168	6594	7049	7316	6409	5710	5276	4303	3411	2736	5717	1576	1240	584	288	175
15	308	673	2118	4369	5741	5039	4883	5099	4601	4103	3807	3101	2510	2081	1542	1161	793	463	231	44
16	436	891	2721	4975	6772	6005	5767	5853	5491	4844	4482	3567	2883	2405	1831	1338	892	496	155	0
17	353	880	2750	4923	6734	6004	5754	6005	5583	4986	4612	3671	2939	2428	2016	1383	938	547	232	0

18	329	790	2561	4649	6459	5732	5514	5742	5381	4931	4506	3598	2969	2427	2066	1402	962	560	256	0
19	222	545	1426	2896	4259	4074	4153	4458	4289	4170	4200	3540	2867	2350	1779	1230	746	402	195	0
20	599	754	1550	3117	4503	4351	4404	4715	4535	4442	4420	3770	3055	2463	2180	1275	801	392	196	0
21	574	985	2624	4380	5179	4533	4580	4810	4521	4492	4563	4408	3013	2425	3661	1294	897	406	186	0
22	599	676	1514	3588	5260	5114	5364	5675	5524	5484	5522	4738	3932	3140	5706	1710	1071	564	278	157
23	537	951	2976	6002	7544	6927	6897	7071	6423	6079	5840	5219	3939	3150	5645	1803	1236	686	340	195
24	275	782	2559	4654	6428	5743	5618	5780	5441	4958	4524	3680	2974	2458	2053	1407	951	447	163	0
25	344	750	2055	4399	6088	5552	5583	5841	5455	4992	4714	3906	3272	2724	4859	1639	1226	695	337	185
26	472	822	2377	4893	6065	5590	5594	5671	5295	4924	4844	4454	3335	2707	5089	1566	1093	606	324	209
27	352	766	2066	4412	6138	5579	5608	5755	5507	5022	4718	2725	3347	2737	4989	1655	1222	700	328	174
28	247	705	2290	4180	5812	5294	5282	5540	5221	4749	4373	3545	2877	2377	2090	1355	913	522	231	0
29	15	303	1477	4026	4862	4513	4452	4614	4091	3624	3348	2763	2229	1817	1538	1033	722	410	192	0
30	327	489	2226	5410	6589	6248	6422	6588	5863	5287	4961	4135	3435	2820	4420	1693	1198	701	333	167
31	418	549	2382	5674	6864	6567	6594	6650	5809	5148	4950	4080	3365	2745	4311	1642	1165	683	325	107
32	380	949	2209	3773	4654	4862	5277	5617	5249	5201	5109	3983	3609	2840	3049	1656	1130	643	313	0
33	17	440	1683	4939	6438	5745	5566	5378	4722	4177	3930	3247	2694	2265	1726	1412	1034	629	295	105
34	24	424	1618	4802	6241	5585	5502	5226	4568	4034	3781	3154	2586	2186	1713	1361	990	608	292	147
35	39	434	1663	4894	6387	5705	5539	5242	4616	4089	3873	3185	2633	2242	1728	1392	1015	619	297	101
36	374	709	2519	6755	8856	7935	7755	7699	6538	5905	5472	4585	3857	3251	4544	2103	1530	940	432	124

37	328	686	2475	6625	8688	7775	7882	7465	6458	5839	5475	4540	3852	3225	4533	2095	1539	930	438	187
38	289	539	2043	5820	7799	7226	7277	7204	6392	5945	5445	4661	3992	3354	4587	2146	1552	923	421	129
39	380	838	2187	4269	5723	5258	5280	4974	4030	3779	3469	3074	2862	2541	2479	1686	1157	585	226	0
40	154	641	1753	4490	5928	5192	5220	4597	3656	3081	2899	2520	2165	1942	1592	1157	763	362	136	0
41	93	573	1636	4286	5716	5111	4971	4490	3647	3094	2912	2563	2181	1965	1538	1190	783	377	152	0
42	106	604	1704	4449	5876	5203	5069	4633	3650	3135	2898	2542	2210	1944	1596	1165	771	374	140	0
43	624	1079	2842	6562	8694	7777	7574	7191	5567	4877	4493	3930	3504	3038	4354	1931	1276	616	231	0
44	576	1046	2763	6376	8393	7540	7377	6845	5323	4638	4344	3776	3358	2920	4320	1828	1215	583	221	0
45	552	1017	2705	6279	8297	7476	7529	6801	5266	4592	4246	3734	3337	2885	4246	1826	1202	581	209	0
46	302	1053	3994	7715	8853	9263	10765	11644	10878	9858	9451	7101	5619	4273	3205	2257	1473	807	327	0
47	275	998	3982	7382	8766	9167	10395	10918	10070	9252	9156	7415	6242	4966	3881	2851	1898	1046	460	211
48	351	1081	4267	7544	8982	9379	10497	11243	10286	9731	9220	7581	6358	5096	3978	2957	1690	1126	518	239
49	219	1835	7736	11291	10823	10019	10317	10502	9779	9288	9306	7508	6368	5138	3792	2879	2005	1266	714	386
50	0	193	1205	3684	4857	4668	5165	5325	4686	4187	3796	3248	2491	2075	1612	1191	819	477	229	0
51	175	295	1110	4236	6114	5899	6031	6256	5976	5537	5166	4301	3390	2537	4241	1167	707	352	163	0
52	199	299	1114	4261	6144	5906	6099	6250	5922	5484	5097	4257	3348	2515	4307	1156	696	353	165	0
53	0	0	0	439	2604	4349	5744	6364	5719	5238	4669	4005	3046	2556	1894	1484	1021	582	283	146
54	334	753	2104	4518	6285	5777	5610	5864	5621	5104	4776	3927	3313	2745	5287	1676	1232	709	342	183
55	38	273	1570	6357	8438	7509	7194	6877	5798	5020	4728	4056	3350	2582	4378	1270	796	407	177	0

56	57	268	1553	6246	8366	7349	7241	6888	5855	5215	4864	4135	3438	2646	4515	1330	830	424	185	0
57	418	890	2343	4985	6612	5886	5631	5111	4039	3446	3192	2852	2494	2205	3131	1350	885	436	157	0
58	295	793	2121	4537	6012	5356	5138	4532	3693	3146	2937	2596	2236	2012	2682	1234	819	387	149	0
59	615	662	2092	3240	4082	4102	4526	4924	4571	4334	4262	3534	2884	2309	1783	1308	938	577	346	226
60	398	705	2846	6220	7460	7155	7716	7989	7166	6311	6138	5318	4613	3728	4983	2050	1361	858	492	298
61	525	668	2598	5758	7208	6850	7438	7710	6743	5999	5828	4924	4195	3321	4912	1830	1211	730	420	258
62	127	401	780	1818	2797	3243	4139	5351	5330	5030	4759	4027	3047	2386	2712	1358	1109	678	426	299
63	690	894	2075	7075	8747	8197	8745	8893	7465	6660	6482	5422	4704	3890	5081	2510	1809	1089	594	345
64	415	496	2005	6886	8458	7904	8372	8500	7074	6234	6143	5127	4486	3725	4969	2392	1671	1045	567	312
65	28	501	1162	4742	6576	6001	6226	6337	5397	4692	4452	3676	3012	2570	2243	1403	920	620	321	0
66	33	286	1260	4855	6762	6174	6378	6397	5442	4755	4432	3665	3024	2569	1858	1527	878	487	240	56
67	0	64	643	3025	4250	4315	4899	5532	4911	4346	4204	3580	3091	2655	2206	1587	1093	654	337	143
68	396	520	2056	7131	9127	8576	9195	8933	7522	6621	6242	5340	4661	3904	5124	2515	1728	1054	554	302
69	9	256	1007	3651	5317	5283	5884	6843	6775	6717	6495	5395	4222	3172	2325	1308	755	339	139	0
70	52	347	1204	3768	5749	6133	7919	8611	7861	7046	6631	5127	3968	2862	3606	1184	645	249	0	0
71	19	304	1242	3935	5831	5644	6268	7291	7331	7416	7032	5662	4444	3306	4185	1404	791	346	38	0
72	159	364	1231	3825	5668	5575	6236	7114	7249	7214	7005	5526	4345	3223	3973	1367	761	343	135	0
73	81	363	1248	3677	5573	6031	7581	8427	7638	6831	6332	5008	3862	2823	3728	1172	637	250	0	0
74	124	399	1289	3680	5730	6591	9122	9747	8151	6792	6182	4558	3404	2386	3902	956	506	165	0	0

75	47	342	1179	3770	5674	6069	7580	8359	7589	6898	6380	4920	3813	2726	3841	1125	606	233	0	0
76	0	243	992	3606	5244	5152	5785	6599	6669	6765	6361	5257	4145	3090	2028	1283	731	330	131	0
77	35	253	1010	3689	5449	5287	5840	6750	6833	6819	6590	5339	4199	3143	1920	1301	739	333	136	0
78	257	582	1513	3702	5734	6924	8875	9045	7508	6544	6232	5217	4477	3710	2793	2002	1129	512	171	0
79	159	705	1905	2956	3825	3960	4507	4900	4671	4707	4461	3805	3289	2657	2462	1587	1105	675	313	55
80	199	657	1748	2760	3572	3706	4500	4701	4792	4796	4593	3791	3422	2740	2485	1635	1286	808	421	101
81	327	772	2021	4268	5431	5586	6623	7305	6825	6725	6278	5106	4310	3277	4366	1795	1203	663	298	0
82	190	1141	3962	4249	6746	8621	10525	12845	11442	12248	11334	9206	6793	5244	3725	2624	1695	1068	589	335
83	91	371	1332	2806	5115	5755	6016	6158	5787	5420	5026	4090	3209	2373	3228	1188	860	392	117	0
84	64	775	4159	5919	5729	5319	5823	4696	3493	2568	1737	1338	711	212	0	0	0	0	0	0
85	22	724	3859	5462	5356	5053	5648	4550	3468	2600	1781	1189	530	97	0	0	0	0	0	0
86	16	301	1066	2082	3312	3835	4471	5290	5244	5040	4836	3913	3319	2521	3451	1431	1024	556	281	0
87	267	852	1915	3384	4872	4946	5245	5933	6254	6449	6869	5730	4187	3241	2521	1780	1139	661	326	0
88	52	439	1438	3325	4540	4865	5392	6062	6125	6200	6333	5517	4183	3335	2614	1927	1321	811	432	62
89	414	1282	4014	8327	9362	9029	9319	8819	8183	7809	7575	6205	5155	3811	2395	1211	501	173	0	0
90	293	959	2276	4975	6908	6680	7536	7628	7150	6564	5998	4983	3950	2918	2061	1349	780	403	162	0
91	395	1235	2582	5392	7488	7564	8473	8322	7269	6805	6643	5444	4265	3149	2291	1468	859	449	180	0
92	225	661	1282	2072	2719	3115	3690	4484	4420	4434	4168	3454	2868	2134	3372	1133	828	368	115	0
93	604	851	2279	3531	4818	4943	5268	6179	6278	6188	6137	5099	4283	3419	2717	1997	1360	856	488	291

94	132	886	2113	3224	4220	4251	4759	5620	6216	6406	6480	5299	4057	3146	2403	1699	1055	559	254	0
95	689	665	1865	4214	5794	5801	6513	6722	6239	5864	5643	4784	3896	3093	2456	1676	1063	604	256	0
96	364	1105	2803	5826	7731	7907	8974	8902	7803	7935	7186	6983	4595	3652	2846	1962	1211	690	327	0
97	261	871	2513	5453	7414	7506	8161	8652	7492	7052	6814	5692	4592	3662	3015	2043	1330	784	370	52
98	560	3198	10955	15815	17183	15417	14466	12155	7180	3239	1606	955	611	396	200	55	0	0	0	0
99	558	3210	10989	15853	17041	15415	14311	12226	7235	3250	1611	956	619	402	201	58	0	0	0	0
100	50	576	1675	2896	3589	3718	4477	5936	7125	7639	7968	7190	4385	3243	2394	1723	1101	628	297	0
101	539	1415	2504	4820	5372	4713	4633	5524	6010	6442	6301	5607	4965	4049	3201	2151	1115	512	205	0
102	126	515	1574	4237	5218	5299	5457	5978	5689	5784	6167	5398	3665	2882	2454	1687	1138	646	315	0
103	121	531	1576	3447	4550	4776	5284	6068	6836	7189	7956	7268	3945	2928	2534	1665	1144	669	353	0
104	422	715	1868	3174	4133	4205	4674	5094	4828	4950	4932	3979	3460	2729	2410	1620	1274	630	269	0
105	114	885	1854	3240	4602	4429	4605	4863	4372	4449	4356	3535	2920	2242	1662	1112	670	338	103	0
106	371	1155	2388	5387	7558	6925	7179	7284	6468	6071	5714	4771	3772	2779	1929	1221	681	328	42	0

Table A.3. Fatty acid methyl ester concentrations in parts per million (PPM) used in the analyses from Chapter 3. Values provides are the average PPM from 3 technical replicates analyzed from the same fuel. Sample descriptions can be seen in table A.1.

Sample	C11:0	C12:0	C14:1	C14:0	C15:0	C16:1	C16:0	C17:0	C18:2	C18:1	C18:0	C20:5	C20:4	C20:3	C20:2	C20:1	C20:0	C22:6	C22:2	C23:0	C24:1	C24:0
1	0	0	385	18	1191	0	8161	76	30822	36740	3872	0	1064	42	0	1588	1064	0	0	0	160	145
2	0	0	599	0	0	0	0	0	0	0	0	0	0	0	0	477	0	0	0	0	0	0
3	0	0	379	0	0	164	0	0	85	0	0	0	0	0	0	587	0	0	0	0	0	0
4	587	0	512	1646	39	276	24143	799	15018	12068	13213	0	497	542	0	1034	497	0	74	51	96	179
5	387	77	274	1451	0	0	37817	376	7343	55086	8211	0	428	0	0	692	428	0	37	14	0	133
6	277	182	64	1527	23	0	46765	175	4626	84340	6580	0	482	0	0	626	482	31	34	0	0	119
7	258	172	0	1468	98	0	46103	167	3208	75017	6369	0	445	0	0	656	445	0	0	0	0	108
8	0	199	221	1719	72	0	50668	153	16591	106386	6937	0	509	0	0	680	509	0	40	0	0	98
9	0	0	423	1520	0	0	22850	748	13083	11825	12526	0	471	112	0	918	471	37	0	52	60	155
10	0	156	179	1528	0	0	46577	155	3852	89082	6561	0	513	0	0	826	513	0	39	0	0	123
11	0	215	1084	1816	64	0	52106	146	17477	110190	7343	0	539	0	0	714	539	0	115	0	0	107
12	0	0	513	2201	0	0	27113	1048	38816	15648	17911	70	337	141	0	897	337	68	0	0	0	127
13	0	0	330	951	0	0	26211	432	44345	48233	9216	14	351	110	0	607	351	21	72	49	0	139
14	434	0	344	720	0	0	13598	396	15027	10226	7759	0	712	314	0	1461	712	0	47	49	184	234
15	0	0	258	956	0	0	26414	411	41468	27246	8812	32	348	116	0	588	348	0	0	33	0	139
16	0	193	362	1600	46	0	50768	113	13650	92579	6112	0	364	0	0	547	364	0	106	0	0	27
17	0	220	364	1696	44	0	51471	138	14634	96082	6503	0	425	0	0	561	425	0	36	0	0	0
18	0	207	158	1670	0	0	51251	144	14207	96356	6572	0	461	0	0	576	461	0	70	0	0	28
19	0	144	92	1453	97	0	45522	161	15330	88953	6285	0	446	0	0	505	446	0	35	0	0	126
20	0	156	88	1492	108	0	46660	172	5172	81398	6364	0	439	0	0	630	439	0	112	0	0	74
21	0	33	0	828	0	0	31154	153	8810	92003	5288	0	563	271	0	957	563	0	78	0	98	149
22	48	176	212	1658	368	0	47468	216	9957	66061	7280	0	548	0	0	707	548	0	0	0	0	140
23	0	0	409	1565	0	0	31247	589	34189	10498	11850	61	549	197	0	1019	549	21	111	50	101	176
24	0	206	447	1680	53	0	51615	142	14673	96786	6660	0	448	0	0	574	448	0	72	0	0	30
25	0	167	89	1500	0	0	46169	143	5394	83283	6411	0	504	106	0	868	504	0	74	0	0	128
26	56	2	222	1344	0	0	28607	399	24627	91232	10651	19	490	247	58	930	490	0	0	47	63	162
27	0	174	254	1511	0	0	46237	144	5251	88722	6436	0	511	0	0	795	511	0	0	0	0	128
28	0	199	435	1644	45	0	50894	139	14421	95209	6466	0	416	0	0	562	416	0	0	0	0	0
29	0	0	133	401	710	1310	27044	116	46863	61064	5662	14	397	98	0	533	397	0	0	0	0	120

30	0	0	615	665	194	0	35303	192	61544	89356	8649	0	640	121	0	800	640	0	0	53	0	154
31	0	0	339	656	972	0	34782	176	59323	85629	8335	0	601	114	0	753	601	0	0	36	0	143
32	0	379	489	1038	949	4220	21989	327	30259	40663	10377	129	586	153	0	1009	586	107	41	69	169	250
33	0	0	329	359	786	2283	25019	128	51796	62864	6149	28	426	72	0	684	426	0	137	18	0	147
34	0	0	74	342	354	2290	24176	116	50049	62699	5887	43	406	137	0	667	406	0	37	50	0	145
35	0	0	379	349	561	1525	24468	140	50760	60868	5955	29	414	121	0	640	414	0	34	50	0	147
36	0	0	337	559	502	0	31531	187	60601	84649	8542	0	558	136	0	899	558	0	0	32	0	133
37	0	0	585	547	766	0	31497	171	60864	82628	8463	0	573	124	0	922	573	0	0	17	0	143
38	0	0	342	556	806	0	32298	183	61192	81704	8919	0	567	156	0	917	567	0	0	17	0	123
39	0	0	404	405	693	0	21923	232	39563	49601	9184	0	779	169	0	748	779	16	0	73	0	228
40	0	0	152	194	554	1232	20631	123	54988	60867	5799	42	415	106	0	573	415	0	0	54	0	157
41	0	0	66	196	553	694	20839	126	55906	59203	5921	15	441	106	0	577	441	0	0	57	0	173
42	0	0	116	193	531	639	20590	117	55492	58978	5806	16	302	111	187	521	302	0	0	36	0	157
43	0	0	281	359	616	0	29199	189	69756	82926	8884	0	651	190	0	828	651	0	0	56	0	170
44	0	0	282	338	784	0	28133	192	68287	81846	8453	0	621	135	0	776	621	0	0	53	0	159
45	0	0	463	331	785	0	27901	189	67939	81650	8432	0	610	145	0	785	610	0	0	39	0	159
46	0	0	697	0	127	0	1448	6	3952	0	534	0	0	0	0	664	0	0	39	0	0	0
47	0	0	610	37	137	0	2436	44	5925	1173	1067	0	0	0	0	871	0	0	0	0	0	0
48	0	0	653	61	88	0	2556	16	6422	1363	1115	0	0	0	0	902	0	0	0	0	0	0
49	0	0	0	0	543	0	3099	11	15030	1341	1129	0	0	0	0	906	0	0	0	0	0	0
50	0	0	296	178	693	2051	20398	113	55756	59044	5732	57	427	124	0	609	427	0	36	61	0	147
51	0	399	513	1556	654	1878	23313	581	37205	77391	11406	67	278	94	52	618	278	18	33	0	0	33
52	0	395	501	1541	720	1198	23154	576	37032	76909	11367	71	279	99	59	627	279	39	0	0	0	66
53	0	0	257	244	842	2446	24699	155	65569	70931	7095	67	531	128	0	748	531	0	0	64	0	182
54	0	171	370	1514	0	0	46336	151	5594	91426	6425	0	510	0	0	859	510	0	37	0	0	126
55	0	192	559	1714	0	2465	24464	644	32995	79670	12547	80	244	102	64	691	244	57	0	0	0	0
56	0	196	545	1758	64	2654	25154	677	33875	81660	12914	96	259	99	73	735	259	62	35	0	0	57
57	0	0	220	235	574	0	21464	136	58612	72473	6499	0	453	119	0	576	453	0	0	49	0	136
58	0	0	286	206	390	0	19709	114	53875	62263	5967	0	428	112	0	528	428	0	0	34	0	132
59	372	0	415	1506	0	306	23891	767	26955	10436	13974	0	345	256	0	737	345	0	95	34	0	134
60	0	0	652	1934	119	0	27044	921	46904	15699	16723	42	284	119	0	964	284	22	39	33	0	82
61	0	0	614	1763	84	0	25802	898	50811	13632	15773	51	371	137	0	873	371	62	39	55	0	139

62	0	0	246	257	0	0	15671	196	18349	6139	6112	0	569	612	0	1027	569	44	83	63	146	209
63	0	69	609	1812	2132	0	34466	745	18949	80287	15514	0	456	490	0	1228	456	0	0	34	0	142
64	0	66	651	1751	2041	0	33636	702	50171	85384	15133	44	413	139	0	1079	413	42	0	0	0	125
65	0	0	354	392	157	2840	17378	180	14788	6161	6191	0	326	254	0	785	326	0	0	0	0	119
66	0	3	385	407	1086	3047	17888	189	49516	69305	6314	11	297	97	0	745	297	0	75	0	0	101
67	0	8	391	791	1492	3387	22106	367	45240	70429	8845	18	306	106	0	805	306	0	36	0	0	116
68	0	64	625	1274	1490	0	29998	541	56905	86242	12892	14	466	115	0	1193	466	0	0	0	0	138
69	0	0	423	384	1038	3730	18212	267	56166	61880	7090	31	364	98	0	619	364	16	0	33	0	145
70	0	0	404	244	1547	0	16812	205	59226	66923	6566	11	324	0	0	522	324	0	0	13	0	101
71	0	0	440	403	1399	0	17963	266	56670	67984	7245	0	327	98	0	559	327	0	0	0	0	99
72	0	0	378	412	1351	0	17626	267	46968	64472	7078	0	351	167	0	568	351	0	0	27	0	109
73	0	0	399	241	582	0	16424	211	59218	66824	6541	0	332	50	0	496	332	0	0	14	0	108
74	0	0	402	91	0	0	15611	159	62874	69979	6091	0	334	25	0	436	334	0	0	29	0	111
75	0	0	409	228	1491	0	16295	195	58167	66687	6406	0	305	0	0	479	305	0	0	14	0	101
76	0	0	427	374	1412	3775	17941	261	56682	60634	6944	0	348	26	0	600	348	0	0	51	0	143
77	0	0	456	384	997	3586	18191	270	55127	61403	7019	13	368	99	0	626	368	0	0	210	0	139
78	0	0	445	0	0	0	0	0	0	0	0	0	0	0	0	514	0	0	0	0	0	0
79	0	0	334	278	979	0	16558	195	34887	45668	6991	0	440	158	0	707	440	0	38	48	0	141
80	0	0	351	214	933	0	17094	198	38111	48756	7498	0	483	122	0	698	483	0	36	51	0	143
81	0	58	444	343	1164	0	22456	178	57824	76165	7322	15	393	96	0	822	393	0	0	0	0	148
82	0	0	547	0	157	241	0	0	851	0	35	0	0	0	0	769	0	0	47	0	0	0
83	0	0	360	188	763	0	10151	106	29662	80903	4321	0	593	0	0	1144	593	0	0	0	65	109
84	0	0	86	0	0	0	0	0	0	0	0	0	0	0	0	0	0	0	0	0	0	0
85	0	0	0	0	50	0	0	0	0	0	0	0	0	0	0	0	0	0	0	0	0	0
86	0	0	418	381	1138	0	13404	190	27126	60909	6618	0	792	0	0	1251	792	0	0	12	112	136
87	0	0	444	0	0	0	0	0	0	0	0	0	0	0	0	382	0	0	0	0	0	0
88	0	0	504	0	0	288	0	0	0	0	0	0	0	0	0	618	0	0	0	0	0	0
89	0	0	468	0	0	0	0	0	0	0	0	0	0	0	0	0	0	0	0	0	0	0
90	0	0	645	0	0	0	0	0	0	0	0	0	0	0	0	264	0	0	0	0	0	0
91	0	0	410	0	1170	3092	238	0	1411	0	91	0	0	0	0	418	0	0	36	0	0	0
92	0	0	424	0	1085	0	7256	67	23003	54445	3418	0	892	0	94	1460	892	0	0	0	140	136
93	0	0	443	0	0	0	0	0	0	0	0	0	0	0	0	619	0	0	0	0	0	0

94	0	0	639	0	0	303	0	0	0	0	0	0	0	0	0	491	0	0	0	0	0	0
95	0	0	457	0	353	1041	721	0	1541	0	154	0	0	0	0	500	0	0	70	0	0	0
96	0	0	935	0	78	196	568	0	3370	0	236	0	0	0	0	563	0	0	0	0	0	0
97	0	0	274	0	1336	0	4186	9	19908	1742	1695	0	76	96	0	651	76	0	0	0	0	50
98	0	0	27	0	0	0	0	0	0	0	0	0	0	0	0	0	0	0	0	0	0	0
99	0	0	41	0	0	0	0	0	0	0	0	0	0	0	0	0	0	0	0	0	0	0
100	0	0	564	0	0	465	0	0	29	0	0	0	0	0	0	530	0	0	0	0	0	0
101	0	0	660	0	0	572	0	0	0	0	0	0	0	0	0	520	0	0	0	0	0	0
102	0	0	376	0	797	0	3306	0	9890	3157	1312	0	132	0	0	706	132	0	0	0	0	79
103	0	0	466	0	826	0	3563	0	10675	3874	1462	0	156	0	0	696	156	0	0	0	26	79
104	0	0	365	364	846	1063	11802	101	14175	34541	3987	95	0	116	0	666	0	95	37	0	0	86
105	0	0	432	0	0	267	0	0	0	0	0	0	0	0	0	264	0	0	0	0	0	0
106	0	0	253	0	51	2050	0	0	0	0	0	0	0	0	0	363	0	0	0	0	0	0